

AD_____

Award Number: DAMD17-98-1-8121

TITLE: Ultrasonic Stimulated Acoustic Emission for Detection of
Breast Microcalcifications

PRINCIPAL INVESTIGATOR: Mostafa Fatemi, Ph.D.

CONTRACTING ORGANIZATION: Mayo Foundation
Rochester, Minnesota 55905

REPORT DATE: May 2000

TYPE OF REPORT: Annual

PREPARED FOR: U.S. Army Medical Research and Materiel Command
Fort Detrick, Maryland 21702-5012

DISTRIBUTION STATEMENT: Approved for Public Release;
Distribution Unlimited

The views, opinions and/or findings contained in this report are those of the author(s) and should not be construed as an official Department of the Army position, policy or decision unless so designated by other documentation.

REPORT DOCUMENTATION PAGE

Form Approved
OMB No. 074-0188

Public reporting burden for this collection of information is estimated to average 1 hour per response, including the time for reviewing instructions, searching existing data sources, gathering and maintaining the data needed, and completing and reviewing this collection of information. Send comments regarding this burden estimate or any other aspect of this collection of information, including suggestions for reducing this burden to Washington Headquarters Services, Directorate for Information Operations and Reports, 1215 Jefferson Davis Highway, Suite 1204, Arlington, VA 22202-4302, and to the Office of Management and Budget, Paperwork Reduction Project (0704-0188), Washington, DC 20503.

1. AGENCY USE ONLY (Leave blank)	2. REPORT DATE May 2000	3. REPORT TYPE AND DATES COVERED Annual (15 Apr 99 - 14 Apr 00)
----------------------------------	----------------------------	--

4. TITLE AND SUBTITLE Ultrasonic Stimulated Acoustic Emission for Detection of Breast Microcalcifications	5. FUNDING NUMBERS DAMD17-98-1-8121
--	--

6. AUTHOR(S) Mostafa Fatemi, Ph.D.	
---------------------------------------	--

7. PERFORMING ORGANIZATION NAME(S) AND ADDRESS(ES) Mayo Foundation Rochester, Minnesota 55905 E-MAIL: fatemi.mayo.edu	8. PERFORMING ORGANIZATION REPORT NUMBER
---	---

9. SPONSORING / MONITORING AGENCY NAME(S) AND ADDRESS(ES) U.S. Army Medical Research and Materiel Command Fort Detrick, Maryland 21702-5012	10. SPONSORING / MONITORING AGENCY REPORT NUMBER
---	---

11. SUPPLEMENTARY NOTES

12a. DISTRIBUTION / AVAILABILITY STATEMENT Approved for public release; distribution unlimited	12b. DISTRIBUTION CODE
---	------------------------

13. ABSTRACT (Maximum 200 Words)

The **purpose** of this research is to build an experimental system based on Ultrasound Stimulated Acoustic Emission for *in vitro* imaging of breast tissue specimens, with the goal of detecting microcalcifications with sufficient accuracy. The **scope** of this research is to improve the laboratory system and evaluate its performance on phantoms and specimens of human breast tissues containing microcalcifications. The first task of this research, which covers a part of the second year, focuses on system improvement for detection of breast microcalcification. The second task which also covers a part the second year, focuses on imaging breast tissue samples using ultrasound stimulated acoustic emission method. Our **findings** include improving our experimental system by substantially reducing the acoustic noise and increasing the scanning speed. Also, we have demonstrated that our method is capable of detecting small breast microcalcifications in human breast tissue samples. We have verified our results with x-ray mammography, and histology.

14. SUBJECT TERMS Breast Cancer	20010228 074	15. NUMBER OF PAGES 84
		16. PRICE CODE

17. SECURITY CLASSIFICATION OF REPORT Unclassified	18. SECURITY CLASSIFICATION OF THIS PAGE Unclassified	19. SECURITY CLASSIFICATION OF ABSTRACT Unclassified	20. LIMITATION OF ABSTRACT Unlimited
--	---	--	---

FOREWORD

Opinions, interpretations, conclusions and recommendations are those of the author and are not necessarily endorsed by the U.S. Army.

___ Where copyrighted material is quoted, permission has been obtained to use such material.

___ Where material from documents designated for limited distribution is quoted, permission has been obtained to use the material.

___ Citations of commercial organizations and trade names in this report do not constitute an official Department of Army endorsement or approval of the products or services of these organizations.

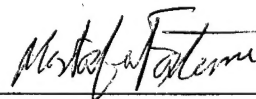
N/A In conducting research using animals, the investigator(s) adhered to the "Guide for the Care and Use of Laboratory Animals," prepared by the Committee on Care and use of Laboratory Animals of the Institute of Laboratory Resources, national Research Council (NIH Publication No. 86-23, Revised 1985).

X For the protection of human subjects, the investigator(s) adhered to policies of applicable Federal Law 45 CFR 46.

N/A In conducting research utilizing recombinant DNA technology, the investigator(s) adhered to current guidelines promulgated by the National Institutes of Health.

N/A In the conduct of research utilizing recombinant DNA, the investigator(s) adhered to the NIH Guidelines for Research Involving Recombinant DNA Molecules.

N/A In the conduct of research involving hazardous organisms, the investigator(s) adhered to the CDC-NIH Guide for Biosafety in Microbiological and Biomedical Laboratories.



PI - Signature

5/24/00
Date

TABLE OF CONTENTS

<u>Front Cover</u>	1
<u>Report Documentation Page</u>	2
<u>Foreword</u>	3
<u>Table of Contents</u>	4
<u>Introduction</u>	5
<u>Body</u>	5-8
<u>Key Research Accomplishments</u>	8
<u>Reportable Outcomes</u>	8
<u>Conclusions</u>	8-9
<u>References</u>	9
<u>Appendices</u>	10 -84

Appendix 1: Figures and legends (pages 11–19 of this report)

Appendix 2: Fatemi, M., and J. F. Greenleaf: Vibro-acoustography: An imaging modality based on ultrasound-stimulated acoustic emission. Proceedings of the National Academy of Sciences USA 96:6603–6608, June 1999 (pages 20–25 of this report)

Appendix 3: Fatemi, M., and J. F. Greenleaf: Probing the dynamics of tissue at low frequencies with the radiation force of ultrasound. Physics in Medicine and Biology 45(6):1449–1464, June 2000 (pages 26–46 of this report)

Appendix 4: Fatemi, M., and J. F. Greenleaf: Vibro-acoustography system modeling. Era of Hope Meeting, DoD Breast Cancer Research Program, Department of Defense, U. S. Army Medical Research and Materiel Command, Atlanta, GA, June 8–12, 2000 (Accepted) (Abstract) (page 47 of this report)

Appendix 5: Fatemi, M., and J. F. Greenleaf: Imaging the viscoelastic properties of tissue. In: M. Fink, J-P. Montagner, and A. Tourin: *Imaging of Complex Media with Acoustic and Seismic Waves* (to be published with the series “Topics in Applied Physics”). Springer-Verlag, 1999 (Submitted) (pages 48–67 of this report)

Appendix 6: Fatemi, M., and J. F. Greenleaf: Application of radiation force in noncontact measurement of the elastic parameters. Ultrasonic Imaging 21(2):147–154, April 1999 (pages 68–75 of this report)

Appendix 7: Fatemi, M., and J. F. Greenleaf: Point response of vibro-acoustography system. 1999 IEEE International Ultrasonics Symposium and Short Courses. Technical Program and Abstracts, Lake Tahoe, NV, October 17–20, 1999, p 68, 1999 (Abstract) (page 76 of this report)

Appendix 8: Greenleaf, J. F., M. Fatemi, and R. R. Kinnick: Vibro-acoustography: Speckle free ultrasonic C-scan. 25th International Acoustical Imaging Symposium, Bristol, United Kingdom, March 19–20, 2000. In: P. N. T. Wells and M. Halliwell: *Acoustical Imaging*, 25, Kluwer Academic/Plenum Publishers, New York (In Press) (pages 77–82 of this report)

Appendix 9: National Science Foundation grant application, “Acquisition of low level sound and vibration measurements system,” submitted January 18, 2000 (pages 83–84 of this report)

1 INTRODUCTION

The general goal of this research is to build an experimental system based on Ultrasound Stimulated Acoustic Emission (USAE) for *in vitro* imaging of breast tissue specimens and test its performance in detecting microcalcification. The general theory of USAE is described in [1,2,3,4,5] and some applications are explained in [6,7,8,9,10]. The first task of this research, which covers the first year and a part of the second year, focuses on system development and optimization for detection of breast microcalcification. The second task, covering parts of the second year, is centered on tissue scanning and studying the manifestation of microcalcifications in USAE images.

This report addresses the activities performed in the second year in both areas. In particular, the report includes experimental results demonstrating the capability of USAE method in imaging and delineating calcifications in breast tissue.

2 BODY

In this section we describe research accomplishments associated with parts of Tasks 1 and 2. First, we report system development activities that improve our measurements. Next, we report some experimental results on human tissue specimens. We will show and discuss USAE images obtained from tissue samples with microcalcifications and compare the results with the corresponding x-ray mammography histology images.

2.a System Development

2.a.1) *Quiet-scanning System*

The step motors used in the present scanner produce loud audio noise that can interfere with the acoustic emission produced by the object. To reduce the vibration and acoustic noise of the scanning, a new scanning system has been designed that is based on analog servo motors instead of the present step motors. The new scanning system has optically encoded axes for precise positioning. Construction of the new system has been successful. The system is now under evaluation test.

2.a.2) *Software development for the new scanning system*

The software for controlling the new scanning system and the data acquisition system has been developed.

2.a.3) *Direct Displacement Measurement by Laser Vibrometer*

Recently we purchased a laser vibrometer for direct measurement of velocity and displacement in the order of nano meters at frequencies up to 250 kHz range. This system allows us to directly measure the vibration that we introduce in an object by the radiation force of ultrasound. Hence, we can validate our acoustic measurements by direct optical measurement.

2.b Breast Tissue Imaging and Detection of Microcalcifications

The hypothesis is that ultrasound stimulated acoustic emission can be used to image tissue and detect microcalcifications. To test this hypothesis, we scanned several excised human breast tissue and compared the results with the x-ray mammography and histology.

2.b.1) Procedure

Experiments were conducted on human breast tissue samples in the following manner:

1. Initial tissue selection — Breast tissues were enlisted within a few days of surgery from Surgical Pathology section of Rochester Methodist Hospital. Patients' records were reviewed to identify those with high probability of having microcalcifications. Tissues from this group of patients were collected.
2. Initial tissue preparation — Tissues were cut into (approximately) 3x3 cm pieces and arranged flat and side-by-side in a plastic bag. The bag was constrained in a rectangular bracket to keep them from moving. Each bag could contain several tissue pieces, but all were from the same patient.
3. Screening mammography — High-resolution x-ray mammography of each tissue bag was obtained using a tissue mammography machine.
4. Reading — Each mammogram was read by our radiologist (Dr. Morton) to identify microcalcifications.
5. Final tissue selection — Tissue pieces identified in the above step were selected. Remaining tissue pieces were put away.
6. Mounting — Each tissue piece selected in the above step was mounted on a Scanning Bracket. This bracket is designed to hold the tissue piece in the water tank for acoustic scanning. Each bracket is shaped like a ring, approximately 10 cm in diameter, and made from plexiglass material. The ring is covered by a thin latex sheet. The tissue piece was mounted on this sheet with a few small drops of glue. Glue drops were carefully placed on locations that would not affect the region of interest with microcalcifications. To identify the position and orientation of the object, small pieces of suture were used as identification marks. For this purpose small knots are placed at different position on the tissue. These markers normally can be seen in the acoustic, x-ray, and photography images.
7. Base Mammography — Tissue mammography images were obtained from each mounted sample. These images were used as a base of comparison with the USAE image. These images were converted into digital form and stored in the computer.
8. Scanning — Mounted samples were scanned in the water tank. Acoustic images were obtained at various difference frequencies. These images were displayed/printed in the same size and orientation as the x-ray mammography images.
9. Image evaluation — Acoustic emission images were evaluated against the x-ray mammography to assess the manifestation of calcifications in the acoustic images.
10. Histology — Sections of the tissue identified with microcalcification were cut for histology. The results were used to validate the existence of microcalcifications and determine their size and locations.

2.b.2) Experiment Results

To demonstrate the procedure outlined above, we present results of some tissue experiments.

The first example illustrates detection of microcalcifications. Figure 1 shows high-resolution x-ray image of a group of tissue samples collected from a 57 year old subject. This x-ray was done for screening (step 3 of the list). It shows several bright spots which are identified as microcalcifications (<400 microns) by the radiologist. The tissue piece that is identified with microcalcifications was chosen for further scanning. Figure 2 shows the photograph of the selected piece mounted on the scanning bracket. Sutures that are knotted on the tissue are for identification purposes. Figure 3 shows the mammogram of the selected tissue pieces mounted on the scanning bracket. This sample was scanned in the water tank. The acoustic emission image of the tissue at 26 kHz is shown in Figure 4. Microcalcifications can be seen in this image as four bright spots. It is interesting to note that the number and position of these spots matches with those microcalcifications identified in the x-ray mammography. Also noticeable is that tissue inhomogeneities appear dim and do not interfere with the calcifications in the acoustic image.

The second example illustrates detection of calcification in a vessel. Figure 5 shows a high-resolution x-ray image of a group of tissue collected from a 78-year old subject after breast removal. This is the screening x-ray. It shows several bright spots which are identified as calcifications by the radiologist. The tissue piece that is identified with having a calcified vessel was chosen for further scanning. We have knotted sutures on three locations on the tissue for identification purpose. Figure 6 shows the mammogram of the selected tissue pieces mounted on the scanning bracket. The sutures are barely visible. This sample was scanned in the water tank. The acoustic emission image of the tissue is shown in Figure 7. Calcification can be clearly seen in this image. It is interesting to note that the shape of calcified region matches with great detail with the corresponding region in the x-ray mammography.

To validate the presence of calcifications, the tissue was examined histologically. The portion of the tissue sample used for this purpose is shown in the x-ray image in Figure 8. Figure 9 shows the histology of the mid-portion of the selected tissue piece in a plane tangential to the vessel. The histology shows the cross section of the vessel with some irregular calcifications on the wall. the thickness of the calcification layer is less than 100 microns.

2.c Discussion

Experimental USAE images presented in this report demonstrates two important facts: (1) USAE imaging method is capable of detecting small microcalcifications, as well as calcifications in vessels, in the breast tissue; (2) Microcalcifications can be delineated from tissue inhomogeneities. Results shown here also indicate that such images have high-spatial resolution, high detectability, good contrast, and high signal-to-noise ratio. Microcalcifications shown in our results are only a few hundred microns in diameter, and the calcifications in the vessel wall were not more than 100 microns thick. Histology image from the second sample also revealed small (<40 microns) microcalcifications below the vessel. These small microcalcifications could not be detected by either USAE or x-ray mammography methods.

A comparison between the USAE image Figure 7 and the corresponding mammography Figure 3 reveals another interesting capability of USAE method. High tissue density in the region surrounding

the microcalcification absorbs a great deal of x-ray energy, hence the x-ray image shows very low contrast within this region, and as a result, microcalcifications are only barely visible. However, the USAE image delineates these microcalcification with high contrast. This is because the acoustic emission is sensitive to the elastic properties of the object.

Acoustic images reported here were obtained at relatively high vibration frequencies (about 20 kHz). At these frequencies we are able to acquire the data at much higher speed, reducing the acquisition time to a few minutes per image (for more details, refer to High-Speed Scanning section in the last year's report). This is because at these frequencies the noise level from the scanner mechanism is negligible, hence we can keep the scanning motor running while collecting the data. Scanning speed is an important factor in our experiments.

2.d Key Research Accomplishments

- Demonstrated that small microcalcification (also vessel calcifications) can be detected by USAE imaging method.
- Demonstrated that breast microcalcifications can be delineated from tissue inhomogeneities in a USAE image.
- Demonstrated that microcalcification can be imaged at high vibrational frequencies.

2.e Reportable Outcomes

1. Fatemi, M., and J. F. Greenleaf: Probing the dynamics of tissue at low frequencies with the radiation force of ultrasound. *Physics in Medicine and Biology* 45(6):1449–1464, June 2000.
2. Fatemi, M., and J. F. Greenleaf: Vibro-acoustography system modeling. Era of Hope Meeting, DoD Breast Cancer Research Program, Department of Defense, U. S. Army Medical Research and Materiel Command, Atlanta, GA, June 8–12, 2000 (Accepted) (Abstract).
3. Fatemi, M., and J. F. Greenleaf: Imaging the viscoelastic properties of tissue. In: M. Fink, J-P. Montagner, and A. Tourin: *Imaging of Complex Media with Acoustic and Seismic Waves* (to be published with the series "Topics in Applied Physics"). Springer-Verlag, 1999 (Submitted).
4. Fatemi, M., and J. F. Greenleaf: Remote measurement of shear viscosity with ultrasound-stimulated vibro-acoustic spectrography. *Acta Physica Sinica* 8:S27–S32, August 1999.
5. Fatemi, M., and J. F. Greenleaf: Point response of vibro-acoustography system. 1999 IEEE International Ultrasonics Symposium and Short Courses. Technical Program and Abstracts, Lake Tahoe, NV, October 17–20, 1999, p 68, 1999 (Abstract).
6. National Science Foundation MRI grant application, "Acquisition of low level sound and vibration measurements system," submitted January 18, 2000.

2.f Conclusions

Small microcalcifications (and vessel calcifications) in breast tissue can be detected by USAE imaging method. In these images microcalcifications appear with high contrast with respect to the soft tissue, hence can be delineated from tissue inhomogeneities.

2.f.1) So what?

Our experimental results support our hypothesis that ultrasound-stimulated acoustic emission method (or vibro-acoustography) is capable of detecting small calcifications in human breast tissue samples. Improvement of this technique such that it can be reliably used in vivo would be a significant contribution to the field, especially where the conventional mammography could not be used for detection of breast microcalcification.

2.g References

1. Fatemi, M., and J. F. Greenleaf: Probing the dynamics of tissue at low frequencies with the radiation force of ultrasound. *Physics in Medicine and Biology* 45(6):1449–1464, June 2000.
2. Fatemi, M., and J. F. Greenleaf: Ultrasound-stimulated vibro-acoustic spectrography. *Science* 280:82–85, April 3, 1998.
3. Fatemi, M., and J. F. Greenleaf: Vibro-acoustography: An imaging modality based on ultrasound-stimulated acoustic emission. *Proceedings of the National Academy of Sciences USA* 96:6603–6608, June 1999.
4. Fatemi, M., and J. F. Greenleaf: Vibro-acoustography system modeling. Era of Hope Meeting, DoD Breast Cancer Research Program, Department of Defense, U. S. Army Medical Research and Materiel Command, Atlanta, GA, June 8–12, 2000 (Accepted) (Abstract).
5. Fatemi, M., and J. F. Greenleaf: Point response of vibro-acoustography system. 1999 IEEE International Ultrasonics Symposium and Short Courses. Technical Program and Abstracts, Lake Tahoe, NV, October 17–20, 1999, p 68, 1999 (Abstract).
6. Fatemi, M., and J. F. Greenleaf: Remote measurement of shear viscosity with ultrasound-stimulated vibro-acoustic spectrography. *Acta Physica Sinica* 8:S27–S32, August 1999.
7. Fatemi, M., and J. F. Greenleaf: Imaging the viscoelastic properties of tissue. In: M. Fink, J-P. Montagner, and A. Tourin: *Imaging of Complex Media with Acoustic and Seismic Waves* (to be published with the series “Topics in Applied Physics”). Springer-Verlag, 1999 (Submitted).
8. Fatemi, M., and J. F. Greenleaf: Application of radiation force in noncontact measurement of the elastic parameters. *Ultrasonic Imaging* 21(2):147–154, April 1999.
9. Greenleaf, J. F., M. Fatemi, and R. R. Kinnick: Vibro-acoustography: Speckle free ultrasonic C-scan. 25th International Acoustical Imaging Symposium, Bristol, United Kingdom, March 19–22, 2000. In: P. N. T. Wells and M. Halliwell: *Acoustical Imaging*, 25, Kluwer Academic/Plenum Publishers, New York (In press).
10. National Science Foundation MRI grant application, “Acquisition of low level sound and vibration measurements system,” submitted January 18, 2000.

3 Appendices

Appendix 1: Figures and legends (pages 11–19 of this report)

Appendix 2: Fatemi, M., and J. F. Greenleaf: Vibro-acoustography: An imaging modality based on ultrasound-stimulated acoustic emission. Proceedings of the National Academy of Sciences USA 96:6603–6608, June 1999 (pages 20–25 of this report)

Appendix 3: Fatemi, M., and J. F. Greenleaf: Probing the dynamics of tissue at low frequencies with the radiation force of ultrasound. Physics in Medicine and Biology 45(6):1449–1464, June 2000 (pages 26–46 of this report)

Appendix 4: Fatemi, M., and J. F. Greenleaf: Vibro-acoustography system modeling. Era of Hope Meeting, DoD Breast Cancer Research Program, Department of Defense, U. S. Army Medical Research and Materiel Command, Atlanta, GA, June 8–12, 2000 (Accepted) (Abstract) (page 47 of this report)

Appendix 5: Fatemi, M., and J. F. Greenleaf: Imaging the viscoelastic properties of tissue. In: M. Fink, J-P. Montagner, and A. Tourin: *Imaging of Complex Media with Acoustic and Seismic Waves* (to be published with the series “Topics in Applied Physics”). Springer-Verlag, 1999 (Submitted) (pages 48–67 of this report)

Appendix 6: Fatemi, M., and J. F. Greenleaf: Application of radiation force in noncontact measurement of the elastic parameters. Ultrasonic Imaging 21(2):147–154, April 1999 (pages 68–75 of this report)

Appendix 7: Fatemi, M., and J. F. Greenleaf: Point response of vibro-acoustography system. 1999 IEEE International Ultrasonics Symposium and Short Courses. Technical Program and Abstracts, Lake Tahoe, NV, October 17–20, 1999, p 68, 1999 (Abstract) (page 76 of this report)

Appendix 8: Greenleaf, J. F., M. Fatemi, and R. R. Kinnick: Vibro-acoustography: Speckle free ultrasonic C-scan. 25th International Acoustical Imaging Symposium, Bristol, United Kingdom, March 19–20, 2000. In: P. N. T. Wells and M. Halliwell: *Acoustical Imaging*, 25, Kluwer Academic/Plenum Publishers, New York (In Press) (pages 77–82 of this report)

Appendix 9: National Science Foundation MRI grant application, “Acquisition of low level sound and vibration measurements system,” submitted January 18, 2000 (pages 83–84 of this report)

APPENDIX A — Figures and Legends

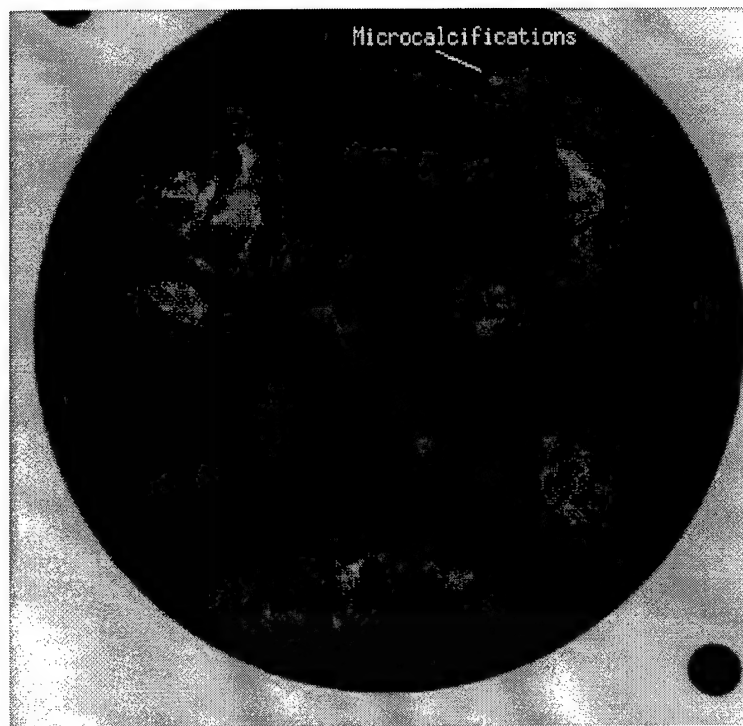


Figure 1 High-resolution x-ray image of breast tissue samples collected from a patient. The piece at the top right corner has some microcalcifications, indicated by the arrow. This piece is selected for scanning.

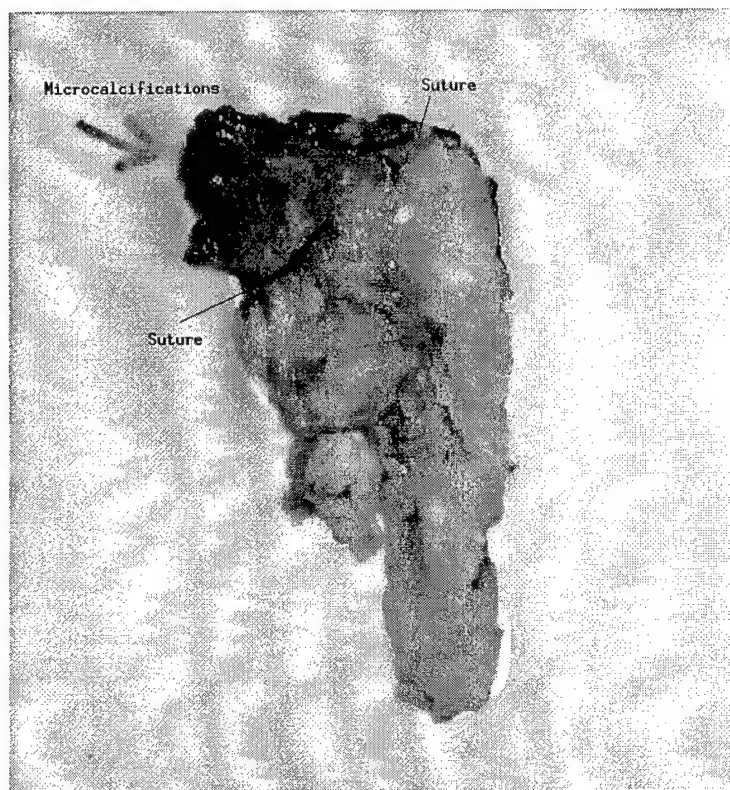


Figure 2 Photograph of the tissue sample selected from the collection shown in the previous figure. Microcalcifications are located at the top-left corner of this sample as indicated by the arrow. Two sutures are knotted at two location on the tissue as indicators and landmarks that will show in the acoustic image. The tissue is glued (using three small droplets at locations far from the calcified region) to a thin latex sheet attached to the scanning bracket for scanning. This sheet is acoustically transparent.



Figure 3 Tissue mammography of the selected sample shown in Figure 2. This sample includes four microcalcification (<400 microns) at the top left corner. The brightness of the image has been reduced to make the microcalcifications stand out from the high density tissue at the top left corner of the sample. As a result most of the tissue is not visible in this x-ray, except for the calcified region and some bright irregular line regions (containing no calcification) at the center.

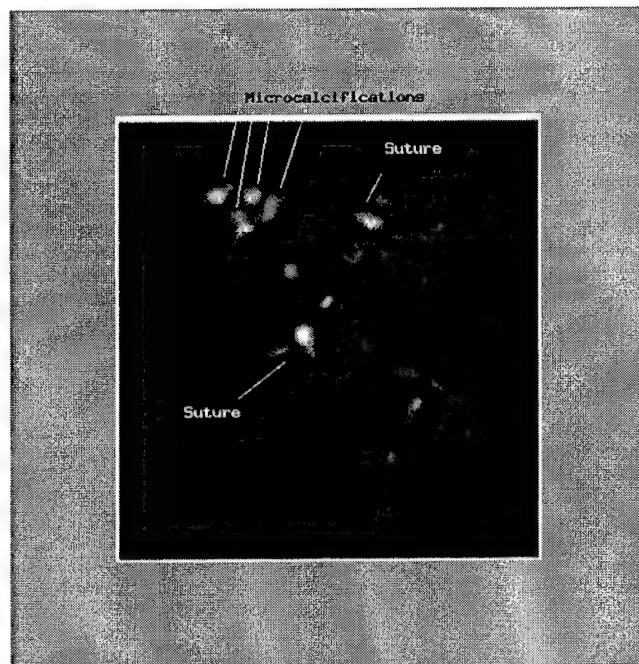


Figure 4 USAE image of the sample shown in Figures 2 and 3. This image clearly shows four microcalcifications (as bright spots) at the top left corner of the tissue sample. The two sutures are also indicated in the image. The location of microcalcifications shown here matches well with those shown in the x-ray mammography.

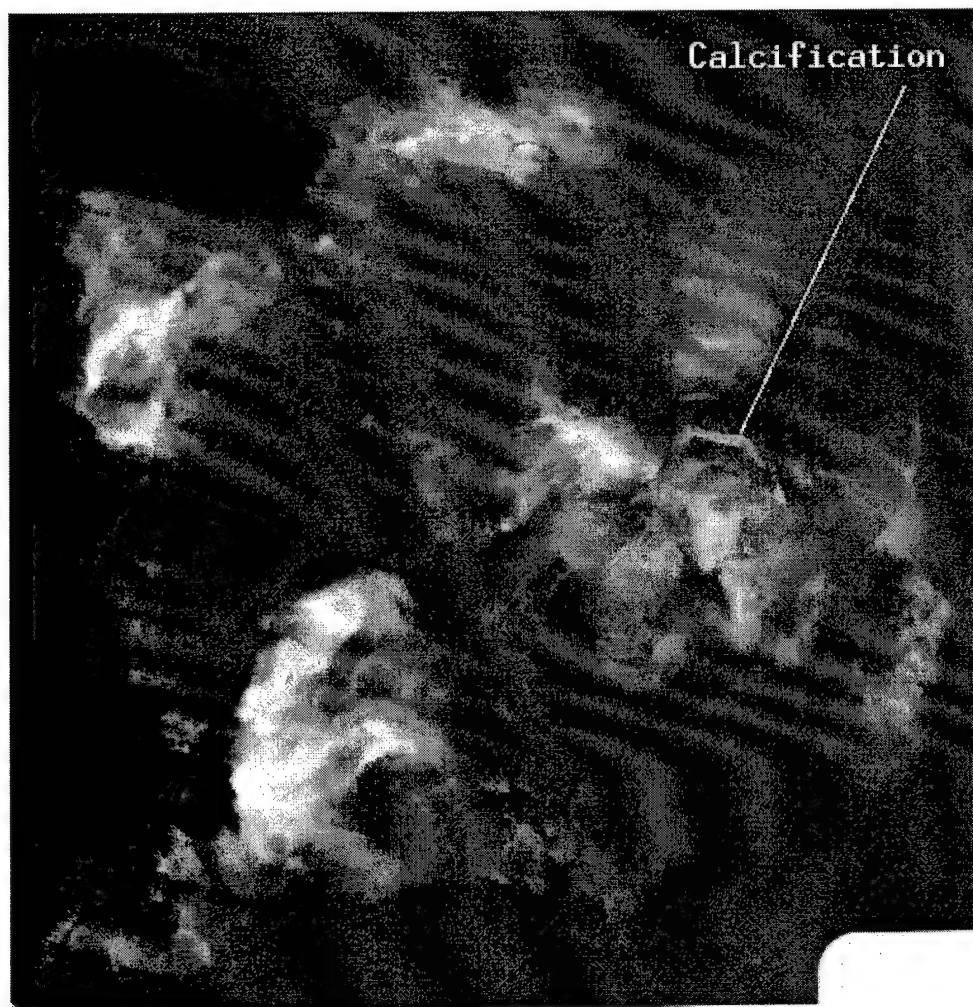


Figure 5 High-resolution x-ray of breast tissue samples from a patient. One of the samples contains a calcified vessel. This sample is selected for scanning.

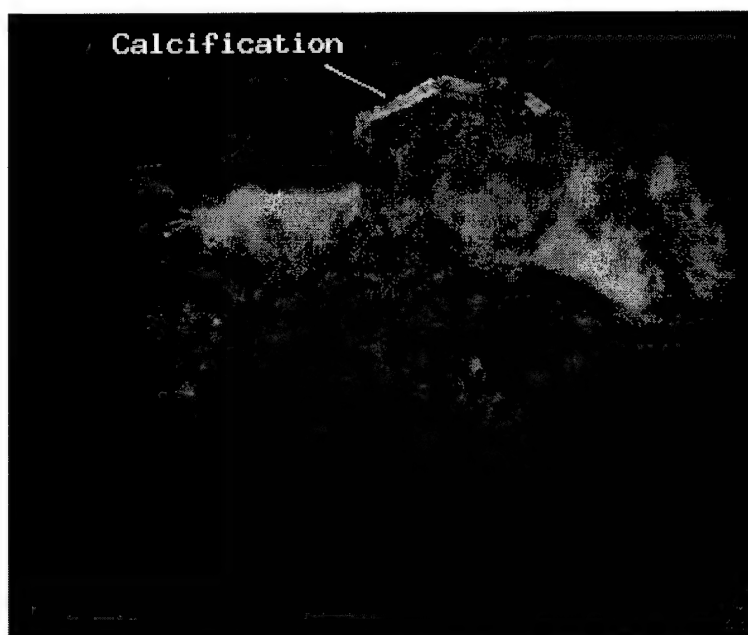


Figure 6 X-ray mammogram of the selected tissue sample indicated in the previous figure. The calcified vessel (bright line) is about one millimeter in diameter. This sample is glued to the latex sheet of the scanning bracket.



Figure 7 USAE image of the tissue sample shown in the previous figure. The calcified vessels shown as a bright line with high contrast with respect to the background tissue. Also seen in this image is the suture that is used for identification. Note that the calcification is displayed with much higher contrast than tissue inhomogeneities.



Figure 8 This x-ray image shows a 12x12 mm portion of the tissue sample shown in Figure 5, which is cut out for histology examination. The thickness of the tissue is about 3 mm. The calcified vessel is seen as a bright line.

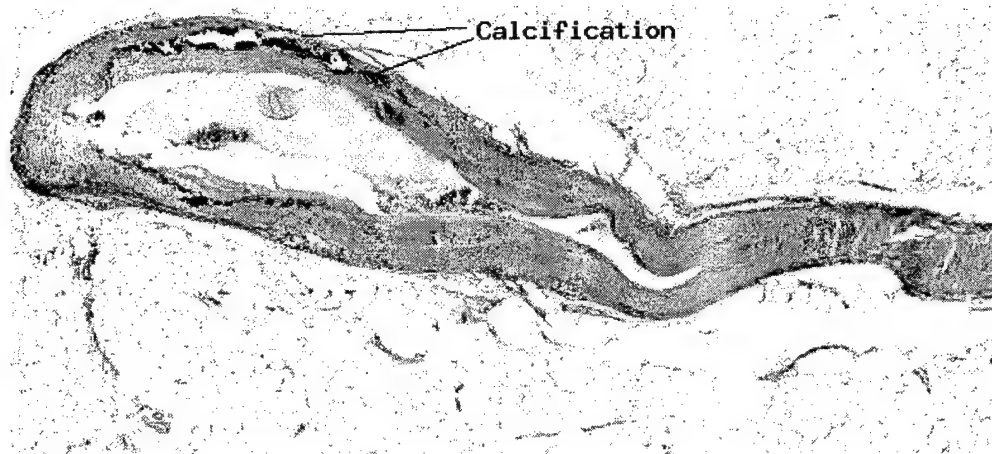


Figure 9 This image shows a histology slide from the center portion of the tissue piece. The slice is cut tangential to the vessel. This magnified slide shows parts of the vessel wall including an irregular calcified layer on the wall. The diameter of the vessel is about 1 mm and the thickness of the calcified layer is less than 100 microns. The layer covers portions of the wall.

Vibro-acoustography: An imaging modality based on ultrasound-stimulated acoustic emission

MOSTAFA FATEMI* AND JAMES F. GREENLEAF

Ultrasound Research, Department of Physiology and Biophysics, Mayo Clinic and Foundation, 200 First Street SW, Rochester, MN 55905

Communicated by Floyd Dunn, Professor Emeritus, University of Illinois, Urbana, IL, March 11, 1999 (received for review August 11, 1998)

ABSTRACT We describe theoretical principles of an imaging modality that uses the acoustic response of an object to a highly localized dynamic radiation force of an ultrasound field. In this method, named ultrasound-stimulated vibro-acoustography (USVA), ultrasound is used to exert a low-frequency (in kHz range) force on the object. In response, a portion of the object vibrates sinusoidally in a pattern determined by its viscoelastic properties. The acoustic emission field resulting from object vibration is detected and used to form an image that represents both the ultrasonic and low-frequency (kHz range) mechanical characteristics of the object. We report the relation between the emitted acoustic field and the incident ultrasonic pressure field in terms of object parameters. Also, we present the point-spread function of the imaging system. The experimental images in this report have a resolution of about 700 μm , high contrast, and high signal-to-noise ratio. USVA is sensitive enough to detect object motions on the order of nanometers. Possible applications include medical imaging and material evaluation.

The study of objects in terms of their mechanical response to external forces is of considerable interest in material science and medical diagnosis. Elastic constants are closely connected to the thermodynamic properties of materials and can be related to a wide range of physical parameters. Elastic constants can be determined by measuring deformation in response to an applied force. Although a static force can be used for this purpose, using a dynamic force is preferred if one is interested in measuring the dynamic characteristics of the material (1).

Changes in elasticity of soft tissues are often related to pathology. Palpation is a traditional example of estimating mechanical parameters for tissue characterization, where a static force is applied and a crude estimation of the tissue elasticity is obtained through the sense of touch. In palpation, force is exerted on the body surface, and the result is an accumulative response of all the tissues below. Physicians can sense abnormalities if the response to palpation of the suspicious tissue is sufficiently different from that of normal tissue. However, if the abnormality lies deep in the body, or if it is too small to be resolved by touch, then the palpation method fails.

Elasticity imaging, a subject extensively investigated in recent years, is a quantitative method that measures the mechanical properties of tissue. The general approach is to measure tissue motion caused by an external (or, in some methods, internal) force/displacement and use it to reconstruct the elastic parameters of the tissue. Some investigators have used static force to compress the tissue and measured the resulting strain by ultrasound (2, 3). Others have used external mechanical vibrators to vibrate the tissue and detected the resulting displacement in tissue by Doppler ultrasound (4-7). For a review of elasticity imaging methods, refer to ref. 8. A recently developed method uses an actuator to vibrate the body

surface and then measures the strain waves with phase-sensitive MRI (9).

Most of the elasticity imaging methods are based on an external source of force resulting in a spatially wide stress-field distribution. This requires the stress field to pass through the superficial portion of an object before reaching the interior part. Analysis of the object response can be complicated because the stress-field pattern changes, often unpredictably, at different depths before it reaches the region of interest within the object. An alternative strategy is to apply a localized stress directly in the region of interest. One way to accomplish this is to use the radiation pressure of an ultrasound source(s). Based on this strategy, Sugimoto *et al.* (10) presented a method to measure tissue hardness by using the radiation force of a single focused ultrasound beam. In this method, impulsive radiation force was used to generate localized deformation of the tissue. Resulting transient deformation was measured as a function of time by an ultrasound Doppler method. Radiation force has also been used to generate shear elastic waves in tissues (11).

In this paper, we describe the principles of an imaging technique that produces a map of the mechanical response of an object to a force applied at each point. The method uses ultrasound radiation force to remotely exert a localized oscillating stress field at a desired frequency within (or on the surface of) an object. In response to this force, a part of the object vibrates. The size of this part and the motion pattern depend on object viscoelastic characteristics. The acoustic field resulting from object vibration, which we refer to as "acoustic emissions,"[†] is detected by a sensitive hydrophone and used to form the image of the object. This method benefits from the high spatial definition of ultrasound radiation force and high motion-detection sensitivity offered by the hydrophone. We call this technique ultrasound-stimulated vibro-acoustography (USVA). Some general aspects of this method, including some experimental results, have been outlined by the authors in ref. 12. Here we present the theoretical foundations of USVA.

METHODS

Our aim is to image an object based on its mechanical characteristics. This is achieved by vibrating the object by applying a highly localized oscillating force to each point of the object. The localized force is produced by modulating the intensity, and thereby the radiation force, of the ultrasound at low frequencies (normally in kHz range). The resulting sound emitted by the object is a function of object mechanical

Abbreviations: USVA, ultrasound-stimulated vibro-acoustography; PSF, point spread function; CW, continuous wave.

*To whom reprint requests should be addressed at: Ultrasound Research, Mayo Clinic. e-mail: fatemi.mostafa@mayo.edu.

[†]The term "acoustic emission" is used to describe the acoustic field in response to a cyclic vibration of the object. Similar terminology is also used in the field of nondestructive testing of materials and in optoacoustic imaging to describe a different phenomenon, usually the acoustic field resulting from structural deformation.

The publication costs of this article were defrayed in part by page charge payment. This article must therefore be hereby marked "advertisement" in accordance with 18 U.S.C. §1734 solely to indicate this fact.

PNAS is available online at www.pnas.org.

characteristics and the location of the excitation point. The image is produced by mapping the amplitude or phase of this sound, which is detected by a sensitive hydrophone, vs. position. Fig. 1 illustrates this method. In the following section, we describe the relationship between the USVA image and the properties of the object.

THEORY

Generation of a Dynamic Radiation Force on a Target. The acoustic radiation force is the time-average force exerted by an acoustic field on an object. This force is an example of a universal phenomenon in any wave motion that introduces some type of unidirectional force on absorbing or reflecting targets in the wave path. Radiation force is produced by a change in the energy density of an incident acoustic field. For a review of this phenomenon, refer to ref. 13. Consider a plane ultrasound beam interacting with a planar object of zero thickness and arbitrary shape and boundary impedance that scatters and absorbs. The radiation force vector, \mathbf{F} , arising from this interaction has a component in the beam direction and another transverse to it. The magnitude of this force is proportional to the average energy density of the incident wave $\langle E \rangle$ at the object, where $\langle \rangle$ represents the time average and S , the projected area of the object (14)

$$\mathbf{F} = \mathbf{d}_r \langle E \rangle S, \quad [1]$$

where \mathbf{d}_r is the vector drag coefficient with a component in the incident beam direction and another transverse to it. The coefficient \mathbf{d}_r is defined per unit incident energy density and unit projected area. For a planar object, \mathbf{d}_r is numerically equal to the force on the object. Physically, \mathbf{d}_r represents the scattering and absorbing properties of the object and is given by (14)

$$\mathbf{d}_r = \hat{\mathbf{p}} S^{-1} (\Pi_a + \Pi_s - \int \gamma \cos \alpha_s dS) + \hat{\mathbf{q}} S^{-1} \int \gamma \sin \alpha_s dS, \quad [2]$$

where $\hat{\mathbf{p}}$ and $\hat{\mathbf{q}}$ are the unit vectors in the beam direction and normal to it, respectively. The quantities Π_a and Π_s are the total absorbed and scattered powers, respectively, and γ is the scattered intensity, all expressed per unit incident intensity. Also, α_s is the angle between the incident and the scattered intensity, and dS is the area element. The drag coefficient can also be interpreted as the ratio of the radiation force magnitude on a given object to the corresponding value if the object were replaced by a totally absorbing object of similar size. This is because $|\mathbf{d}_r| = 1$ for a totally absorbing object. This coefficient can be determined for objects of different shapes and sizes. For simplicity, we assume a planar object normal to the beam axis. In this case, the transverse component vanishes, thus the drag coefficient (force) will have only a component normal to the target surface, which we denote by scalar $d_r(F)$. Values of d_r for spheres, in terms of the diameter and the wavelength, are given in ref. 14.

To produce a dynamic radiation force, one can use an amplitude-modulated beam (15). Consider an amplitude-modulated incident (ultrasonic) pressure field, $p(t)$, as

$$p(t) = P_{\omega_0} \cos(\Delta\omega t/2) \cos\omega_0 t, \quad [3]$$

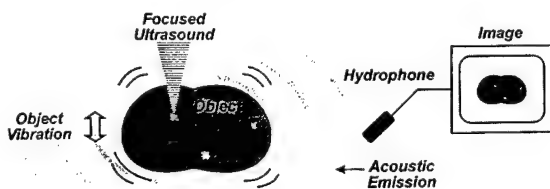


FIG. 1. Principle of ultrasound-stimulated vibro-acoustography.

where P_{ω_0} , $\Delta\omega/2$, and ω_0 are the pressure amplitude, modulating frequency, and center frequency, respectively. In our analysis and experiments, we assume that the condition $\Delta\omega \ll \omega_0$ holds. In such a case, the energy density of the incident field has slow variations in time. To discriminate the slow time variations of a function, let us define the *short-term time average* of an arbitrary function $\xi(t)$ over the interval of T seconds at time instance t , as $\langle \xi(t) \rangle_T = 1/T \int_{t-T/2}^{t+T/2} \xi(\tau) d\tau$, which is a function of t . The long-term time average (or simply the time average) is obtained by setting $T \rightarrow \infty$. To compute the short-term time average of the acoustic-energy density relevant to field variations at $\Delta\omega/2$, we choose T longer than the ultrasound wave period but much shorter than the modulation period, that is $2\pi/\omega_0 \ll T \ll 4\pi/\Delta\omega$. Under this condition, the short-term time average of $p^2(t)$ is $\langle p^2(t) \rangle_T = (P_{\omega_0}^2/4) (1 + \cos \Delta\omega t)$. The energy density is given by $p^2(t)/\rho c^2$, where ρ and c are the density and propagation speed in the medium (16). We are interested in the time-varying component of the short-term time average of the energy density. Denoting this component by $e_{\Delta\omega}(t)$, we can write: $e_{\Delta\omega}(t) = (P_{\omega_0}^2/4\rho c^2) \cos \Delta\omega t$. This component of the energy density produces a time-varying radiation force on the target (Eq. 1) at frequency $\Delta\omega$. The amplitude of this force, $F_{\Delta\omega}$, is

$$F_{\Delta\omega} = P_{\omega_0}^2 S d_r / 4\rho c^2. \quad [4]$$

This equation states that the time-varying force amplitude is proportional to the square of incident ultrasound pressure, or equivalently, to the incident power. If the object moves in response to this force, then the high-frequency ultrasound energy would convert to low-frequency mechanical energy.

Acoustic Emission from a Target Caused by a Dynamic Force. The radiation force $F_{\Delta\omega}$ vibrates the target object at frequency $\Delta\omega$. Object vibration results in an acoustic field in the medium (acoustic emission). This field is related to object shape, size, and viscoelastic properties. To present a conclusive analysis of this relationship, we have to assume an object with specific characteristics. Here we assume that the vibrating object has a circular cross-section of radius b and uniformly vibrates back and forth like a piston. This choice allows us to illustrate the concept in a simple form. We also consider an area $S \leq \pi b^2$ of the piston surface to be projected normally by the beam. Similar solutions can be carried out for other objects.[‡]

The steady-state normal velocity amplitude of a piston, $U_{\Delta\omega}$, caused by a harmonic force $F_{\Delta\omega}$ at frequency $\Delta\omega$, can be described in terms of the mechanical impedance $Z_{\Delta\omega}$,

$$U_{\Delta\omega} = F_{\Delta\omega} / Z_{\Delta\omega}, \quad [5]$$

where $Z_{\Delta\omega} = Z'_m + Z_r$ is comprised of the mechanical impedance of the object in vacuum Z'_m , and the radiation impedance of the object Z_r , all defined at $\Delta\omega$. Modeling the object as a mass-spring system, Z'_m can be written in terms of $\Delta\omega$ as (16, 17)

$$Z'_m = R'_m - j(m\Delta\omega - K'/\Delta\omega), \quad [6]$$

where m , R'_m , and K' are the mass, mechanical resistance, and spring constants of the object, respectively. The radiation impedance of the piston can be written (17) as $Z_r = \pi b^2 (R_r - jX_r)$ [7], where $R_r = \rho c [1 - (c/2\Delta\omega b) J_1(c/2\Delta\omega b)]$, [8], and $X_r = (4\rho c/\pi) \int_0^{\pi/2} \sin[(2b\Delta\omega/c) \cos \alpha] \sin^2 \alpha d\alpha$ [9], where $J_1(\cdot)$ is the first-order Bessel function of the first kind. In many applications of our interest, the wavelength is much greater than the object size, hence, $(\Delta\omega/c)b \rightarrow 0$. In such cases Z_r assumes a simpler form as $Z_r = \pi b^3 \rho \Delta\omega (b\Delta\omega/2c - j8/3\pi)$

[‡]The theory can be extended to include arbitrary vibrating-part shapes and nonuniform displacement of the object. Nonuniform displacement would be an important issue when the vibration wavelength in the object material is smaller than $2b$.

[10]. The mechanical impedance of the piston object can now be written as

$$\begin{aligned} Z_{\Delta\omega} &= (R'_m + \pi b^2 R_r) - j(m\Delta\omega - K'/\Delta\omega + \pi b^2 X_r) \\ &\approx (R'_m + \pi \rho b^4 \Delta\omega^2/2c) - j(m\Delta\omega - K'/\Delta\omega \\ &\quad + 8\rho b^3 \Delta\omega/3), \quad b(\Delta\omega/c) \rightarrow 0. \end{aligned} \quad [11]$$

Once we calculate $U_{\Delta\omega}$, we can calculate the pressure field it produces in the medium. We assume that the acoustic emission signal propagates in a free and homogenous medium. The farfield acoustic pressure caused by a piston source of radius b set in a planar boundary of infinite extent is given by (17),

$$\begin{aligned} P_{\Delta\omega} &= -j\Delta\omega\rho \frac{\exp(j\Delta\omega l/c)}{4\pi l} \left[\frac{2J_1[(b\Delta\omega/c) \sin \vartheta]}{(b\Delta\omega/c) \sin \vartheta} \times \frac{\cos \vartheta}{\cos \vartheta + \beta_B} \right] \\ &\quad \times (2\pi b^2 U_{\Delta\omega}), \end{aligned} \quad [12]$$

where l is the distance from the observation point to the center of the piston, ϑ is the angle between this line and the piston axis, and β_B is the specific acoustic admittance of the boundary surface.[§] The factor of two comes from the presence of the boundary wall, which would be replaced by unity if the boundary wall were not present (16). The acoustic emission field resulting from object vibration can be written in terms of the incident ultrasound pressure by combining Eqs. 4, 5, and 12, as

$$\begin{aligned} P_{\Delta\omega} &= \left\{ j \frac{\Delta\omega}{c^2} \times \frac{\exp(j\Delta\omega l/c)}{4\pi l} \left[\frac{2J_1[(b\Delta\omega/c) \sin \vartheta]}{(b\Delta\omega/c) \sin \vartheta} \times \frac{\cos \vartheta}{\cos \vartheta + \beta_B} \right] \right\} \\ &\quad \times \{1/[(R'_m + \pi b^2 R_r) - j(m\Delta\omega - K'/\Delta\omega + \pi b^2 X_r)](2\pi b^2)P_{\omega_0}^2 S d_r\}. \end{aligned} \quad [13]$$

For wavelengths long compared to the object size, i.e., when $b\Delta\omega/c \rightarrow 0$, the term in the first brace approaches a constant, hence we may consider the contents of the first brace to be an object-independent function (the specific acoustic admittance β_B relates to the surrounding boundary surface). Under these conditions, the first brace in the above equation represents the effect of the medium on the acoustic emission field, which we may call the *medium transfer function*, and denote it by

$$H_{\Delta\omega}(l) = j \frac{\Delta\omega}{c^2} \times \frac{\exp(j\Delta\omega l/c)}{4\pi l} \left[\frac{2J_1[(b\Delta\omega/c) \sin \vartheta]}{(b\Delta\omega/c) \sin \vartheta} \times \frac{\cos \vartheta}{\cos \vartheta + \beta_B} \right]. \quad [14]$$

The second brace in Eq. 13 is $1/Z_{\Delta\omega}$, or the mechanical admittance of the object at the frequency of the acoustic emission ($\Delta\omega$), and we denote it by $Y_{\Delta\omega}$. It is convenient to combine this term with the next term ($2\pi b^2$) in Eq. 13, as $Q_{\Delta\omega} = 2\pi b^2 Y_{\Delta\omega} = 2\pi b^2/Z_{\Delta\omega}$, which is the total acoustic outflow by the object per unit force (acoustic outflow is the volume of the medium (e.g., the fluid) in front of the object surface that is displaced per unit time because of object vibration.). Function $Q_{\Delta\omega}$ represents the object characteristics at the acoustic frequency. We may thus rewrite Eq. 13 in a more compact form as

$$P_{\Delta\omega} = H_{\Delta\omega}(l) Q_{\Delta\omega} P_{\omega_0}^2 S d_r. \quad [15]$$

Eq. 15 indicates that the acoustic emission pressure is proportional to: (i) the square of ultrasound pressure P_{ω_0} ; (ii) the ultrasound characteristics of the object, d_r , in the projected

area S ; (iii) the acoustic outflow by this object, $Q_{\Delta\omega}$, representing the object size b and its mechanical admittance at the acoustic frequency, $Y_{\Delta\omega}$; and (iv) the transfer function of the medium at the acoustic frequency, $H_{\Delta\omega}(l)$. The above equation illustrates the basic nonlinear relationship between the ultrasound and acoustic emission pressure amplitudes. Note that neither the medium nor the object needs to be nonlinear for this relationship to hold. It is interesting to note that the projection area S and the vibrating area πb^2 play different roles. The projection area determines the extent of the force applied to the object (Eq. 4). The vibrating area, however, influences the total acoustic outflow in the medium caused by object vibration. The mechanism of object vibration is somewhat analogous to that of a loudspeaker, where the electromotive force is exerted at a small area of the membrane (usually at the center), causing the entire membrane surface to vibrate. In our method, the size of the vibrating area depends on the object structure. For a free suspended point object, smaller than the beam cross-section, the vibrating area would be the same as the projected area. For a large stiff plate, however, the vibrating area could be much larger than the projected area (similar to a loudspeaker). In some cases, it is more convenient to write the acoustic emission field in terms of the applied force $F_{\Delta\omega}$. Referring to Eq. 4, we can rewrite Eq. 15 as

$$P_{\Delta\omega} = 4\rho c^2 H_{\Delta\omega}(l) Q_{\Delta\omega} F_{\Delta\omega}. \quad [16]$$

Again in analogy to a loudspeaker, $F_{\Delta\omega}$, $Q_{\Delta\omega}$, and $H_{\Delta\omega}(l)$ represent the electromotive force, dynamic characteristics of the membrane, and propagation medium transfer function.

Beam Forming. To probe an object with the dynamic radiation force at high spatial resolution, it is ideal to confine the dynamic stress field to a very small region in three-dimensional space. We may define the resolution cell of the system as the volume within which the amplitude of the modulated field is high enough to produce a stress field on a target. The purpose of beam forming is to produce a resolution cell as small as possible. An amplitude modulated single-focused beam can provide a resolution cell that is small in diameter but long in depth direction. A superior strategy that can achieve a small resolution cell in all dimensions is to use two unmodulated focused beams at slightly different frequencies and allow them to cross each other at their focal regions. This is accomplished by projecting two coaxial confocal continuous-wave (CW) ultrasound beams on the object. An amplitude-modulated field is produced only at the interference region of the two unmodulated beams around their focal areas, resulting in a small resolution cell. For this purpose, elements of a two-element spherically focused annular array (consisting of a central disc with radius a_1 and an outer ring with the inner radius of a'_2 and outer radius of a_2) are excited by separate CW signals at frequencies $\omega_1 = \omega_0 - \Delta\omega/2$ and $\omega_2 = \omega_0 + \Delta\omega/2$. We assume that the beams are propagating in a lossless medium, in the $+z$ direction of a Cartesian coordinate system (x, y, z), with the joint focal point at $z = 0$. The resultant pressure field on the $z = 0$ plane may be written as

$$p(r) = P_1(r) \cos(\omega_1 t + \psi_1(r)) + P_2(r) \cos(\omega_2 t + \psi_2(r)), \quad [17]$$

where $r = \sqrt{x^2 + y^2}$ is the radial distance. The amplitude functions are (16, 18)

$$P_1(r) = \rho c U_{01} (\pi a_1^2 / \lambda_{1z_0}) \text{jinc}(ra_1 / \lambda_{1z_0}), \quad [18]$$

and

$$P_2(r) = \rho c U_{02} (\pi / \lambda_{2z_0}) [a_2^2 \text{jinc}(ra_2 / \lambda_{2z_0}) - a_2'^2 \text{jinc}(ra_2' / \lambda_{2z_0})], \quad [19]$$

where $\lambda_i = 2\pi/\omega_i$, $i = 1, 2$, is the ultrasound wavelength, U_{0i} is the particle velocity amplitude at the i -th transducer element surface, and $\text{jinc}(X) = J_1(2\pi X)/\pi X$. The phase functions,

[§]The specific acoustic admittance is $\beta_B = \rho c/Z_B$, where Z_B , the acoustic impedance of the boundary, represents the ratio between the pressure and normal fluid velocity at a point on the surface.

$\psi_i(r) = -\pi r^2/\lambda_i z_0$, for $i = 1, 2$, are conveniently set to be zero at the origin.

Now, we define a unit point target at position (x_0, y_0) on the focal plane with a drag coefficient distribution as

$$d_r(x, y) = \delta(x - x_0, y - y_0), \quad [20]$$

such that $d_r(x, y)dxdy$ is unity at (x_0, y_0) and zero elsewhere. This equation is merely used as a mathematical model because d_r is physically finite. In this case, the projected area can be considered to be $S = dxdy$. We replace $d_r S$ in Eq. 1 with $d_r(x, y)dxdy$ and follow the steps similar to those outlined in Eqs. 3 and 4 for the pressure field expressed by Eq. 17, then the complex amplitude of the normal component of the force on the unit point target can be found as

$$F_{\Delta\omega}(x_0, y_0) = \rho U_{01} U_{02} (\pi a_1^2/4\lambda_1 z_0) \text{jinc}(r_0 a_1/\lambda_1 z_0) [(\pi a_2^2/\lambda_2 z_0) \text{jinc}(r_0 a_2/\lambda_2 z_0) - (\pi a_2'^2/\lambda_2 z_0) \text{jinc}(r_0 a_2'/\lambda_2 z_0)] \exp(-jr_0^2 \Delta\omega/2cz_0), \quad [21]$$

where the arguments x_0 and y_0 are added to denote the position of the point target and $r_0 = \sqrt{x_0^2 + y_0^2}$. Eq. 21 describes the spatial distribution of the force (the stress field). This equation shows that the stress field is confined to the regions near the beam axis ($r_0 = 0$) and decays as the radial distance r_0 increases. The lateral extent of the stress field, and hence the resolution cell diameter, would be smaller at higher ultrasound frequencies (smaller λ_1 and λ_2). One can calculate the total force on an arbitrary object by integrating the force over the projected area. The axial extent of the resolution cell (depth resolution or the depth of field) can be determined by calculating the force $F_{\Delta\omega}$ as a function of the depth variable, in a fashion as outlined in Eqs. 17 to 21. For conciseness, we will present only the measured values for the depth resolution in Results.

Loss in the propagation path would attenuate both ultrasound beams, thus less radiation force would be generated by the remaining ultrasound energy. In the case of soft tissues, the force attenuation factor is $A(z_0) = \exp[\alpha z_0(\omega_1 + \omega_2)]$, where α is the attenuation coefficient of the tissue. Energy loss in the medium would also result in generation of a separate radiation stress on the medium along the ultrasound paths. However, because the two beams propagate along separate paths in the CW form, they exert mainly steady radiation stresses to the medium, which does not cause object or medium vibrations. Dynamic radiation force is produced only in the interference region around the focal area, which is another advantage of using two unmodulated beams over a modulated single beam.

Image Formation. To produce an image, we scan the object in a plane and record the complex amplitude of the acoustic emission, $P_{\Delta\omega}$, at different positions. In this process, we keep $\Delta\omega$ fixed. For transverse view images, the scan plane is the focal plane ($x-y$). Alternatively, for the parallel view the scan plane is the $x-z$ plane. In the conventional ultrasound imaging context, these two views are called the C-scan and B-scan, respectively. Our main focus here is the transverse view imaging. In this case, the acoustic emission data obtained by vibrating the object at point (x, y) are assigned to the corresponding point (x, y) in the image.

Before defining the image, we need to define the function that represents the object. Referring to Eq. 15, the terms that are object dependent are the drag coefficient d_r and the function $Q_{\Delta\omega}$ (assuming that $H_{\Delta\omega}(l)$ is object independent). The object function $g(x, y)$ is thus defined as the spatial distribution of these terms,

$$g(x, y) = Q_{\Delta\omega}(x, y)d_r(x, y). \quad [22]$$

Variables x and y are added to denote the dependency of d_r and $Q_{\Delta\omega}$ on position. In particular, $Q_{\Delta\omega}(x, y)$ implies the total

acoustic outflow by the object when unit force is applied at point (x, y) .

Commonly, an imaging system is studied through its point-spread function (PSF), which is defined as the image of a point object. To determine the PSF of our system, we consider a unit point target at the origin with unit mechanical response, $Q_{\Delta\omega}(x, y) = 1$. Hence, referring to Eqs. 20 and 22, we can write $g(x, y) = \delta(x, y)$. To obtain the PSF, we move this point object to every possible position (x_0, y_0) on the $z = 0$ plane and form the image using the resulting acoustic emission field, $P_{\Delta\omega}(x_0, y_0)$. Because x_0 and y_0 are now being treated as variables, we may replace them by variables x and y , respectively. We define the normalized PSF of the coherent imaging system as the complex function

$$h(x, y) = P_{\Delta\omega}(x, y)/P_{\Delta\omega}(0, 0). \quad [23]$$

Division by $P_{\Delta\omega}(0, 0)$ cancels the constant multipliers. Referring to Eqs. 16 and 21, we can write

$$h(x, y) = (a_2^2 - a_2'^2)^{-1} \text{jinc}(ra_1/\lambda_1 z_0) [a_2^2 \text{jinc}(ra_2/\lambda_2 z_0) - a_2'^2 \text{jinc}(ra_2'/\lambda_2 z_0)] \exp(-jr^2 \Delta\omega/2cz_0). \quad [24]$$

This equation illustrates that the system PSF is a circularly symmetric function with the peak at the origin and decaying amplitude with increasing the radial distance r . Amplitude decays faster for higher ultrasound frequency. This function will be discussed further in the next section.

EXPERIMENTS

The experimental setup is shown in Fig. 2. The confocal transducer is constructed by using a spherical piezoelectric cap. The two elements are constructed by dividing the back electrode of the piezoelectric wafer into a central disc and the outer ring, such that the elements have identical beam axes and focal lengths. Radii of the elements are $a_1 = 14.8$ mm, $a_2 = 22.5$ mm, and $a_2' = 16.8$ mm, and the focal distance is 70 mm. Transducer elements were driven by two stable radio frequency synthesizers [Hewlett-Packard 33120A and Analogic 2045 (Peabody, MA)] at frequencies of $f_0 - \Delta f/2$ and $f_0 + \Delta f/2$, where $f_0 = 3$ MHz, and the value of $\Delta f = \Delta\omega/2\pi$ is stated separately for each experiment. The object was placed at the focal plane of the ultrasound beams in a water tank. Sound produced by the object vibration was detected by an audio hydrophone (International Transducer, Santa Barbara, CA, model 680, sensitivity -154 dB re $1\text{V}/\mu\text{Pa}$) placed within the water tank. The received signal was filtered and amplified by a programmable filter (Stanford Research Sunnyvale, CA, SR650) to reject noise, then digitized by a 12 bits/sample digitizer (Hewlett-Packard E1429A) at a rate sufficiently higher than the Nyquist rate for the particular Δf used. Data were recorded on a computer disc. For coherent imaging, which requires the phase information, the reference signal (i.e., $\cos \Delta\omega t$) was obtained by electronic downmixing of the

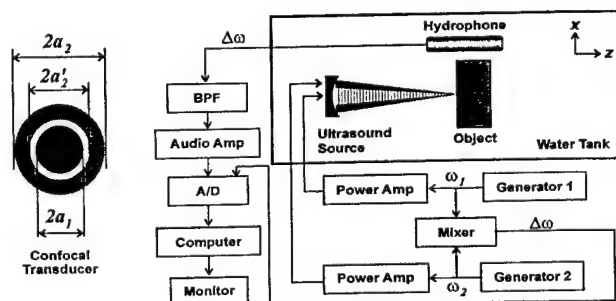


FIG. 2. Ultrasound-stimulated vibro-acoustography system. The confocal ultrasound annular array transducer with two elements is shown on the left.

two driving signals and was recorded along with the hydrophone signal. The relative phase of the acoustic emission data was then calculated at each point by discrete Hilbert transform. We conducted two experiments. The first experiment is designed to verify the relationship between the acoustic emission pressure and the ultrasound pressure (Eq. 15), and the second is designed to experimentally measure the PSF stated in Eq. 24. These experiments are presented to prove the principles of the method. Further experiments, illustrating applications of the method for evaluation of object mechanical properties and tissue imaging, are presented in ref. 12.

RESULTS

Acoustic Emission vs. Ultrasound Pressure. Eq. 15 states that the acoustic emission field amplitude is linearly proportional to the square of the incident ultrasound pressure, or equivalently, to the incident power. To test this hypothesis, a calibrated 1-mm-diameter ultrasound needle hydrophone, with its tip facing the ultrasound beam, was used to measure the ultrasound field at the focal point. The tip of the hydrophone also served as an object to generate the acoustic emission. Here, Δf was set at 40 kHz, and the radial distance from the tip of the needle hydrophone to the audio hydrophone was about 65 mm. The result is shown in Fig. 3. The slope of the acoustic emission intensity vs. ultrasonic intensity indicates that the intensity of the acoustic emission field is proportional to the square of the ultrasound intensity, or equivalently, the acoustic emission pressure amplitude is linearly proportional to the ultrasound power, as predicted by Eq. 15. In another experiment, a 450- μ m-diameter glass bead was used as a point object. In this case, Δf was set at either 7 or 40 kHz. The radial distance from the glass bead to the audio hydrophone was about 50 mm. Again, the data indicate a quadratic relationship between the acoustic emission and ultrasonic intensities. These glass-bead data also show that increasing the frequency increases the acoustic intensity. This can be better understood by investigating the theoretical model presented in Eq. 13. If we assume that the mechanical admittance of the object is approximately constant at these frequencies, then the object behaves almost as a point source, and the acoustic pressure amplitude is proportional to $\Delta\omega$. Hence the acoustic emission intensities $I_{\Delta\omega_1}$ and $I_{\Delta\omega_2}$ at frequencies $\Delta\omega_1$ and $\Delta\omega_2$, respectively, are related by $I_{\Delta\omega_2}/I_{\Delta\omega_1} = (\Delta\omega_2/\Delta\omega_1)^2$. Now, letting $\Delta\omega_1$ and $\Delta\omega_2$ correspond to 7 and 40 kHz, respectively, we can write the intensity ratio as: $[I_{\Delta\omega_2}/I_{\Delta\omega_1}]_{dB} = 20 \log (\Delta\omega_2/\Delta\omega_1) = 15$ dB. The mean value of the intensity ratio calculated from the glass-bead data at 7 and 40 kHz is 16 dB, which is in close agreement with the theoretical result.

PSF Measurement. To demonstrate the image-formation process and support the theoretical derivation of the PSF (Eq. 24), we evaluated this function experimentally. For this purpose, we used a 380- μ m diameter glass bead as a model for a point and placed it on a thin latex sheet. The latex sheet produces only a small change in the incident energy, and hence does not produce significant radiation force or acoustic emission. The entire object was placed in a water tank and the latex

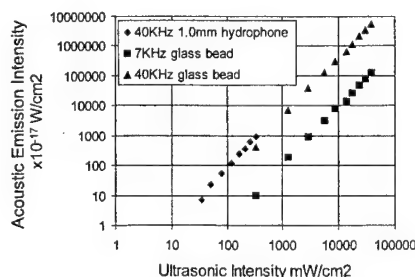


FIG. 3. Acoustic-emission field intensity vs. the combined ultrasound intensity.

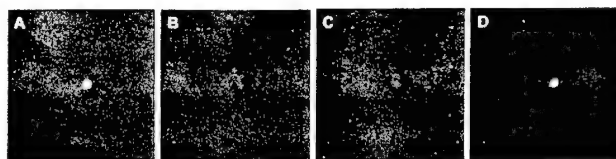


FIG. 4. USVA images of a 380- μ m glass bead: (A) in-phase, (B) quadrature, (C) phase, and (D) magnitude. The phase in C ranges from $-\pi$ radians (black regions) to $+\pi$ radians (white regions), and was normalized to be zero at the center of the glass bead. (Modified with permission from ref. 12, copyright 1998, American Association for the Advancement of Science.)

sheet surface was scanned in a raster format at 0.2-mm increments in either direction at $\Delta f = 7.3$ kHz. The amplitude and phase of the acoustic emission signal were calculated at each point relative to the reference signal data. The phase was normalized to the phase value at the center of the bead. The resulting in-phase, quadrature, phase, and magnitude images are shown in Fig. 4A–D. Transverse image resolution, defined as the -6 -dB width of the bead image, is approximately 700 μ m for the in-phase image in either dimension (refer to Fig. 5). To compare the experimental results with those of the theory, we calculated the profile of the PSF for the transducer parameters used in this experiment according to Eq. 24. Fig. 5 shows the theoretical PSF profile and the glass-bead profile obtained from the experiment (in-phase image profile, shifted to center at zero). This figure shows excellent agreement between theory and experiment for amplitudes above 20% of the peak. The experimental data show some background offset about 12% of the peak. We believe that this background offset is caused at least by the following sources: (i) acoustic emission by the latex sheet; (ii) the background acoustic noise in the experimental setup caused by equipment fans and some structural and building vibrations; (iii) nonlinearity of water that can produce a nonlinear mix of the two beams even in the absence of the object; and (iv) streaming as a result of energy absorption by water (14), which in turn can vibrate the latex sheet blocking the stream. To evaluate the depth resolution (or the slice thickness), we placed the glass bead on the beam axis and scanned it in the z-direction about the focal point. The depth resolution, defined as the distance between the points where the amplitude of the acoustic emission field drops to -6 dB of its peak, was 9 mm.

DISCUSSION

System Properties. Spectral characteristics. In general, USVA images represent object characteristics at two ends of the spectrum: the drag coefficient at the ultrasound frequency and the mechanical admittance at the low acoustic frequency Δf . The ultrasound frequency is usually set at a value suitable to form the beam, whereas Δf can vary in a wide range depending on the application. If the two beams are produced by similar ultrasound transducer elements, then the practical

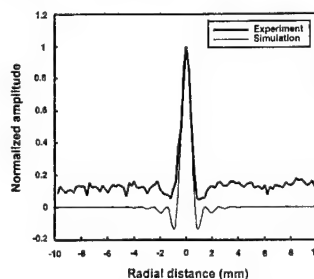


FIG. 5. The theoretical PSF profile of the USVA system according to Eq. 24 and the glass-bead in-phase image profile (Fig. 4A) obtained from the experiment.

upper limit for Δf is about equal to the transducer bandwidth. The lower limit of Δf is zero.

Sensitivity. System sensitivity in detecting very small displacements is an important practical issue, especially when the allowable ultrasound power is limited (for example, in medical imaging). Motion measurement with ultrasound pulse echo has been used previously to study "stiffness" of tissues (10). However, the sensitivity of ultrasound pulse echo to motion, at common medical ultrasound frequencies, is limited to several micrometers. An advantage of USVA is its high displacement sensitivity. Cyclic displacement of 100 nm at 10 kHz produces an acoustic intensity of about 3.0×10^{-3} watts/cm². Hydrophones similar to the one used in these experiments are sensitive to as little as 10^{-15} watts/cm² and therefore are capable of detecting very small cyclic displacements. For instance, the hydrophone detected an acoustic pressure of about 15×10^{-3} Pa at a distance of 5 cm from the glass bead shown in Fig. 4. Under assumptions of isotropic vibration, this pressure would be produced by a similar-sized sphere vibrating with a displacement amplitude of about 6 nm. Sensitivity increases at higher frequencies because the acoustic emission pressure is proportional to frequency for constant mechanical admittance (Eq. 13).

Comparisons with pulse-echo systems. Some contrasting features of USVA with respect to the conventional ultrasound pulse-echo imaging (B-mode and C-mode) are: (i) A pulse-echo image represents object microstructure by displaying its ultrasonic reflectivity distribution. The acoustic emission signal in a USVA system is proportional to the drag coefficient $d_r(x, y)$, which is a local ultrasound parameter, and to the function $Q_{\Delta\omega}(x, y)$, which represents the bulk response of the object at acoustic frequency $\Delta\omega$. Hence, a USVA image, in general, represents both the microstructure and macrostructure of the object. (ii) The echo signal in a pulse-echo system is a linear function of the incident ultrasound pressure amplitude and the amplitude reflection coefficient of the object. In USVA, however, the acoustic emission signal is proportional to the ultrasound power and the power reflection coefficient of the object. (iii) Pulse-echo systems are not directly sensitive to medium absorption. Absorption is indicated as relative changes in the amplitude of the echoes resulting from the scatterers within the medium. In a USVA system, the acoustic emission can be produced directly as a result of energy absorption by the medium, even if the medium is homogeneous (refer to Eq. 2). (iv) Pulse-echo systems are generally broadband. The USVA method presented here is basically a narrowband technique. (v) Pulse-echo systems achieve high depth resolution by transmitting short wideband pulses. A USVA system gains its depth resolution by tailoring beam geometry to limit the depth of the region where the two beams interfere. A USVA system does not require a wide bandwidth signal to achieve a high depth resolution. (vi) The data of USVA images are acquired one point at a time, which resembles the data acquisition in C-mode pulse-echo systems. B-mode pulse-echo systems, however, require much less acquisition time because the data are collected one line at a time.

Applications. USVA promises applications in two general areas: medical imaging and material evaluation.

Medical applications. USVA can be used to image tissues and evaluate their mechanical characteristics. To use USVA for *in vivo* applications, one must take into account limitations such as safe (ultrasound) power limit, tissue attenuation, body noise, and phase aberration. The ultrasound power required to generate a detectable acoustic emission depends on the object, acoustic noise, and receiver sensitivity. Experimental results shown in Fig. 3 demonstrate that ultrasound intensities as low as 30 mW/cm² are sufficient to detect the acoustic emission from a 1-mm-diameter object with our hydrophone in the water tank. This power value is much smaller than the FDA limit for safe diagnostic ultrasound applications. Tissue attenuation reduces the ultrasound intensity at the target, and hence the acoustic

emission [by the factor $A(z_0)$]. Attenuation limits the usable ultrasound frequency, and hence, lowers the resolution. It also limits the signal-to-noise-ratio (SNR) because of the loss in the acoustic emission energy as a result of ultrasound attenuation by tissue. Direct effect of tissue attenuation on the acoustic emission signal is probably negligible because attenuation of the compressional waves at frequencies in the order of a few kHz in soft tissues is low. Sources of biological noise of the human body include cardiovascular and respiratory systems and muscle movements. Body noise is usually concentrated below 1 kHz and can be filtered out if Δf is above this value. The SNR can be improved by increasing the time duration of the signal recorded at each point (to increase the signal energy) and by using very narrow-band filters (to reject the noise), while keeping the ultrasound power within the safe level. Phase aberration in tissue can reduce the sensitivity of the system by decreasing the effective ultrasound energy density at the beam interaction region. One may use known phase aberration correcting methods to reduce such an effect. The practical value of these methods for USVA remains to be studied.

Material evaluation. Another field in which USVA can be potentially useful is material characterization, including mechanical parameter evaluation, imaging, and nondestructive testing of materials. USVA can be used for detection and imaging flaws in materials. Also, one may use USVA to evaluate the mechanical frequency response of an object at low frequencies. In such case, we are interested in determining $Q_{\Delta\omega}(x, y)$ vs. frequency. We assume that the object is uniform within the projected area S . Then, the total radiation force on this object, $F_{\Delta\omega}$, can be calculated by integrating $F_{\Delta\omega}(x, y)$ over S . Referring to Eq. 21, one can show that for $\Delta\omega \ll \omega_0$, $F_{\Delta\omega}$ is virtually independent of $\Delta\omega$. If $H_{\Delta\omega}(l)$ is known and nonzero, then the function $Q_{\Delta\omega}(x, y)$ can be estimated using Eq. 16 as $Q_{\Delta\omega}(x, y) = P_{\Delta\omega}(x, y)/F_{\Delta\omega}H_{\Delta\omega}(l)$. In practice, $P_{\Delta\omega}(x, y)$ is obtained by sweeping $\Delta\omega$ in the range of interest and recording the resulting acoustic emission (12).

This work was supported in part by grant DAMD17-98-1-8121 from the Army Medical Research and Materiel Command. The authors thank R. R. Kinnick, T. Kinter, E. C. Quarve, and J. M. Patterson for their support.

1. Maynard, J. (1996) *Phys. Today* **49**(1), 26–31.
2. O'Donnell, M., Skovoroda, A. R., Shapo, B. M. & Emelianov, S. Y. (1994) *IEEE Trans. Ultrason. Ferroelectr. Freq. Contr.* **41**, 314–325.
3. Ophir, J., Cespedes, I., Ponnankanti, H., Yazdi, Y. & Li, X. (1991) *Ultrason. Imaging* **13**, 111–134.
4. Yamakoshi, Y., Sato, J. & Sato, T. (1990) *IEEE Trans. Ultrason. Ferroelectr. Freq. Contr.* **47**, 45–53.
5. Krouskop, T. A., Dougherty, D. R. & Vinson, F. S. (1987) *J. Rehabil. Res. Dev.* **24**, 1–8.
6. Lerner, R. M., Huang, S. R. & Parker, K. J. (1990) *Ultrasound Med. Biol.* **16**, 231–239.
7. Alam, S. K., Richards, D. W. & Parker, K. J. (1994) *Ultrasound Med. Biol.* **20**, 751–758.
8. Gao, L., Parker, K. J., Lerner, R. M. & Levinson, S. F. (1996) *Ultrasound Med. Biol.* **22**(8), 959–977.
9. Muthupillai, R., Lomas, D. J., Rossman, P. J., Greenleaf, J. F., Manduca, A. & Ehman, R. L. (1995) *Science* **269**, 1854–1857.
10. Sugimoto, T., Ueha, S. & Itoh, K. (1990) *Ultrason. Symp. Proc.*, 1377–1380.
11. Sarvazyan, A. P., Rudenko, O. V., Swanson, S. D., Fowlkes, J. B. & Emelianov, S. Y. (1998) *Ultrasound Med. Biol.* **24**, 1419–1435.
12. Fatemi, M. & Greenleaf, J. F. (1998) *Science* **280**, 82–85.
13. Beyer, R. T. (1978) *J. Acoust. Soc. Am.* **63**(4), 1025–1030.
14. Westervelt, P. J. (1951) *J. Acoust. Soc. Am.* **23**(4), 312–315.
15. Greenspan, M., Breckenridge, F. R. & Tschiegg, C. E. (1978) *J. Acoust. Soc. Am.* **63**(4), 1031–1038.
16. Morse, P. M. & Ingard, K. U. (1968) *Theoretical Acoustics* (McGraw-Hill, New York).
17. Morse, P. M. (1981) *Vibration and Sound* (The Acoustical Society of America, Woodbury, NY), 3rd Ed.
18. Kino, G. S. (1987) *Acoustics Waves: Devices, Imaging, and Analog Signal Processing* (Prentice-Hall Signal Processing Series, Englewood Cliffs, NJ).

Probing the Dynamics of Tissue at Low Frequencies with the Radiation Force of Ultrasound

Mostafa Fatemi¹ and James F. Greenleaf²

Department of Physiology and Biophysics, Mayo Clinic
and Mayo Foundation, Rochester, MN 55905 U.S.A.

Short title: Probing the Dynamics of Tissue with Radiation Force

Classification numbers: 43.25 Qp, 43.30 Jx, 43.35 Yb, 43.35 Zc, 43.40 Rj, 43.40 Yq, 43.80 Jz, 43.80 Qf, 87.63 Df

Abstract: In the past few years there has been an increasing interest in using the radiation force of ultrasound for evaluating, characterizing, and imaging biological tissues. Of particular interest are those methods that measure the dynamic properties of tissue at low frequencies. In this paper we present dynamic radiation force methods for probing tissue as a new field and discuss the inter-relationship of several methods within this field and comparing their features. The techniques in this field can be categorized in three groups: transient methods, shear wave measurement methods, and a recently developed method called vibro-acoustography. The last method is the focus of this paper. After briefly describing the key concepts of the first two methods, we will present a detailed description of vibro-acoustography. Finally, we will compare capabilities and limitations of these methods.

1. Introduction

It is well known that changes in elasticity of soft tissues are often related to pathology. Traditionally, physicians use palpation as a simple method for estimating mechanical properties of tissue. In this method, a static force is applied and a crude estimation of tissue elasticity is obtained through the sense of touch. In palpation, the force is applied on the body surface and the result is a collective response of all the tissues below. Clinicians can sense abnormalities if the response to palpation of the suspicious tissue is sufficiently different from that of normal tissue. However, if the abnormality lies deep in the body, or if it is too small to be resolved by touch, then the palpation method fails. The dynamic response of soft tissue to a force is also valuable in medical diagnosis. For instance, rebound of tissue upon sudden release of pressure exerted by the physician's finger on the skin provides useful diagnostic information about the tissue.

Quantitative measurement of the mechanical properties of tissues and their display in a raster format is the aim of a class of techniques generally called elasticity imaging or elastography. The general approach is to measure tissue motion caused by an external (or, in some methods, internal) force or displacement and use it to reconstruct the elastic parameters of the tissue. The excitation stress can be either static or dynamic (vibration). Dynamic excitation is of particular

¹ E-mail: fatemi.mostafa@mayo.edu

² E-mail: jfg@mayo.edu

interest because it provides more comprehensive information about tissue properties in a spectrum of frequencies, or alternatively, the transient behavior of the tissue could be deduced from the measurements. In most elasticity imaging methods, ultrasound is used to detect the motion or displacement resulting from the applied stress. Magnetic resonance elastography is a recently developed method (Muthupillai *et al* 1995) that employs a mechanical actuator to vibrate the body surface and then measures the strain waves with phase sensitive Magnetic Resonance Imaging (MRI) machine.

The majority of elasticity imaging methods are based on an external source of force. In these methods the object is pressed by a known amount of force or displacement, and the resulting internal deformations are measured by means of pulse-echo ultrasound. Elasticity of the region of interest is then calculated based on the resulting deformation in relation to the magnitude of applied force (or displacement). Normally, the region of interest rests deep in the body and away from the source of the force. The force that is actually exerted on the region of interest depends on the elastic properties of the tissues located between the source and the region of interest. Hence, the deformation, and the estimated elasticity of the region of interest, are subject to variables of the intervening tissues.

An alternative strategy is to apply a localized stress directly in the region of interest. One way to accomplish this is to use the radiation pressure of ultrasound. Acoustic radiation force is the time average force exerted by an acoustic field on an object. This force is produced by a change in the energy density of an incident acoustic field (Chu and Apfel 1982), for example, due to absorption or reflection. Several benefits may result from using ultrasound radiation force for evaluating tissue properties, including: (a) acoustic (ultrasound) energy is a noninvasive means of exerting force, (b) existing ultrasound technology and devices can be readily modified for this purpose, thus eliminating the need for developing a new technology, (c) radiation force can be generated remotely inside tissue without disturbing its superficial layers, (d) the radiation stress field can be highly localized, thus allowing for precise positioning of the excitation point, and (e) radiation force can be produced in a wide range of frequencies or temporal shapes. These features make radiation force methods more attractive than other, mostly mechanical, excitation methods used in elasticity imaging.

Tissue probing with the radiation force of ultrasound can be accomplished by a variety of techniques, depending on the excitation and detection methods used. As in elasticity imaging methods with mechanical excitation, the radiation force methods can use either a static or dynamic stress.

It is the opinion of the authors that using the dynamic radiation force to remotely probe tissue has certain unique characteristics and capabilities that can open a new chapter in the field of tissue characterization and imaging. We believe that the techniques based on this phenomenon have the potential to provide a new set of information about tissue that has never been available from other methods. We also believe that it is important to recognize and treat this set of techniques as a new field. Especially, it is insightful to set this new field apart from the conventional ultrasound tissue characterization/imaging field. A major difference being the fact that using the dynamic radiation stress allows one to analyze the object based on its structural vibration properties as opposed to its ultrasonic parameters.

Our intention in writing this paper is to present the dynamic radiation force methods for probing tissue as a new field by discussing the inter-relationship of several methods within this field and compare their features. To the best of our knowledge, such a discussion has not been presented before in the literature.

The dynamic radiation force methods may be categorized as: (a) transient methods, where an impulsive radiation force is used and the transient response of the tissue is detected by Doppler ultrasound (Sugimoto *et al* 1990); (b) shear-wave methods, where an impulsive or oscillating radiation is applied to the tissue and the resulting shear wave is detected by ultrasound or other methods (Andreev *et al* 1997; Sarvazyan *et al* 1998; Walker 1999); (c) vibro-acoustography, a method recently developed by the authors, where a localized oscillating radiation force is applied to the tissue and the acoustic response of the tissue is detected by a hydrophone or microphone.

In this paper we systematically discuss the features and capabilities that are offered by the dynamic radiation force techniques. Here, we describe the general approach used in the transient, shear wave, and vibro-acoustography methods. We pay particular attention to the last method, present its theory, and discuss its features. Then, we compare the capabilities and limitations of all three methods and discuss their possible applications.

2. Radiation force methods

The acoustic radiation force is a time average force exerted by an acoustic field on an object. This force is an example of a universal phenomenon in any wave motion that introduces some type of unidirectional force on absorbing or reflecting targets in the wave path. For a review of this topic the reader may refer to (Chu and Apfel 1982).

Consider a plane ultrasound beam interacting with a planar object of zero thickness and arbitrary shape and boundary impedance that scatters and absorbs. The radiation force vector, \mathbf{F} , arising from this interaction has a component in the beam direction and another transverse to it. The magnitude of this force, is proportional to the average energy density of the incident wave $\langle E \rangle$ at the object, where $\langle \rangle$ represents the time average, and S , the area of the projected portion of the object (Westervelt 1951):

$$\mathbf{F} = \mathbf{d}_r S \langle E \rangle, \quad (1)$$

where \mathbf{d}_r is the vector drag coefficient with a component in the incident beam direction and another transverse to it. The coefficient \mathbf{d}_r is defined per unit incident energy density and unit projected area. For a planar object, \mathbf{d}_r is numerically equal to the force on the unit area of the object per unit energy density. Physically, the drag coefficient represents the scattering and absorbing properties of the object and is given by (Westervelt 1951)

$$\mathbf{d}_r = \hat{\mathbf{p}} \frac{1}{S} \left(\Pi_a + \Pi_s - \int \gamma \cos \alpha_s dS \right) + \hat{\mathbf{q}} \frac{1}{S} \int \gamma \sin \alpha_s dS, \quad (2)$$

where $\hat{\mathbf{p}}$ and $\hat{\mathbf{q}}$ are the unit vectors in the beam direction and normal to it, respectively. The quantities Π_a and Π_s are the total absorbed and scattered powers, respectively, and γ is the scattered intensity, all expressed per unit incident intensity. Also, α_s is the angle between the incident and the scattered intensity, and dS is the scalar area element. The drag coefficient

can also be interpreted as the ratio of the radiation force magnitude on a given object to the corresponding value if the object were replaced by a totally absorbing object of similar size. For simplicity, we assume a planar object oriented perpendicular to the beam axis. In this case, the transverse component vanishes, thus, the drag coefficient (force) will have only a component normal to the target surface which we denote by scalar $d_r(F)$.

To produce a time varying radiation force, the intensity of the incident beam can be shaped in various ways. For example, a short ultrasound pulse can produce a transient pulsed radiation force, and a sinusoidally modulated beam can result in a sinusoidally varying force.

2.1. Transient methods

In the transient methods the radiation force of ultrasound is used to make a minute deformation in the tissue. The transient recoil of the tissue resulting from this deformation is measured and used for evaluation of tissue elastic properties.

A method for measuring tissue hardness, presented by Sugimoto *et al* (1990), uses the radiation force of a single focused ultrasound beam. Ideally, hardness may be represented by the spring constant of the object, which is the ratio of the applied force to the displacement. Because it is difficult to measure the absolute values of force or deformation *in vivo*, this method relies on evaluating the hardness based on changes in relative values. In this method an ultrasound pulse is used to generate a short duration radiation force which produces localized deformation of the tissue. Immediately after the force pulse, the resulting transient deformation of tissue is measured as a function of time with Doppler ultrasound using a separate transducer. The deformation includes an initial rapid squeeze of the tissue, followed by a relaxation and possibly a rebound. This function is a function of tissue viscoelastic parameters, as well as the applied force. Sugimoto *et al* (1990) argue that because measuring the internal radiation force in an absolute sense is difficult, it is advantageous to derive a relative quantity that is representative of tissue hardness. To derive a single relative quantity from the deformation data, the relaxation part of the function is approximated by a sum of several exponential curves, and the sum of the first order derivatives of such exponential is calculated. It is shown that this quantity is correlated to the spring constant of the tissue, thus may be used as a measure of tissue hardness.

2.2. Shear wave methods

Shear modulus is related to the hardness or elasticity of the material. It is known that the shear modulus of various soft tissues range over several orders of magnitude, while bulk modulus, a parameter that is associated with the conventional pulse-echo ultrasound compressional wave speed, varies significantly less than an order of magnitude (Goss *et al* 1978; Frizzell and Carstensen 1976). These features indicate that shear modulus may be a better parameter for tissue characterization than bulk modulus. One way to induce localized shear waves inside tissue is to use the radiation force of focused ultrasound (Andreev *et al* 1997). In a method called shear wave elasticity imaging (SWEI) (Sarvazyan *et al* 1998), an amplitude modulated single focused ultrasound beam is used to induce a localized radiation stress inside the soft tissue. Localization of the stress field is the key in success of the method. To achieve a high degree of localization, the method uses a focused ultrasound beam. It is shown that the radiation stress exerted within a dissipative medium peaks near the focal region of highly focused transducer.

It has also been suggested that localization can be improved by designing the transducer and selecting the beam parameters such that a nonlinear shock wave is produced in the focal region, increasing the magnitude of the stress field in the vicinity of the focal region, thus augmenting localization of the stress field (Sarvazyan *et al* 1998).

Modulation of the ultrasound beam can be in the form of an oscillating wave or short pulse. The resulting radiation force elicits a shear wave propagating in the radial direction with respect to the beam axis, with particle motion parallel to the beam axis. Shear waves in soft tissue travel at very low speed, typically around a few meters per second (Frizzell and Carstensen 1976; Sarvazyan *et al* 1998), thus the corresponding wavelength is much shorter than that of the compressional waves for the same frequency. Shear waves are also highly attenuated in soft tissue, with an attenuation coefficient two or three orders of magnitude higher than that of the compressional waves (Frizzell and Carstensen 1976; Sarvazyan *et al* 1998). Because of high attenuation of shear waves, it is possible to induce them in a very limited region in the vicinity of the focal point of the ultrasound beam, hence avoiding the influence of tissue boundaries. In SWEI, a short ultrasound pulse is delivered to the tissue causing a radial shear oscillation around the beam axis. By measuring the amplitude and the temporal characteristics of this wave, shear parameters of the tissue, such as shear modulus and shear viscosity can be calculated. For example, the time required for the wave front to propagate from one point to another can be used to calculate the shear wave speed, and consequently, the shear wave modulus μ , as

$$\mu = \rho c_t^2 \quad (3)$$

where ρ and c_t are the density and the shear wave velocity, respectively.

Shear waves may be detected optically. In this method a laser source and a photo detector are used to detect the displacement of particles due to the shear wave in a transparent phantom (Sarvazyan *et al* 1998). Because this method requires a transparent medium, its application *in vivo* is difficult. Phase sensitive magnetic resonance imaging (Muthupillai *et al* 1995; Sarvazyan *et al* 1998) is an alternative method that can be used to measure the two-dimensional distribution of particle displacement in a given direction versus time in a material. In an experiment presented in (Sarvazyan *et al* 1998), an ultrasound pulse of 3.6 ms duration produced by a 70 mm diameter transducer focused at 100 mm was transmitted within a cylindrical rubber phantom. The displacement was measured by 2.0 T MRI system at two different times after the acoustic pulse was applied. The position of the peak displacement at these time points was used to estimate the shear velocity, which was shown to be consistent with the independently measured value. Shear waves can also be detected by Doppler ultrasound (Andreev *et al* 1997). It has been shown (Walker 1999) that to achieve an appreciable displacement needed for Doppler detection, most soft tissues require high ultrasound intensities which might be beyond the recommended maximum intensity level for diagnostic ultrasound (FDA report, see reference 9).

2.3. Vibro-acoustography

2.3.1. Method

This technique produces a map of the mechanical response of an object to a dynamic force applied at each point. The method utilizes ultrasound radiation force to remotely exert a localized

oscillating stress field at a desired frequency within (or on the surface of) an object and records the resultant acoustic response (Fatemi and Greenleaf 1998; Fatemi and Greenleaf 1999). This acoustic response, which is normally at low kHz range, is a function of the viscoelastic properties of the object and can be used to produce an image of the object.

To produce an oscillating radiation force the intensity of the incident ultrasound must be amplitude modulated at the desired low frequency. Using a single amplitude modulated beam seems to be the simplest means to attain this purpose. However, such a beam will exert a radiation force on any object that is present along the beam path, producing undesirable acoustic emission. To confine the oscillating radiation stress to the desired region, vibro-acoustography uses two unmodulated CW beams at slightly different frequency, propagating along separate paths. The beams are arranged to cross each other at their respective foci, and thus produce a modulated field at a confined, small, cross-sectional region. The single and double beam arrangements are illustrated in Fig. 1.

2.3.2. System diagram and image formation

Figure 2 illustrates a vibro-acoustography system. The elements of the annular array transducer are driven by two CW signals at frequencies $f_1 = \omega_1/2\pi$ and $f_1 + \Delta f = (\omega_1 + \Delta\omega)/2\pi$. The object to be imaged is placed at the joint focal plane of the transducer elements (the scanning plane). The ultrasound field produces a localized radiation stress field at the focal point on the object at frequency Δf . Depending on the elastic properties of the object, the radiation force may cause a portion of the object, or the entire object, to vibrate at this frequency. The acoustic emission resulting from object vibration is received by a hydrophone which is located nearby. Normally the wavelength of vibration is large compare to the object size, hence the acoustic emission field is almost omnidirectional. Therefore, hydrophone position is not a critical parameter in this measurement. The filter is used to eliminate noise and other interfering signals. To form an image the focal point of the transducer is moved across the scanning plane on the object in a raster pattern. The acoustic emission is received at each position, and an image is formed by displaying the amplitude (or phase) of such signals at corresponding positions on the image plane. The spatial resolution of this imaging method is determined by the ultrasound beamwidth at the focal plane, which is normally in the order of the incident ultrasound wavelength.

2.3.3. Theory

In the beam forming method to be described the amplitude modulated field is obtained by the interference of two unmodulated ultrasound beams. Radially symmetric interfering beams are obtained when two coaxial, confocal transducers are used (Fatemi and Greenleaf 1999). For this purpose, elements of a two-element spherically focused annular array (consisting of a central disc with radius a_1 and an outer ring with the inner radius of a'_2 and outer radius of a_2) are excited by separate CW signals at frequencies $\omega_1 = \omega_0 - \Delta\omega/2$ and $\omega_2 = \omega_0 + \Delta\omega/2$. We assume that the beams are propagating in the $+z$ direction with the joint focal point at $z = 0$. The resultant field on the $z = 0$ plane may be written as:

$$p(t) = P_1(r) \cos(\omega_1 t + \psi_1(r)) + P_2(r) \cos(\omega_2 t + \psi_2(r)), \quad (4)$$

where $r = \sqrt{x^2 + y^2}$ is the radial distance. The amplitude functions are (Morse and Ingard 1968; Kino 1987)

$$P_1(r) = \rho c U_{01} \frac{\pi a_1^2}{\lambda_1 z_0} \text{jinc}\left(\frac{r a_1}{\lambda_1 z_0}\right), \quad (5)$$

and

$$P_2(r) = \rho c U_{02} \frac{\pi}{\lambda_2 z_0} \left[a_2^2 \text{jinc}\left(\frac{r a_2}{\lambda_2 z_0}\right) - a_2'^2 \text{jinc}\left(\frac{r a_2'}{\lambda_2 z_0}\right) \right], \quad (6)$$

where U_{0i} is the velocity amplitude at the i -th transducer element surface, and $\lambda_i = 2\pi/\omega_i$ for $i=1,2$ are the ultrasound wavelengths. The phase functions,

$$\psi_i(r) = -\frac{\pi r^2}{\lambda_i z_0}, \quad (7)$$

for $i=1, 2$, are conveniently set to be zero at the origin. Also, $\text{jinc}(X) = J_1(2\pi X)/\pi X$, where $J_1(\cdot)$ is the first order Bessel function of the first kind.

The instantaneous energy is $E = p^2(t)/\rho c^2$. Replacing $p(t)$ from Eq. 4, this energy will have a time independent component, a component at the difference frequency $\Delta\omega = \omega_2 - \omega_1$ which results from the cross product of the two pressure fields, and high frequency components at ω_1 and ω_2 and their harmonics. The energy component at the difference frequency is:

$$e_{\Delta\omega}(t) = \frac{P_1(r_0)P_2(r_0)}{\rho c^2} \cos[\Delta\omega t + \Delta\psi(r_0)], \quad (8)$$

where $\Delta\psi(r_0) = \psi_2(r_0) - \psi_1(r_0)$.

Now, we define a *unit point target* with an area of $dxdy$ at position (x_0, y_0) on the focal plane, and with a drag coefficient $d_r(x_0, y_0)$ such that: $d_r(x_0, y_0)dxdy = 1$ on the target and zero elsewhere. This equation is merely used as a mathematical model. In this case, the projected area can be considered to be $S = dxdy$. Therefore, if the projected area is unity, then $d_r(x, y) = 1$, which according to Eq. 2 corresponds to a totally absorptive object.

Referring to Eq. 1, and replacing $d_r S$ with unity and $\langle E \rangle$ by $e_{\Delta\omega}(t)$ of Eq. 8, then we can write the low-frequency component of the radiation force on the unit point target as:

$$f_{\Delta\omega}(x_0, y_0; t) = \frac{1}{\rho c^2} P_1(r_0) P_2(r_0) \cos[\Delta\omega t + \Delta\psi(r_0)], \quad (9)$$

where arguments x_0 and y_0 are added to denote the position of the point target, and $r_0 = \sqrt{x_0^2 + y_0^2}$. Referring to Eqs. 5 and 6, the complex amplitude of the stress field can be found as

$$\begin{aligned} F_{\Delta\omega}(x_0, y_0) = & \rho U_{01} U_{02} \frac{\pi a_1^2}{\lambda_1 z_0} \text{jinc}\left(\frac{r_0 a_1}{\lambda_1 z_0}\right) \times \\ & \left[\frac{\pi a_2^2}{\lambda_2 z_0} \text{jinc}\left(\frac{r_0 a_2}{\lambda_2 z_0}\right) - \frac{\pi a_2'^2}{\lambda_2 z_0} \text{jinc}\left(\frac{r_0 a_2'}{\lambda_2 z_0}\right) \right] \times \\ & \exp\left(-j \frac{r_0^2}{2\Delta\lambda z_0}\right), \end{aligned} \quad (10)$$

where $\Delta\lambda = 2\pi c/\Delta\omega$ is the wavelength associated with $\Delta\omega$. The above equation indicates that the radiation stress is concentrated at the focal point and decays down quickly with distance as $\text{jinc}(\cdot)^2$.

As an example, we consider a confocal transducer with dimensions $a_1 = 14.8$ mm, $a'_2 = 16.8$ mm, $a_2 = 22.5$ mm, and the focal length 70 mm. Also, we assume that the center frequency is 3 MHz, and the difference frequency is 7.3 kHz. The radiation stress at the focal plane of a this transducer is plotted in Fig. 3.

In medical applications the maximum ultrasonic intensity is regulated for safety reasons. It is, therefore, useful to write the stress field in terms of the peak ultrasonic intensity at the focal point. The long-term average of ultrasonic intensity at the focal point can be written as

$$I(0) = \frac{P_1^2(0) + P_2^2(0)}{2\rho c} \quad (11)$$

where $P_1(0)$ and $P_2(0)$ can be found from Eqs. 5 and 6 as

$$I(0) = \frac{\rho c}{2} \left[U_{01}^2 \left(\frac{\pi a_1^2}{\lambda_1 z_0} \right)^2 + U_{02}^2 \left(\frac{\pi}{\lambda_2 z_0} \right)^2 (a_2^2 - a_2'^2)^2 \right]. \quad (12)$$

Assuming $U_{01} = U_{02} = U_0$, we can write the focal plane stress field in terms of $I(0)$:

$$\begin{aligned} F_{\Delta\omega}(x_0, y_0) = & \frac{2I(0)}{c} \times \frac{\frac{\pi a_1^2}{\lambda_1 z_0}}{\left(\frac{\pi a_1^2}{\lambda_1 z_0} \right)^2 + \left(\frac{\pi}{\lambda_2 z_0} \right)^2 (a_2^2 - a_2'^2)^2} \times \\ & \text{jinc}\left(\frac{r_0 a_1}{\lambda_1 z_0}\right) \left[\frac{\pi a_2^2}{\lambda_2 z_0} \text{jinc}\left(\frac{r_0 a_2}{\lambda_2 z_0}\right) - \frac{\pi a_2'^2}{\lambda_2 z_0} \text{jinc}\left(\frac{r_0 a_2'}{\lambda_2 z_0}\right) \right] \times \\ & \exp\left(-j \frac{r_0^2}{2\Delta\lambda z_0}\right). \end{aligned} \quad (13)$$

The first fraction in the above equation represents the static radiation force produced by the two beams on a total absorber, the second fraction is a constant factor, and the rest represents the spatial distribution of the stress field on the focal plane. If $\Delta\omega \ll \omega_2$, then we may replace λ_1 and λ_2 by with λ_0 , and simplify the expression for the stress field. Under these conditions, the stress at the focal point is

$$F_{\Delta\omega}(0, 0) = \frac{2I(0)}{c} \times \frac{a_1^2(a_2^2 - a_2'^2)}{a_1^4 + (a_2^2 - a_2'^2)^2}. \quad (14)$$

The fraction on the right represents the effect of transducer dimension on the stress field. For the transducer used in the previous example, the value of this fraction is 0.4999. (This fraction can be also calculated for a single element transducer of the same diameter, excited by an amplitude modulated signal. For this purpose, we may let $a_1 = a_2$ and $a_2'^2 = 0$. For these values, the last fraction in Eq. 14 is 0.5.) The resulting radiation stress (assuming $c = 1500$ m/sec for water) is $F_{\Delta\omega}(0, 0) = 6.67 \times 10^{-4} I(0)$ N/m². Now letting $I(0) = 7200$ W/m², which is the maximum spatial peak, time average intensity suggested by FDA for *in vivo* applications (FDA report, see reference 9), the resulting stress at the focal point is $F_{\Delta\omega}(0, 0) = 4.80$ N/m². Referring to Fig. 3, we note that this stress field is applied only in a small region around the focal point to the object.

2.3.4. Acoustic emission

To explain the acoustic emission we consider an "object" within a homogeneous infinite medium. This model allows us to separate the roles played by the parameters of the object and the surrounding medium, and can be fitted to various applications. When an oscillating stress field is applied to the object, the object vibrates at the frequency of the stress field. Vibrational energy of the object is partly transferred to the surrounding medium, which is called the acoustic emission field. Here, we calculate the acoustic emission of an object resulting from applying the radiation stress.

To explain the physics in more generalized terms, for the moment we consider an object in the form of a flat disk facing the beam. Here, we assume that the vibrating object has a circular cross section of radius b and uniformly vibrates back and forth like a piston. This choice allows us to illustrate the concept in a simple form. We also consider an area $S \leq \pi b^2$ of the piston surface to be projected normally by the beam. We can always return to our elementary point object by reducing the area of this disk to $dxdy$. Similar solutions can be carried out for objects of other forms. The theory can be also extended to include arbitrary vibrating-part shapes and nonuniform displacement of the object. The total radiation force on this object $\overline{F_{\Delta\omega}}$, can be found by integrating the radiation stress over the area of the object. This force vibrates the target object at frequency $\Delta\omega$. The steady state normal velocity amplitude of a piston at frequency $\Delta\omega$, $U_{\Delta\omega}$, due to a harmonic force $\overline{F_{\Delta\omega}}$, can be written as

$$U_{\Delta\omega} = \frac{\overline{F_{\Delta\omega}}}{Z_{\Delta\omega}}, \quad (15)$$

where $Z_{\Delta\omega}$ is the mechanical impedance of the object at $\Delta\omega$. The mechanical impedance of the object has two components, one resulting from the inertia, friction, and the elasticity of the object itself, and the other resulting from the loading effect of the surrounding medium on the vibrating object. The mechanical impedance can be interpreted as a measure of object rigidity and how much it yields to the applied force. For example, for a rigid object, $Z_{\Delta\omega}$ is high, and hence the object resists the force.

Knowing $U_{\Delta\omega}$, we can calculate the pressure field it produces in the medium. We assume that the acoustic emission signal propagates in a free and homogenous medium. The farfield acoustic pressure due to a piston source of radius b set in a planar boundary of infinite extent is given by (Morse and Ingard 1968),

$$P_{\Delta\omega} = -j\Delta\omega\rho \frac{\exp(j\Delta\omega l/c)}{4\pi l} \left[\frac{2J_1\left(\frac{\Delta\omega b}{c} \sin \vartheta\right)}{\frac{\Delta\omega b}{c} \sin \vartheta} \times \frac{\cos \vartheta}{\cos \vartheta + \beta_B} \right] (2\pi b^2 U_{\Delta\omega}), \quad (16)$$

where l is the distance from the observation point to the center of the piston, ϑ is the angle between this line and the piston axis, and β_B is the specific acoustic admittance of the boundary surface (The specific acoustic admittance is $\beta_B = \frac{\rho c}{Z_B}$, where Z_B , the acoustic impedance of the boundary, represents the ratio between the pressure and normal fluid velocity at a point on the object). The factor two in the parenthesis comes from the presence of the boundary wall. It would be replaced by unity if the boundary wall were not present (Morse and Ingard 1968).

The acoustic emission field resulting from object vibration can be written in terms of object mechanical impedance by combining Eqs. 15 and 16, as

$$P_{\Delta\omega} = \rho c^2 \left\{ j \frac{\Delta\omega}{c^2} \times \frac{\exp(j\Delta\omega l/c)}{4\pi l} \left[\frac{2J_1\left(\frac{\Delta\omega b}{c} \sin \vartheta\right)}{\frac{\Delta\omega b}{c} \sin \vartheta} \times \frac{\cos \vartheta}{\cos \vartheta + \beta_B} \right] \right\} \times \frac{2\pi b^2}{Z_{\Delta\omega}} \overline{F_{\Delta\omega}}. \quad (17)$$

For wavelengths long compared to the object size, i.e., when $b\Delta\omega/c \rightarrow 0$, the term in the bracket approaches a constant because $2J(X)/X \rightarrow 1$ for $X \rightarrow 0$. Hence, ignoring the first fraction in the brackets, we may consider the contents of the brace to be an object independent function (the specific acoustic admittance β_B relates to the surrounding boundary surface). Under these conditions, the brace in the above equation represents the effect of the medium on the acoustic emission field, which we may call the *medium transfer function*, and denote it by

$$H_{\Delta\omega}(l) = j \frac{\Delta\omega}{c^2} \times \frac{\exp(j\Delta\omega l/c)}{4\pi l} \times \frac{\cos \vartheta}{\cos \vartheta + \beta_B}. \quad (18)$$

The last fraction in Eq. 17 includes $\frac{1}{Z_{\Delta\omega}}$, which is the mechanical admittance of the object at the frequency of the acoustic emission ($\Delta\omega$), and we denote this by $Y_{\Delta\omega}$. It is convenient to combine this term with the next term ($2\pi b^2$) in Eq. 17, as $Q_{\Delta\omega} = 2\pi b^2 Y_{\Delta\omega} = 2\pi b^2 / Z_{\Delta\omega}$, which is the total acoustic outflow by the object per unit force (acoustic outflow is the volume of the medium, e.g., the fluid, in front of the object surface that is displaced per unit time due to object motion). Function $Q_{\Delta\omega}$ represents the object characteristics at the acoustic frequency. We may thus rewrite Eq. 17 in a more compact form as

$$P_{\Delta\omega} = \rho c^2 H_{\Delta\omega}(l) Q_{\Delta\omega} \overline{F_{\Delta\omega}}. \quad (19)$$

Equation 19 indicates that the acoustic emission pressure is proportional to: (1) the radiation force, which itself is proportional to the square of ultrasound pressure and the ultrasound characteristics of the object, d_r , and the projected area S ; (2) the acoustic outflow by this object, $Q_{\Delta\omega}$, representing the object size b and its mechanical admittance at the acoustic frequency, $Y_{\Delta\omega}$; and (3) the transfer function of the medium at the acoustic frequency, $H_{\Delta\omega}(l)$. Note the difference between the projection area S and the vibrating area πb^2 . The projection area determines the extent of the force applied to the object (Eq. 1). The vibrating area, however, influences the total acoustic outflow in the medium caused by object vibration.

2.3.5. Measuring the acoustic emission

A hydrophone is used to measure the acoustic emission field. Equation 18 indicates that for long wavelengths compare to the object size, the acoustic emission field pattern resembles that of a dipole with an angle dependency represented by the last fraction to the right of this equation. This angle dependency is normally weak and hence the position of the receiving hydrophone is not critical. Also, because the attenuation of low frequency acoustic waves in tissue and liquids is normally low, one may place the hydrophone at a distance from the object without

losing too much intensity. The simplified diagram presented in Fig. 2 describes how to measure the amplitude of the acoustic emission field. To measure the phase of the acoustic emission, a phase reference needs to be set. One way to accomplish this is to generate a reference signal by electronic down mixing of the two CW excitation signals to produce a beat signal at the difference frequency Δf . Then, using this reference signal, the phase of the acoustic emission signal (hydrophone output) can be calculated by conventional phase detection methods.

2.3.6. Applications

Evaluation of the characteristics of an object (or a medium) by listening to its sound is a traditional approach that has been used for many purposes. Qualitative evaluation of a crystal glass by tapping on it is a simple example. Vibro-acoustography implements the same approach but in micro-scale, and in a way that could be applied to tissues.

Equation 19 presents a general relationship between the mechanical parameters of the objects, surrounding medium, and the acoustic emission field resulting from object vibration. By measuring the acoustic emission field, it would be possible, in principle, to estimate some of the object or medium parameters, either in an absolute or in a relative sense. For example, one can use vibro-acoustography to measure the resonance frequency of an object, and from that information it is possible to estimate some viscoelastic parameters of the object or the medium. This method has been used to measure the Young's modulus of a metallic rod (Fatemi and Greenleaf 1999a). In another experiment, by measuring the resonance frequency of a known resonator in a liquid medium, the viscosity of the fluid has been estimated with good accuracy (Fatemi and Greenleaf 1999b). These applications are not necessarily medical, but the principle could be used for evaluation of soft tissues, blood, bone, etc.

In medical applications, one can use vibro-acoustography to obtain an image of the object for diagnostic purposes. In such applications, the image may not represent a physical quantity, rather it provides a means to visualize object details.

2.3.7. Experimental results

In the following experiment vibro-acoustography has been used to image excised human carotid arteries that include calcifications. Characteristics of the ultrasound transducer used here are those described in the example presented in Theory section. The object consists of two excised human carotid arteries secured on a thin sheet of latex. This sheet is almost transparent to the ultrasound and x-ray. Figure 4a shows an x-ray image of these arteries. The left artery is from a young person and has shows no calcification. The left artery is from an older person and includes some calcium deposit which can be seen as a bright region near the bifurcation. The arteries were immersed in a water tank for scanning. The difference frequency Δf in this experiment is 7 kHz. The lead number "2" was placed on the latex sheet for identification purposes. Figure 4b shows the vibro-acoustography image (displaying the amplitude of the acoustic emission signal) of the object. In this image, the calcified region is seen as a bright region, resembling its x-ray image. Calcification, which is formed from stiff (compare to the arterial wall) material, is an efficient acoustic radiator, producing strong acoustic emission when

exposed to the radiation force of the incident ultrasound. Hence, it stands out in the vibro-acoustography image. This image has a high spatial resolution (about 0.7 mm), low speckle, and high signal-to-noise ratio. The number "2", which is also made from a hard material, is seen with high contrast. This experiment demonstrates the utility of the method in delineating stiff material in a soft background.

3. Comparisons of the methods

In this paper we presented three approaches for using localized ultrasound radiation force to probe biological materials. Here we compare the features and capabilities of the methods.

3.1. Objectives

The transient method estimates a quantity that correlates to the hardness of tissue. While it does not estimate a specific physical parameter, the estimated parameter is quantitative and may be useful for diagnosis.

Shear wave methods aim specifically at the shear wave characteristics in soft tissue, in particular, estimating the shear wave velocity. Shear wave velocity in soft tissue is very low (typically in the order of a few m/sec), allowing localized measurement of the parameter. Also, because shear wave attenuation in soft tissue is high, the boundaries of the object have minimal effect on the measurement. This method is not intended for use in hard materials.

Vibro-acoustography seeks a two-fold objective. In this method, the acoustic emission signal is dependent on both microstructure (local drag coefficient) and macrostructure (the mechanical admittance) of the object. The acoustic emission signal can be analyzed to estimate different characteristics of the object. In some applications, both the local parameters and those that are related to the large-scale structure of an object are needed. An instructive example presented in Fatemi and Greenleaf (1999) demonstrates that vibro-acoustography can be used to produce an image of a tuning fork displaying its detail (microstructures) while measuring its resonance frequency (a parameter related to the macrostructure) represented by color.

3.2. Excitation method

In the first two methods the radiation force is produced by a single focused transducer which is driven by an amplitude modulated signal, in particular, pulse shaped (the shear wave method can, in principle, operate using a single sinusoidally modulated beam). Vibro-acoustography, however, uses two CW excitation signals (or long tone bursts of CW signals). The major difference in these excitation techniques is the distribution of the radiation stress in the depth direction. A possible drawback of using a single amplitude modulated beam method is that the pulsed ultrasound exerts a radiation stress on all tissue through which it propagates. Also, a shock can be produced on the transducer surface, and then transmitted to the tissue. Such phenomena result in extraneous motion of the object that could introduce errors in the measurements. In vibro-acoustography, the two CW beams pass through separate paths. Outside of their interaction at the focal region, they can only produce a static radiation force on the object, which produces no sound. The beams mix near the focal point to produce a modulated field that can generate an oscillating radiation force only in that location. The resulting acoustic field, therefore, is directly

related to the excitation of the object at the focal area. This is an important feature, because the acoustic emission from other parts of the object or the transducer should not be allowed to interfere with the acoustic emission from the focal area.

3.3. Detection method

The transient method and the shear wave method are based on localized detection of material displacement. This is implemented by using either Doppler ultrasound, optical displacement measurement, or a more sophisticated method such as MRI. Vibro-acoustography uses an audio hydrophone or microphone for detection, which is a much simpler detection method than Doppler or MRI.

3.4. Sensitivity

Detection sensitivity is critical to the success of any of the above methods. More ultrasound intensity would be needed if the detection sensitivity is poor. Ultrasound Doppler methods, at conventional ultrasound frequencies, probably can detect displacements in the order of a few micrometers. The sensitivity of the MRI technique is in the order of 100 nm (Muthupillai *et al* 1995). Vibro-acoustography has been shown to detect motions as small as a few nanometers (Fatemi and Greenleaf 1998). The high sensitivity of this method is a result of the fact that small motions of the object can produce an acoustic emission pressure field that is easily detectable by a sensitive hydrophone.

3.5. Measured quantities

The quantity measured in the transient method is somewhat arbitrary, and not a direct measure of any physical quantity. The merit of this method is that tissue hardness is measured from relative displacement values, without the need to measure the applied force. The shear wave methods directly measure a physical parameter of the material in an absolute sense. The acoustic emission field measured in vibro-acoustography is a function of several physical parameters that relate to the object and the surrounding medium. It is possible to measure a single parameter only if one has enough knowledge about other parameters involved. For example, one can measure the shear viscosity of a liquid using a known resonator as an object in the liquid (Fatemi and Greenleaf 1999b), or, for a given the geometry, the Young's modulus of a metallic object can be measured (Fatemi and Greenleaf 1999a) by vibro-acoustography.

3.6. Exposure safety

The shear wave method presented in (Sarvazyan *et al* 1998) uses high intensity pulsed ultrasound for excitation and either the optical or MRI methods for detection. It is argued that, although the intensity is high, the total exposure is within the FDA limits (FDA report, see reference 9). These limits are recommended based on possible thermal and mechanical effects of ultrasound on tissue. However, *in vivo* use of such detection methods would be difficult. Using Doppler ultrasound for detection is less sensitive, hence, requires higher peak ultrasound intensity to produce enough displacement of the tissue. This intensity level may exceed the recommended spatial peak pulse average intensity limit.

Vibro-acoustography uses either CW or tone burst ultrasound. Therefore, the continuous ultrasound intensity (spatial peak time average intensity) limit must be observed. This limit according to the FDA is 720 mW/cm^2 (FDA report, see reference 9). However, because of high sensitivity of the hydrophone detector, it is possible to detect very small levels of the acoustic emission while using low transmit power. For example, it has been shown that a submillimeter object can be detected at ultrasound intensities far below the FDA limit (Fatemi and Greenleaf 1999).

3.7. *In vivo* applicability

In vivo application of the transient method is not clear because it requires high ultrasound power to produce a detectable displacement. Application of the shear wave methods in human body largely depends on the detection method used. Optical methods are not likely usable *in vivo*. MRI detection methods are generally complex, especially when the operation is to be linked to the ultrasound system in the magnetic field. Ultrasound Doppler is a more practical detection method for shear wave detection; however, its sensitivity may not be sufficient for ultrasound intensities within the recommended maximum level (Walker 1999). Vibro-acoustography uses a hydrophone for detection which is simple to operate in clinical settings. It, however, requires an acoustically quiet environment for proper detection. The biological noise spectrum seems to be below 1 kHz, which can be easily filtered out if the operation frequency is above this limit (Fatemi and Greenleaf 1999).

3.8. Image resolution

Imaging complex objects using the transient or the shear wave methods has not been fully explored in the literature. Vibro-acoustography can be used for high quality imaging. The spatial resolution is proportional to the width of the stress field main lobe. For example, for the 3 MHz ultrasound transducer presented in Fig. 3, the spatial resolution is about 700 micrometers.

3.9. Material properties

Both the transient and shear wave methods are based on local deformation of soft tissue in the beam direction. These methods work best if the material under test supports the shear wave, has enough attenuation to allow the build up of enough radiation force, and is compliant enough to allow appreciable displacement. Application of these methods for hard material, such as bone and calcifications, would be difficult or impractical because: (a) stiff materials have low compliance, hence, their displacement in response to the force is relatively small and difficult to detect; (b) the shear wave travels at high speed in such material. In vibro-acoustography hard materials produce structural vibrations which are often stronger than that of soft tissue. Such vibrations result in strong and easily detectable acoustic emissions. The bright appearance of the arterial calcifications in the experiment presented in Fig. 4 is a demonstration of this phenomenon.

In contrast to the other two methods, vibro-acoustography can be used to detect particles in materials that do not support shear waves, for example, detecting gas bubbles in liquids. The acoustic emission resulting from particle vibration includes a compressional wave component that can travel in the surrounding medium including the liquid. Tissue attenuation for compressional

waves at low frequencies is small, hence such waves can be detected by the hydrophone from a distance. Shear waves in liquid medium decay very rapidly and are difficult to detect by most methods.

4. Summary

Recent progress on techniques for evaluation of dynamic viscoelastic parameters of tissue, based on the radiation force of ultrasound, has prompted us to view these techniques as an emerging new field. We recognize the capabilities and potentials of this new field as unique and distinguishable from those of conventional elasticity or ultrasound imaging techniques.

Three methods for probing biological tissue using the dynamic radiation force of ultrasound were presented. The first method measures a minute transient tissue deformation versus time. The second method, also uses a transient excitation, but measures the resulting shear wave amplitude and velocity. The last method, vibro-acoustography, measures the acoustic field resulting from object vibration at a specified frequency. Capabilities and limitations of these methods for probing different materials and their potentials for *in vivo* applications were discussed.

5. Acknowledgments

This work was supported in part by grant DAMD17-98-1-8121 from the Army Medical Research and Materiel Command and grant HL 61451 from the National Institutes of Health.

6. References

1. Andreev V, Dmitriev V, Rudenko O V, and Sarvazyan A 1997 *J. Acoust. Soc. Am.* **102** 3155.
2. Chu B-T and Apfel R E 1982 *J. Acoust. Soc. Am.* **72**(6) 1673-87.
3. Fatemi M and Greenleaf J F 1998 *Science* **280** 82-5.
4. Fatemi M and Greenleaf J F 1999 *Proc. Natl. Acad. Sci. USA (PNAS)* **96** 6603-08.
5. Fatemi M and Greenleaf J F 1999a *Ultrasonic Imaging* **21**(2) 147-54.
6. Fatemi M and Greenleaf J F 1999b *Acta Physica Sinica* **8** S27-32.
7. Frizzell L A and Carstensen E L 1976 *J. Acoust. Soc. Am.* **60**(6) 1409-11.
8. Goss S A, Johnston R L, Dunn F 1978 *J. Acoust. Soc. Am.* **64**(2) 423-57.
9. Information for manufacturers seeking marketing clearance of diagnostic ultrasound systems and transducers Sept. 30, 1997 Report by U.S. Dept. of Health and Human Services Food and Drug Administration, Rockville, MD USA.
10. Kino G S 1987 *Acoustics Waves: Devices, Imaging, and Analog Signal Processing* (Englewood Cliffs, NJ: Prentice-Hall Signal Processing Series).
11. Morse P M and Ingard K U 1968 *Theoretical Acoustics* (New York: McGraw Hill, New York).
12. Muthupillai R, Lomas D J, Rossman P J, Greenleaf J F, Manduca A and Ehman R L *Science* **269** 1854-57.
13. Sarvazyan A P, Rudenko O V, Swanson S D Fowlkes J B, Emelianov S Y 1998 *Ultrasound Med. Biol.* **24**(9) 1419-35.
14. Sugimoto T, Ueha S and Itoh K 1990 *IEEE Ultrason. Symp. Proc.* **3** 1377-80.

15. Walker W F 1999 *J. Acoust. Soc. Am.* **105** 2508–18.
16. Westervelt P J 1951 *J. Acoust. Soc. Am.* **23**(4) 312–5.

7. Legends

Figure 1 Generation of a modulated ultrasound field by single and confocal beams. The single beam produces a field that is modulated throughout the beam path. This field can produce an oscillating radiation force on any object in the beam path. The confocal annular array transducer generates two CW beams propagating separate paths. These beams interfere near the focal zone, producing a modulated field only in that region. Hence, the oscillating radiation force can only be generated on objects in the beam crossing region.

Figure 2 Vibro-acoustography system. The two elements of the confocal annular array are excited by separate CW signals at two different frequencies. The object is placed at the focal plane of the transducer. The ultrasound field produces a radiation force at the difference frequency Δf on the object. This force vibrates the object, which in turn produces a sound field in the medium. This sound field is received by an audio hydrophone placed near the object. To form an image, the beams are scanned in a raster motion across the scanning plane, and the resulting acoustic emission is recorded from each point. Brightness of each corresponding point on the image plane is determined by the amplitude (or phase) of the recorded acoustic emission.

Figure 3 Three-dimensional plot of the stress field amplitude of a confocal annular array transducer at the focal plane at a point in time. Transducer dimensions are: $a_1 = 14.8$ mm, $a'_2 = 16.8$ mm, $a_2 = 22.5$ mm, and the focal length is 70 mm. The center frequency is 3 MHz, and the difference frequency is 7.3 kHz.

Figure 4 Vibro-acoustography of excised human carotid arteries: (a) x-ray image showing a normal (left) and a calcified (right) artery placed on a sheet of latex; (b) vibro-acoustography of the arteries in (a) measured at a vibration frequency of 7 kHz. The calcification is seen as a bright region in both x-ray and vibro-acoustography images. Lead number "2" is used for identification.

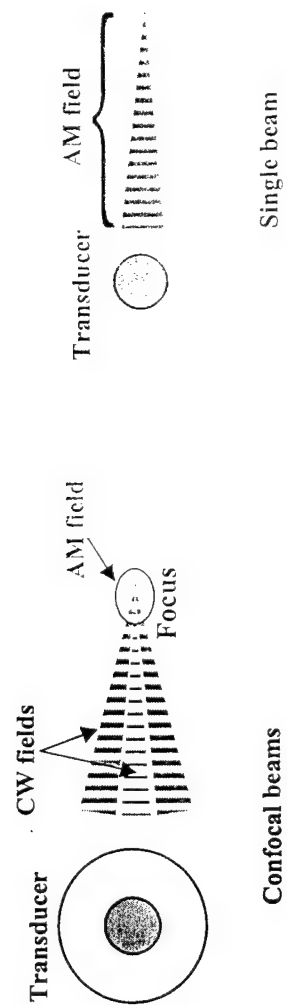


Figure 1

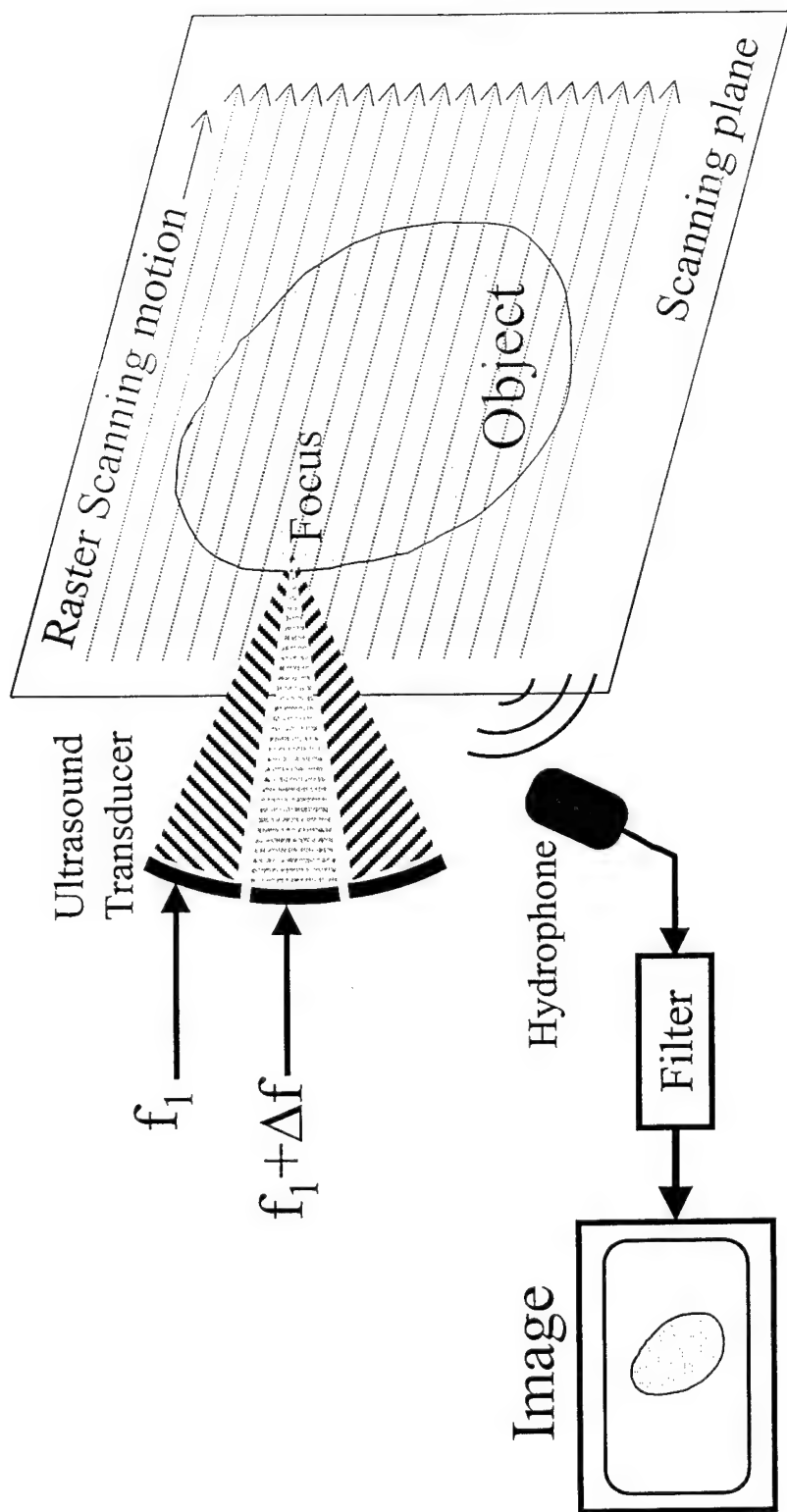


Figure 2

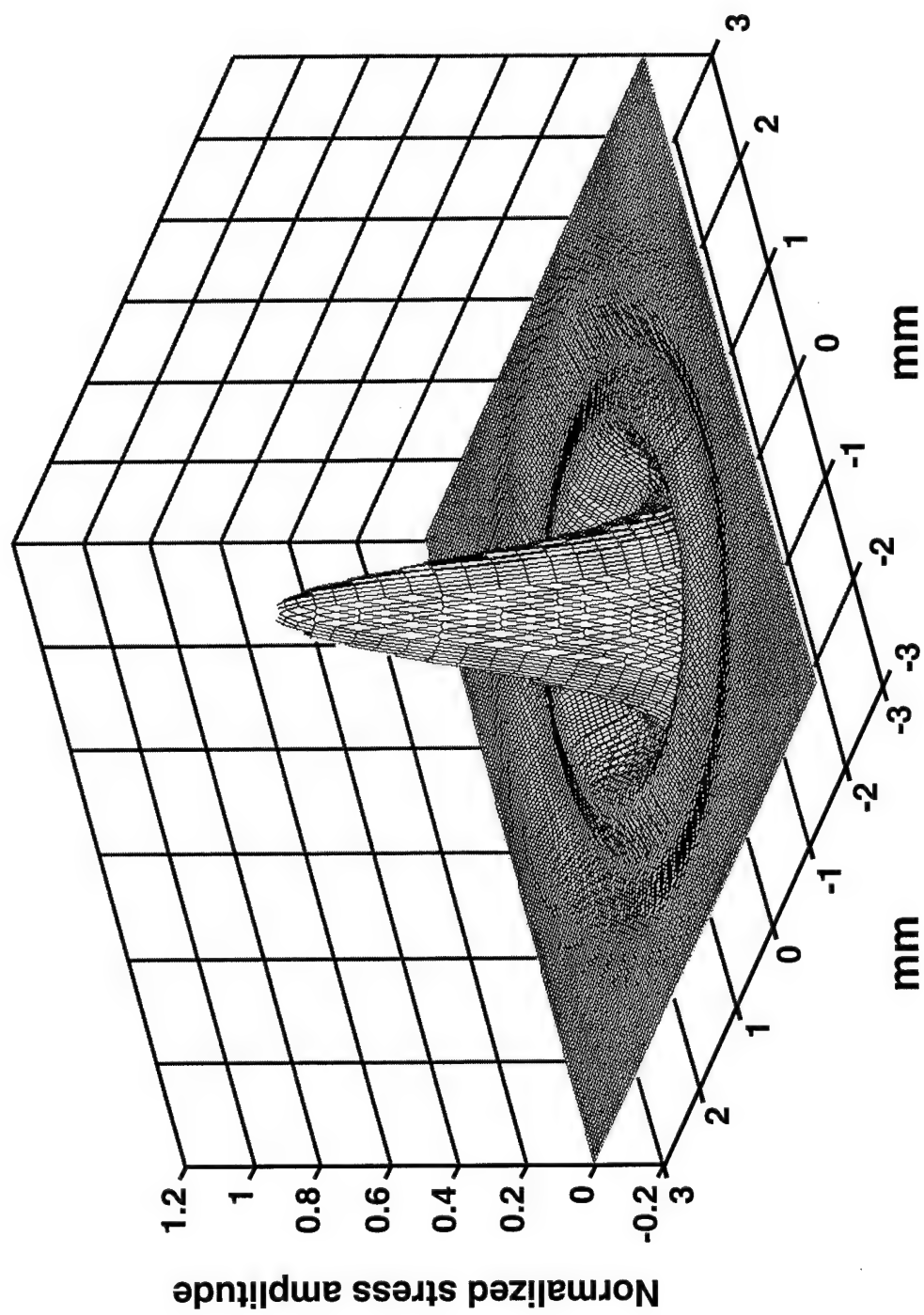
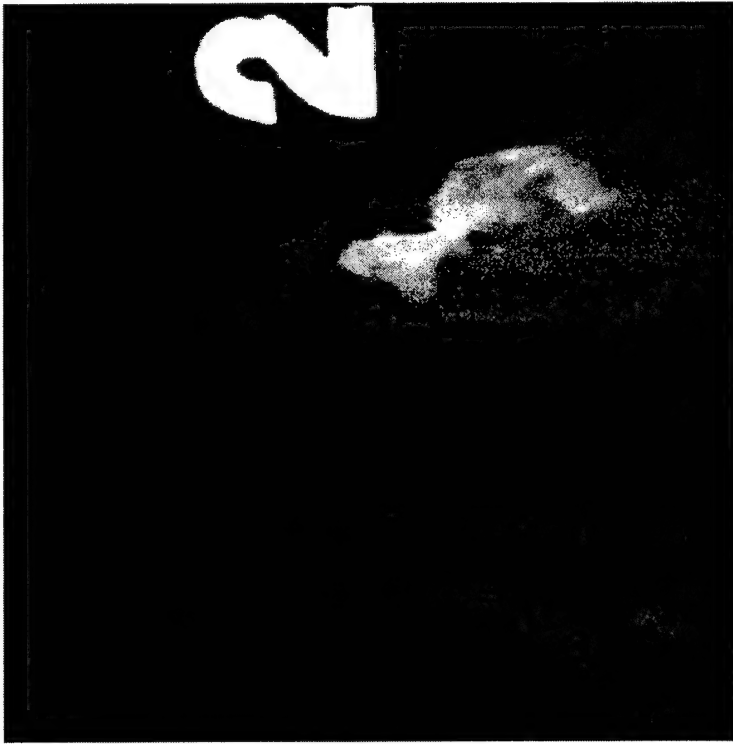
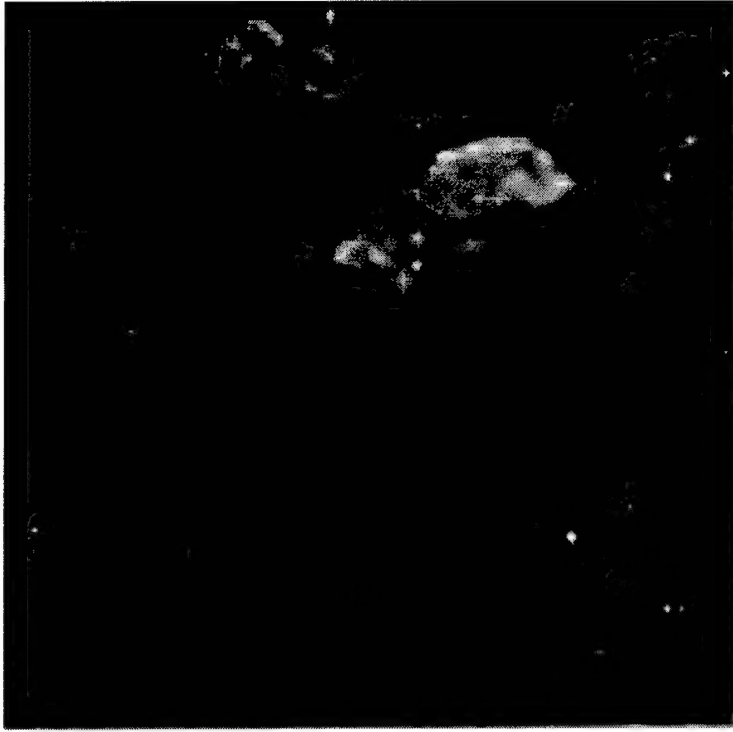


Figure 3



a



b

Figure 4

VIBRO-ACOUSTOGRAPHY SYSTEM MODELING

Mostafa Fatemi and James F. Greenleaf

Department of Physiology and Biophysics, Mayo Clinic
and Mayo Foundation, Rochester, MN 55905 USA

fatemi.mostafa@mayo.edu

Vibro-acoustography is a new imaging method that utilizes the radiation force of ultrasound to vibrate objects at low (kHz range) frequencies. The acoustic emission resulting from such vibration is detected by a hydrophone and is used to obtain an image that is a function of object elastic characteristics [*Proc Natl Acad Sci USA* 96:6603-6608, June 1999]. Elastic parameters, such as object stiffness, are valuable in delineating hard objects such as breast micro calcifications from the surrounding soft tissue. This method offers a high spatial resolution provided by two focused ultrasound beams, and produces a highly localized dynamic stress field to probe the object point-by-point with low-frequency elastic waves. The principles used for beam forming in vibro-acoustography are fundamentally different from those for the conventional ultrasound imaging methods. The reason is that in vibro-acoustography the ultrasound field is designed to interact nonlinearly with the object whereas in the conventional ultrasound they interact linearly. In order to understand the roles of different parameters of the system and the object in the final image it is important to analyze the input-output relationship of the system.

The approach taken in this paper is to derive an analytical model for vibro-acoustography system. This model includes three parts: (a) the incident beam characteristics and the resulting radiation stress field, (b) a model for the mechanical response of the object to the stress field, and (c) a model for the propagation medium. Using this model we can calculate the acoustic emission field from an object such as a sphere or a disc. Also this model allows us to calculate the complex point spread function of the imaging system.

The results show that the acoustic emission is inversely proportional to the impedance of the object, which is comprised of two components, the mechanical impedance and the radiation impedance. These impedances can be written in terms of object mass, shape and elastic parameters. The quadratic relationship between the ultrasound pressure and the resulting acoustic emission pressure is determined theoretically and verified experimentally. To verify the theoretical point spread function, the experimental point spread function is obtained and shown to be in agreement with the theoretical results.

We conclude that the model presented here can adequately represent the imaging system.

The U.S. Army Medical Research and Materiel Command under DAMD17-98-1-8121 supported this work.

IMAGING THE VISCOELASTIC PROPERTIES OF TISSUE

M. Fatemi and J.F. Greenleaf

Department of Physiology and Biophysics, Mayo Clinic
and Mayo Foundation, Rochester, MN 55905 USA

fatemi.mostafa@mayo, jfg@mayo.edu

1. Introduction

It is well known that changes in elasticity of soft tissues are often related to pathology. Traditionally, physicians use palpation as a simple method for estimating mechanical properties of tissue. In palpation, a static force is applied and a crude estimation of tissue elasticity is obtained through the sense of touch. The force is applied on the body surface and the result is a collective response of all the tissues below. Clinicians can sense abnormalities if the response to palpation of the suspicious tissue is sufficiently different from that of normal tissue. However, if the abnormality lies deep in the body, or if it is too small to be resolved by touch, then the palpation method fails. The dynamic response of soft tissue to a force is also valuable in medical diagnosis. For instance, rebound of tissue upon sudden release of pressure exerted by the physician's finger on the skin provides useful diagnostic information about the tissue.

Quantitative measurement of the mechanical properties of tissues and their display in a raster format is the aim of a class of techniques generally called elasticity imaging or elastography [1]. The general approach is to measure tissue motion caused by an external (or, in some methods, internal) force or displacement and use it to reconstruct the elastic parameters of the tissue. The excitation stress can be either static, or dynamic (vibration). The dynamic excitation is of particular interest because it provides more comprehensive information about tissue properties in a spectrum of frequencies, or alternatively, the transient behavior of the tissue could be deduced from the measurements. In most elasticity imaging methods ultrasound is used to detect the motion or displacement resulting from the applied stress. Magnetic resonance elastography is a recently developed method [2] that employs a mechanical actuator to vibrate the body surface and then measures the strain waves with phase sensitive Magnetic Resonance Imaging (MRI). The majority of elasticity imaging methods are based on an external source of force, resulting in a spatially wide stress field distribution. This requires the stress field to pass through the superficial portion of the object before reaching the region of interest within the interior. This requirement can complicate the estimation of stiffness because the stress field patterns change at different depths. Also, because the stress field is widely distributed the response of the object is an integral sum of the stress field. An alternative strategy is to apply a localized stress directly in the region of interest. One way to accomplish this is to use the radiation pressure of ultrasound.

Acoustic radiation force is the time average force exerted by an acoustic field on an object. This force is produced by a change in the energy density of an incident acoustic field [3], for example, due to absorption or reflection. Several benefits may result from using ultrasound

radiation force for evaluating tissue properties, including: a) acoustic (ultrasound) energy is a non invasive means of exerting force, b) existing ultrasound technology and devices can be readily modified for this purpose, thus eliminating the need for developing a new technology, c) radiation force can be generated remotely inside tissue without disturbing its superficial layers, d) the radiation stress field can be highly localized, thus allowing for precise positioning of the excitation point, and e) radiation force can be produced in a wide range of frequencies or temporal shapes. These features make radiation force methods more attractive than other, mostly mechanical, excitation methods used in elasticity imaging.

Tissue probing with the radiation force produced by ultrasound can be accomplished in a variety of techniques, depending on the excitation and detection methods used. We may categorize these method as: a) transient methods, where an impulsive radiation force is used and the transient response of the tissue is detected by Doppler ultrasound [4]; b) shear-wave methods, where an oscillating radiation is applied to the tissue and the resulting shear wave is detected by ultrasound or other methods [5, 6, 7]; c) vibro-acoustography, recently developed by the authors, where a localized oscillating radiation force is applied to the tissue and the acoustic response of the tissue is detected by a hydrophone [15, 16]. Figure [1] illustrates the relationship between various methods that have been developed for evaluating or imaging the elastic properties of tissue.

Dynamic radiation force methods seem to be evolving rapidly as a new field in tissue characterization and imaging. The purpose of this chapter is to systematically discuss the features and capabilities that are offered in this group of elasticity measurement techniques. Here, we describe the general approach used in the transient, shear wave, and vibro-acoustography methods. We pay particular attention to the last method, present its theory, and discuss its features. Finally we discuss the capabilities and limitations of all three methods.

2. Theory of the Radiation Force

Study of radiation force and radiation pressure dates back nearly one century, to the time of Rayleigh [8]. Since then, this subject has been under continuous investigation. A historical review of radiation force and radiation pressure is presented in [9], and a critical review of the subject can be found in [3]. Some recent analyses of radiation force/pressure in attenuating medium, which may be applicable to biological tissues, are presented in [10] and [11].

The acoustic radiation force is an example of a universal phenomenon in any wave motion that introduces some type of unidirectional force on absorbing or reflecting targets in the wave path. Radiation force in fluids is often studied in the context of radiation pressure. Depending on the boundary conditions, radiation pressure can be defined differently. Simple explanations of these definitions can be presented by considering a sound traveling inside, and along the axis of, a cylindrical container toward the opposite wall [9]. Rayleigh radiation pressure is the excess pressure produced on the opposite wall when the container's side wall is confining the fluid inside. Langevin radiation pressure is the excess pressure on the opposite wall when we remove the confining side wall, so that the fluid is free to move (fig. 2). Here we will focus

on Langevin radiation pressure because the conditions for which this pressure is defined apply to our experimental situation. It can be shown that the Langevin radiation pressure of a plane wave impinging normally on a perfectly absorbing wall is equal to the total energy density $\langle E \rangle$, where $\langle \rangle$ represents the time average. If the wall is partially reflecting, this pressure would be equal to $(1 + R)\langle E \rangle$, where R is the power reflection coefficient [9]. Thus, in general, we can write the radiation force of a normally impinging sound beam on a wall as

$$F = d_r S \langle E \rangle, \quad (1)$$

where F is the force in the beam direction, and d_r is the “radiation force function” or the drag coefficient. This dimensionless coefficient is defined per unit incident energy density and unit projected area. For a planar object, d_r is numerically equal to the force on the object. Physically, the drag coefficient represents the scattering and absorbing properties of the object [12]. For a perfectly absorbing object $d_r = 1$, and for a perfectly reflecting object $d_r = 2$. In the case of oblique incidence, the radiation force will have a normal as well as a transverse component. A more detailed description of d_r is presented in [12].

To produce a time varying radiation force, the intensity of the incident beam can be modulated in various ways. For example, a short ultrasound pulse can produce a transient pulsed radiation force, and a sinusoidally modulated beam can result in a sinusoidally varying force.

3. Radiation Force Methods

3.1 Transient Method

In transient methods the radiation force of ultrasound is used to make a minute deformation in the tissue. The transient recoil of the tissue resulting from this deformation is measured and used for evaluation of tissue elastic properties. A method for measuring tissue hardness, presented by Sugimoto, et al. [4], uses the radiation force of a single focused ultrasound beam. Ideally, hardness may be represented by the spring constant of the object, which is the ratio of the applied force to the displacement. Principles of the transient methods are presented in fig. 3.

In this method an ultrasound pulse is used to generate a short duration radiation force which produces localized deformation of the tissue. Immediately after the force pulse, the resulting transient deformation of tissue is measured as a function of time with Doppler ultrasound using a separate transducer. The deformation includes an initial rapid squeeze of the tissue, followed by a relaxation and possibly a rebound. The deformation is a function of tissue viscoelastic parameters, as well as the applied force. The authors argue that because quantitatively measuring the internal radiation force is difficult, it is advantageous to derive a relative quantity that is representative of tissue hardness. To derive a single relative quantity from the deformation data, the relaxation part of the function is approximated by a sum of several exponential curves, and the sum of the first order derivatives of such exponential is calculated. Sugimoto, et al. [4] show that this quantity is correlated to the spring constant of the tissue, thus may be used as a measure of tissue hardness.

3.2 Shear Wave Methods

Shear modulus is related to the hardness or elasticity of the material. It is known that the shear modulus of various soft tissues range over several magnitudes of order, while bulk modulus, a parameter that is associated with the conventional pulse-echo ultrasound compressional wave speed, varies significantly less than an order of magnitude [13, 14]. These features indicate that shear modulus may be a better parameter for tissue characterization than bulk modulus. Tissue attenuation of the shear wave is very large even at low kHz frequencies. One way to induce localized shear waves inside tissue is to use the radiation force of focused ultrasound [5]. In a method called shear wave elasticity imaging (SWEI) [6], an amplitude modulated single focused ultrasound beam is used to induce a localized radiation stress inside the soft tissue. Localization of the stress field is critical to success of the method. To achieve a high degree of localization, the method uses a focused ultrasound beam. It is shown that the radiation stress exerted within a dissipative medium peaks about the focal region of the highly focused transducer. Also, it has been suggested that localization can be improved by designing the transducer and selecting the beam parameters such that a nonlinear shock wave is produced in the focal region, increasing the magnitude of the stress field in the vicinity of the focal region, thus augmenting localization of the stress field.

Modulation of the ultrasound beam can be in the form of an oscillating wave or short pulse. The resulting radiation force elicits a shear wave propagating in the radial direction with respect to the beam axis, with particle motion parallel to the beam axis. Shear waves in soft tissue travel at very low speed, typically around a few meters per second, thus the corresponding wavelength is much shorter than that of the compressional waves for the same frequency. Shear waves are also highly attenuated in soft tissue, with an attenuation coefficient two or three orders of magnitude higher than that of the compressional waves. Because of high attenuation of shear waves, it is possible to induce them in a very limited region in the vicinity of the focal point of the ultrasound beam, hence avoiding the influence of tissue boundaries. Shear parameters of the tissue, such as shear modulus and shear viscosity, can be calculated by measuring the amplitude and the temporal characteristics of this wave. For example, the time required for the wave front to propagate from one point to another can be used to calculate the shear wave speed, and consequently, the shear wave modulus μ , as

$$\mu = \rho c_t^2 \quad (2)$$

Where ρ and c_t are the density and the shear wave velocity, respectively.

Shear waves may be detected optically. In this method a laser source and a photo detector are used to detect the displacement of particles due to the shear wave in a transparent phantom [6]. Because this method requires a transparent medium, its application *in vivo* is difficult. Phase sensitive magnetic resonance imaging [2, 6] is an alternative method that can be used to measure the three-dimensional distribution of particle displacement in a given direction versus time in a material. Figure 4 illustrates a simplified system for shear wave elasticity measurement using magnetic resonance imaging. In an experiment presented in [6], an ultrasound pulse of 3.6 ms

duration produced by a 70 mm diameter transducer focused at 100 mm was transmitted within a cylindrical rubber phantom. The displacement was measured by 2.0 T MRI system at two different times after the acoustic pulse was applied. The position of the peak displacement at these time points was used to estimate the shear velocity, which was shown to be consistent with the independently measured value. Shear waves can also be detected by Doppler ultrasound [5]. It has been shown [7] that to achieve an appreciable displacement needed for Doppler detection, most soft tissues require high ultrasound intensities which might be beyond the safe limit.

3.3 Vibro-acoustography

3.3.1 Method

This technique produces a map of the mechanical response of an object to a dynamic force applied at each point. The method utilizes ultrasound radiation force to remotely exert a localized oscillating stress field at a desired frequency within (or on the surface of) an object, and records the resultant acoustic response [15, 16]. Figure 5 illustrates the principle of this method. This acoustic response, which is normally at low kHz range, is a function of the viscoelastic properties of the object and can be used to produce an image of the object.

This method operates on an oscillating radiation force to vibrate the tissue and consequently produce an acoustic emission from the object. To produce an oscillating radiation force the intensity of the incident ultrasound must be amplitude modulated at the desired low frequency. Using a single amplitude modulated beam seems to be the simplest means to attain this purpose. However, such a beam could exert a radiation force on any object that is present along the beam path, producing undesirable acoustic emission. To confine the radiation stress to the desired region, we use two unmodulated CW beams at slightly different frequency, propagating along separate paths. The beams are positioned to cross each other at their respective foci, and thus produce a modulated field at a confined, small, cross-section region.

3.3.2 Theory

In the beam forming method to be described the amplitude modulated field is obtained by the interference of two unmodulated ultrasound beams. The main advantage of this approach is that the interference volume size can be limited to a small region. Radially symmetric interfering beams are obtained when two coaxial, confocal transducers are used [16]. For this purpose, elements of a two-element spherically focused annular array (consisting of a central disc with radius a_1 and an outer ring with the inner radius of a_2' and outer radius of a_2) are excited by separate CW signals at frequencies $\omega_1 = \omega_0 - \Delta\omega/2$ and $\omega_2 = \omega_0 + \Delta\omega/2$, respectively. We assume that the beams are propagating in the $+z$ direction with the joint focal point at $z = 0$, as shown in fig. 6. The resultant field on the $z = 0$ plane may be written as:

$$p(t) = P_1(r) \cos(\omega_1 t + \psi_1(r)) + P_2(r) \cos(\omega_2 t + \psi_2(r)), \quad (3)$$

where $r = \sqrt{x^2 + y^2}$ is the radial distance. The amplitude functions are [17, 18]

$$P_1(r) = \rho c U_{01} \frac{\pi a_1^2}{\lambda_1 z_0} \text{jinc}\left(\frac{r a_1}{\lambda_1 z_0}\right), \quad (4)$$

and

$$P_2(r) = \rho c U_{02} \frac{\pi}{\lambda_2 z_0} \left[a_2^2 \text{jinc} \left(\frac{r a_2}{\lambda_2 z_0} \right) - a_2'^2 \text{jinc} \left(\frac{r a_2'}{\lambda_2 z_0} \right) \right], \quad (5)$$

where U_{0i} is the velocity amplitude at the i -th transducer element surface, and $\lambda_i = 2\pi/\omega_i$ for $i=1,2$ are the ultrasound wavelengths. The phase functions,

$$\psi_i(r) = -\frac{\pi r^2}{\lambda_i z_0}, \quad (6)$$

for $i=1, 2$, are conveniently set to be zero at the origin. Also, $\text{jinc}(X) = J_1(2\pi X)/\pi X$, where $J_1(\cdot)$ is the first order Bessel function of the first kind.

The instantaneous energy is $E = p^2(t)/\rho c^2$. Replacing $p(t)$ from (3), this energy will have a time independent component, a component at the difference frequency $\Delta\omega = \omega_2 - \omega_1$ which results from the cross product of the two pressure fields, and high frequency components at ω_1 and ω_2 and their harmonics. The energy component at the difference frequency is:

$$e_{\Delta\omega}(t) = \frac{P_1(r_0)P_2(r_0)}{4\rho c^2} \cos[\Delta\omega t - \Delta\psi(r_0)], \quad (7)$$

where $\Delta\psi(r_0) = \psi_2(r_0) - \psi_1(r_0)$.

Now, we define a *unit point target* with an area of $dxdy$ at position (x_0, y_0) on the focal plane, and with a drag coefficient $d_r(x_0, y_0)$ such that: $d_r(x_0, y_0)dxdy = 1$ on the target and zero elsewhere. This equation is merely used as a mathematical model. In this case, the projected area can be considered to be $S = dxdy$. Therefore, if the projected area is unity, then $d_r(x, y) = 1$, which corresponds to a totally absorptive object.

Referring to (1), and replacing $d_r S$ with unity and $\langle E \rangle$ by $e_{\Delta\omega}(t)$ of (7), then we can write the low-frequency component of the radiation force on the unit point target as:

$$f_{\Delta\omega}(x_0, y_0; t) = \frac{1}{\rho c^2} P_1(r_0) P_2(r_0) \cos[\Delta\omega t + \Delta\psi(r_0)], \quad (8)$$

where arguments x_0 and y_0 are added to denote the position of the point target, and $r_0 = \sqrt{x_0^2 + y_0^2}$. Referring to (4) and (5), the complex amplitude of the stress field can be found as

$$\begin{aligned} F_{\Delta\omega}(x_0, y_0) = & \rho U_{01} U_{02} \frac{\pi a_1^2}{\lambda_1 z_0} \text{jinc} \left(\frac{r_0 a_1}{\lambda_1 z_0} \right) \times \\ & \left[\frac{\pi a_2^2}{\lambda_2 z_0} \text{jinc} \left(\frac{r_0 a_2}{\lambda_2 z_0} \right) - \frac{\pi a_2'^2}{\lambda_2 z_0} \text{jinc} \left(\frac{r_0 a_2'}{\lambda_2 z_0} \right) \right] \times \\ & \exp \left(-j \frac{r_0^2}{2\Delta\lambda z_0} \right), \end{aligned} \quad (9)$$

where $\Delta\lambda = 2\pi c/\Delta\omega$ is the wavelength associated with $\Delta\omega$. The above equation indicates that the radiation stress is concentrated at the focal point and decays quickly as $\text{jinc}(\cdot)^2$. It should be

noted that because $f_{\Delta\omega}(x_0, y_0; t)$ and $F_{\Delta\omega}(x_0, y_0)$ are defined per unit point target, they have the dimension of force per unit area, or equivalently the unit of stress. As an example, we consider a confocal transducer with dimensions $a_1 = 14.8$ mm, $a'_2 = 16.8$ mm, $a_2 = 22.5$ mm, and the focal length 70 mm. Also, we assume that the center frequency is 3 MHz, and the difference frequency is 7.3 kHz. The radiation stress at the focal plane of this transducer is plotted in fig. 7.

In medical applications the maximum ultrasonic intensity is regulated for safety reasons. It is therefore useful to write the stress field in terms of the peak ultrasonic intensity at the focal point. The long-term average of ultrasonic intensity at the focal point can be written as

$$I(0) = \frac{P_1^2(0) + P_2^2(0)}{2\rho c}, \quad (10)$$

where $P_1(0)$ and $P_2(0)$ can be found from (4) and (5) as

$$I(0) = \frac{\rho c}{2} \left[U_{01}^2 \left(\frac{\pi a_1^2}{\lambda_1 z_0} \right)^2 + U_{02}^2 \left(\frac{\pi}{\lambda_2 z_0} \right)^2 (a_2^2 - a_2'^2)^2 \right], \quad (11)$$

Assuming $U_{01} = U_{02} = U_0$, we can write the focal plane stress field in terms of $I(0)$:

$$\begin{aligned} F_{\Delta\omega}(x_0, y_0) = & \frac{2I(0)}{c} \times \frac{\frac{\pi a_1^2}{\lambda_1 z_0}}{\left(\frac{\pi a_1^2}{\lambda_1 z_0} \right)^2 + \left(\frac{\pi}{\lambda_2 z_0} \right)^2 (a_2^2 - a_2'^2)^2} \times \\ & \text{jinc} \left(\frac{r_0 a_1}{\lambda_1 z_0} \right) \left[\frac{\pi a_2^2}{\lambda_2 z_0} \text{jinc} \left(\frac{r_0 a_2}{\lambda_2 z_0} \right) - \frac{\pi a_2'^2}{\lambda_2 z_0} \text{jinc} \left(\frac{r_0 a_2'}{\lambda_2 z_0} \right) \right] \times \\ & \exp \left(-j \frac{r_0^2}{2\Delta\lambda z_0} \right). \end{aligned} \quad (12)$$

The first fraction in the above equation represents the static radiation force produced by the two beams on a total absorber, the second fraction is a constant factor, and the rest represents the spatial distribution of the stress field on the focal plane. If $\Delta\omega \ll \omega_2$, then we may replace λ_1 and λ_2 by with λ_0 , and simplify the expression for the stress field. Under these conditions, the stress at the focal point is

$$F_{\Delta\omega}(0, 0) = \frac{2I(0)}{c} \times \frac{a_1^2 (a_2^2 - a_2'^2)}{a_1^4 + (a_2^2 - a_2'^2)^2}. \quad (13)$$

The fraction on the right represents the effect of transducer dimension on the stress field. For the transducer used in the previous example, the value of this fraction is 0.4999. (This fraction can be also calculated for a single element transducer of the same diameter excited by an amplitude modulated signal. For this purpose, we may let $a_1 = a_2$ and $a_2' = 0$. For these values, the last fraction in (13) is 0.5.) The resulting radiation stress (assuming $c = 1500$ m/sec for water) is $F_{\Delta\omega}(0, 0) = 6.67 \times 10^{-4} I(0)$ N/m². Now letting $I(0) = 7200$ W/m², which is the intensity suggested by FDA for safe *in vivo* applications, the resulting stress at the focal point is $F_{\Delta\omega}(0, 0) = 4.80$ N/m². Referring to fig. 7, we note that this stress field is applied only in a small region around the focal point to the object.

3.3.2.1 Acoustic Emission

To explain the acoustic emission we consider an "object" within a homogeneous infinite medium. This model allows us to separate the roles played by the parameters of the object and the surrounding medium. Also, this model can be fitted to various applications. When an oscillating stress field is applied to the object, the object vibrates at the frequency of the stress field. Vibrational energy of the object is partly transferred to the surrounding medium, resulting in an acoustic emission field. Here, we calculate the acoustic emission of an object subjected to cyclic radiation stress.

To explain the physics in an analytical form, we consider a flat plate facing the beam. Here, we assume that the vibrating object has a circular cross section of radius b and uniformly vibrates back and forth like a piston. We also consider an area $S \leq \pi b^2$ of the piston surface to be projected normally to the beam. We can always return to our elementary point object by reducing the area of this disk to $dxdy$. Similar solutions can be carried out for objects of other forms. The theory can be also extended to include arbitrary vibrating-part shapes and non uniform displacement of the object. The total radiation force on this object $\overline{F_{\Delta\omega}}$, can be found by integrating the radiation stress over the area of the object. This force vibrates the target object at frequency $\Delta\omega$. The steady state normal velocity amplitude of a piston at frequency $\Delta\omega$, $U_{\Delta\omega}$, due to a harmonic force $\overline{F_{\Delta\omega}}$, can be written as

$$U_{\Delta\omega} = \frac{\overline{F_{\Delta\omega}}}{Z_{\Delta\omega}}, \quad (14)$$

where $Z_{\Delta\omega}$ is the mechanical impedance of the object at $\Delta\omega$. The mechanical impedance of the object has two components, one resulting from the inertia, friction, and the elasticity of the object itself, and the other resulting from the loading effect of the surrounding medium on the vibrating object. The mechanical impedance can be interpreted as a measure of object rigidity and how much it yields to the applied force. For example, for a rigid object, $Z_{\Delta\omega}$ is high, and hence resisting the force.

Knowing $U_{\Delta\omega}$, we can calculate the pressure field it produces in the medium. We assume that the acoustic emission signal propagates in a free and homogenous medium. The farfield acoustic pressure due to a piston source of radius b set in a planar boundary of infinite extent is given by [17],

$$P_{\Delta\omega} = -j\Delta\omega\rho \frac{\exp(j\Delta\omega l/c)}{4\pi l} \left[\frac{2J_1\left(\frac{\Delta\omega b}{c} \sin \vartheta\right)}{\frac{\Delta\omega b}{c} \sin \vartheta} \times \frac{\cos \vartheta}{\cos \vartheta + \beta_B} \right] (2\pi b^2 U_{\Delta\omega}), \quad (15)$$

where l is the distance from the observation point to the center of the piston, ϑ is the angle between this line and the piston axis, and β_B is the specific acoustic admittance of the boundary surface (the specific acoustic admittance is $\beta_B = \frac{\rho c}{Z_B}$, where Z_B , the acoustic impedance of the boundary, represents the ratio between the pressure and normal fluid velocity at a point on the object). The factor two comes from the presence of the boundary wall. It would be replaced by unity if the boundary wall were not present [17].

The acoustic emission field resulting from object vibration can be written in terms of object mechanical impedance by combining (14) and (15), as

$$P_{\Delta\omega} = \rho c^2 \left\{ j \frac{\Delta\omega}{c^2} \times \frac{\exp(j\Delta\omega l/c)}{4\pi l} \left[\frac{2J_1\left(\frac{\Delta\omega b}{c} \sin \vartheta\right)}{\frac{\Delta\omega b}{c} \sin \vartheta} \times \frac{\cos \vartheta}{\cos \vartheta + \beta_B} \right] \right\} \times \frac{2\pi b^2}{Z_m} \overline{F_{\Delta\omega}}. \quad (16)$$

For wavelengths long compared to the object size, i.e., when $b\Delta\omega/c \rightarrow 0$, the term in the bracket approaches a constant, hence we may consider the contents of the brace to be an object independent function (the specific acoustic admittance β_B relates to the surrounding boundary surface). Under these conditions, the brace in the above equation represents the effect of the medium on the acoustic emission field, which we may call the *medium transfer function*, and denote it by

$$H_{\Delta\omega}(l) = j \frac{\Delta\omega}{c^2} \times \frac{\exp(j\Delta\omega l/c)}{4\pi l} \times \frac{\cos \vartheta}{\cos \vartheta + \beta_B}. \quad (17)$$

The last fraction in (16) includes $\frac{1}{Z_{\Delta\omega}}$, which is the mechanical admittance of the object at the frequency of the acoustic emission ($\Delta\omega$), and we denote this by $Y_{\Delta\omega}$. It is convenient to combine this term with the next term ($2\pi b^2$) in (16), as $Q_{\Delta\omega} = 2\pi b^2 Y_{\Delta\omega} = 2\pi b^2 / Z_{\Delta\omega}$, which is the total acoustic outflow by the object per unit force (acoustic outflow is the volume of the medium, e.g., the fluid, in front of the object surface that is displaced per unit time due to object motion). Function $Q_{\Delta\omega}$ represents the object characteristics at the acoustic frequency. We may thus rewrite (16) in a more compact form as

$$P_{\Delta\omega} = \rho c^2 H_{\Delta\omega}(l) Q_{\Delta\omega} \overline{F_{\Delta\omega}}. \quad (18)$$

Equation 18 indicates that the acoustic emission pressure is proportional to: a) the radiation force, which itself is proportional to the square of ultrasound pressure and the ultrasound characteristics of the object, d_r , in the projected area S ; b) the acoustic outflow by this object, $Q_{\Delta\omega}$, representing the object size b and its mechanical admittance at the acoustic frequency, $Y_{\Delta\omega}$; and c) the transfer function of the medium at the acoustic frequency, $H_{\Delta\omega}(l)$. Note the difference between the projection area S and the vibrating area πb^2 . The projection area determines the extent of the force applied to the object (1). The vibrating area, however, influences the total acoustic outflow in the medium caused by object vibration.

3.3.3 Applications

Evaluating the characteristics of an object (or a medium) by listening to its sound is a traditional approach that has been used for many purposes. Qualitative evaluation of a crystal glass by tapping on it is a simple example. Vibro-acoustography implements the same approach but in micro-scale, and in a way that could be applied to tissues.

Equation 18 presents a general relationship between the mechanical parameters of the objects, surrounding medium, and the acoustic emission field resulting from object vibration. By measuring the acoustic emission field, it would be possible, in principle, to estimate some of the object or medium parameters, either in absolute or in relative sense. For example, one can use vibro-acoustography to measure the resonance frequency of an object, and from that information it is possible to estimate some viscoelastic parameters of the object or the medium. This method has been used to measure the Young's modulus of a metallic rod [19]. In another experiment, by measuring the resonance frequency of a known resonator in a liquid medium, the viscosity of the fluid has been estimated with good accuracy [20]. These applications are not necessarily medical, but the principle could be used for evaluation of soft tissues, blood, bone, etc.

In medical applications, one can use vibro-acoustography to obtain images of human body for diagnostic purposes. In such applications, the image may not represent a physical quantity, rather it provides a means to visualize object details. To demonstrate the capability of vibro-acoustography, we used this method to image a specimen of human iliac artery that included calcifications. A 3MHz confocal transducer with dimensions $a_1 = 14.8$ mm, $a'_2 = 16.8$ mm, $a_2 = 22.5$ mm, and the focal length of 70 mm, was used for this experiment. The difference frequency was set at 44 kHz. Figure 9 shows a photo of the artery that is cut open. The areas with calcification are marked by letter "C". The vibro-acoustic image of the same artery is shown on the right. Calcium deposits, which are formed in large (a few mm to a few cm long) and stiff (compare to the arterial wall) plates, are efficient acoustic radiators, producing strong acoustic emission when they are exposed to the radiation force of the incident ultrasound. Hence, they stand out in the vibro-acoustography image. The vibro-acoustic image has high resolution, no speckle, and high signal-to-noise ratio. These features allow vibro-acoustography to delineate calcium deposits with high definition and contrast.

4. Capabilities and Limitations

Although the methods described above tend to estimate the mechanical properties of the object, the quantities they measure are different. The quantity measured in the transient method is somewhat arbitrary, and not a direct measure of any physical quantity. The merit of this method is that tissue hardness is measured from relative displacement values, without the need to measure the applied force. The shear wave method directly measures a physical parameter of the material in an absolute sense. The acoustic emission field measured in vibro-acoustography is a function of several physical parameters that relate to the object and the surrounding medium. It is possible to measure a single parameter only if one has enough knowledge about other parameters involved. For example, one can measure the shear viscosity of a liquid using a known resonator as an object in the liquid [20], or, for a given the geometry, the Young's modulus of a metallic object can be measured [19] by vibro-acoustography.

Detection sensitivity is critical to the success of any of the above methods. Greater ultrasound intensity would be needed if the detection sensitivity is poor. As a result, the peak ultrasound intensity at focal area may be limited by the safe *in vivo* limit. Ultrasound Doppler methods,

at conventional ultrasound frequencies, probably can detect displacements in the order of a few micrometers. The sensitivity of the MRI technique is in the order of 100 nm [2]. Vibro-acoustography has been shown to detect motions as small as a few nanometers [15]. The high sensitivity of this method is a result of the fact that small motions of the object can produce an acoustic emission pressure field that is easily detectable by a sensitive hydrophone.

Image spatial resolution is an important parameter when assessing the capability of an imaging method in delineating fine structures in the object. Vibro-acoustography can be used for high quality imaging. The spatial resolution is proportional to the width of the stress field main lobe. For example, for the 3 MHz ultrasound transducer presented in fig. 7, the spatial resolution is about 700 micrometers. Imaging complex objects using the transient or the shear wave methods have not been fully explored in the literature.

Performance of each method is partly influenced by viscoelastic properties of the material. Both the transient and shear wave methods work best if the material under test supports the shear wave, has enough attenuation to allow the build up of enough radiation force, and is compliant enough to allow appreciable displacement. Application of these methods for hard material, such as bone and calcifications, would be difficult or impractical because: a) stiff materials have low compliance, hence their displacement in response to the force is relatively small and difficult to detect; b) the shear wave travels at high speed in such material. In vibro-acoustography hard materials produce structural vibrations which are often stronger than that of soft tissue. Such vibrations result in strong and easily detectable acoustic emissions. The bright appearance of the arterial calcifications in the experiment presented in [15] is a demonstration of this phenomenon. Vibro-acoustography can be used to detect particles in materials that do not support shear waves, for example, detecting gas bubbles in liquids. The acoustic emission resulting from particle vibration includes a compressional wave component that can travel in the surrounding medium including the liquid. Tissue attenuation for compressional waves at low frequencies is small, hence such waves can be detected by the hydrophone from a distance. Shear waves in liquid medium decay very rapidly and are difficult to detect by most methods.

The ultimate goal of viscoelastic parameter imaging methods is to measure these parameters in human body. *In vivo* application of the transient method is not clear because it requires high ultrasound power to produce a detectable displacement. Application of the shear wave method in human body largely depends on the detection method used. Optical methods are not likely usable *in vivo*. MRI detection methods are generally complex, especially when the technique is to be linked to the ultrasound system in the magnetic field. Ultrasound Doppler is a more practical detection method for shear wave detection, however its sensitivity may not be sufficient for ultrasound intensities in the safe limit [7]. Vibro-acoustography uses a hydrophone for detection which is simple to operate in clinical settings. It however requires an acoustically quiet environment for proper detection. The biological noise spectrum seems to be below 1 kHz, which can be easily filtered out if the operation frequency is above this limit [15].

Before any of the methods discussed here are used in the in human body, one must be certain that the ultrasound exposure does not harm the subject. Vibro-acoustography uses either CW

or tone burst ultrasound. Therefore, the continuous ultrasound intensity (spatial peak temporal average intensity) limit must be observed for the safety reasons. This limit according to the FDA is 720 mW/cm^2 . However, because of the high sensitivity of hydrophone detectors, it is possible to detect very small levels of the acoustic emission while using low transmit power. For example, it is shown that a submillimeter object can be detected at ultrasound intensities far below the FDA limit [16]. The shear wave method presented in [6] uses high intensity pulsed ultrasound for excitation and either the optical or MRI methods for detection. It is argued that, although the intensity is high, the total exposure is within the FDA limits. However, *in vivo* use of such detection methods would be difficult. Using Doppler ultrasound for detection is less sensitive, hence requires higher peak ultrasound intensity to produce enough radiation force on the tissue. This intensity level may exceed the safe spatial peak pulse average intensity limit.

5. Summary

Radiation force or ultrasound is a non invasive means for introducing highly localized vibrating force inside tissue. The three methods described here utilize this tool to evaluate the dynamic viscoelastic properties of tissue. The transient method measures minute transient tissue deformation versus time. The shear wave method measures the amplitude and velocity of the shear waves resulting from excitation by radiation force. Finally, Vibro-acoustography measures the acoustic field resulting from object vibration at a specified frequency.

6. Acknowledgments

This work was supported in part by grant BC971878 from the Army Medical Research and Materiel Command and grant HL 61451 from the National Institutes of Health.

7. References

1. Gao L, Parker KJ, Lerner RM, Levinson SF. Imaging of the elastic properties of tissue — a review. *Ultrasound Med Biol* 1996 22(8): 959–77.
2. Muthupillai R, Lomas DJ, Rossman PJ, Greenleaf JF, Manduca A, Ehman RL. Magnetic resonance elastography by direct visualization of propagating acoustic strain waves. *Science* 1995 269: 1854–7.
3. Chu B-T, Apfel RE. Acoustic radiation pressure produced by a beam of sound. *J Acoust Soc Am* 1982 72(6): 1673–87.
4. Sugimoto T, Ueha S, Itoh K. Tissue hardness measurement using the radiation force of focused ultrasound. 1990 IEEE Ultrasonics Symposium Proceedings 1990 3: 1377–80.
5. Andreev V, Dmitriev V, Rudenko OV, Sarvazyan A. A remote generation of shear wave in soft tissue by pulsed radiation pressure. *J Acoust Soc Am* 1997 102: 3155 (Abst).
6. Sarvazyan AP, Rudenko OV, Swanson SD, Fowlkes JB, Emelianov SY. Shear wave elasticity imaging: a new ultrasonic technology of medical diagnostics. *Ultrasound Med Biol* 1998 24(9): 1419–35.

7. Walker WF. Internal deformation of a uniform elastic solid by acoustic radiation. *J Acoust Soc Am* 1999 105: 2508-18.
8. Lord Raleigh. *Philos Mag* 3, 338-346, 1902. Also, see: Lord Raleigh. *Philos Mag* 1905 10: 364-74.
9. Beyer RT. Radiation pressure—the history of a mislabeled tensor. *J Acoust Soc Am* April 1978 63(4): 1025-30.
10. Rudenko OV, Sarvazian AP, Emelionov SY. Acoustic radiation force and streaming induced by focused nonlinear ultrasound in a dissipative medium. (May 1996) *J Acoust Soc Am* May 1996 99(5): 1-8.
11. Jiang Z-Y, Greenleaf JF. Acoustic radiation pressure in a three-dimensional lossy medium. *J Acoust Am* August 1996 100(2, Pt. 1): 741-7.
12. Westervelt PJ. The theory of steady force caused by sound waves. *J Acoust Soc Am* May 1951 23(4): 312-5.
13. Goss SA, Johnston RL, Dunn F. Comprehensive compilation of empirical ultrasonic properties of mammalian tissues. *J Acoust Soc Am* 1978 64(2): 423-57.
14. Frizzell LA, Carstensen EL. Shear properties of mammalian tissues at low megahertz frequencies. *J Acoust Soc Am* 1976 60(6): 1409-11.
15. Fatemi M, Greenleaf JF. Ultrasound-stimulated vibro-acoustic spectrography. *Science* 1998 280, 82-5.
16. Fatemi M, Greenleaf JF. Vibro-acoustography: An imaging modality based on ultrasound-stimulated acoustic emission. *Proc Natl Acad Sci USA (PNAS)* 1999 96:6603-8.
17. Morse PM, Ingard KU, editors. *Theoretical Acoustics*. New York: McGraw Hill, 1968.
18. Kino GS, editor. *Acoustics Waves: Devices, Imaging, and Analog Signal Processing*. Englewood Cliffs, NJ: Prentice-Hall Signal Processing Series, 1987.
19. Fatemi M, Greenleaf JF. Application of radiation force in noncontact measurement of the elastic parameters. *Ultrasonic Imaging* April 1999 21(2): 147-54.
20. Fatemi M, Greenleaf JF. Remote measurement of shear viscosity with ultrasound-stimulated vibro-acoustic spectrography. *Acta Physica Sinica* August 1999 8:S27-S32.

8. Legends

Figure 1 Tissue elasticity evaluation and imaging methods. These methods can be divided into two general groups. The static group employs a steady force to deform the object. The dynamic group use either a momentary or an oscillating force to vibrate the object and can be divided into two subgroups. Mechanical drive methods use a mechanical actuator, whereas the radiation force drive methods use the radiation force of ultrasound to excite the object. The latter subgroup is divided into three sub-subgroups based on the detection method used. Vibro-acoustography uses a hydrophone to detect object response.

Figure 2 Radiation force produced by projection of ultrasound on an object. Interaction of an ultrasound beam with an object that scatters and/or absorbs results in a force on the object in the beam direction. The magnitude of this force is proportional to the time average energy density of the incident beam and a factor that represents the scattering and absorbing properties of the object.

Figure 3 Principle of the transient method. The excitation transducer produces a momentary radiation force which induces a minute deformation in the object. Doppler methods are used to measure this deformation using the probe transducer.

Figure 4 Principle of shear wave elastography. The focused ultrasound beam is absorbed by the object, resulting a localized radiation stress, which squeezes the elastic object. This deformation propagates in the form of shear waves through the object. The phase sensitive MRI machine detects the spatial distribution of the resulting displacement in the object.

Figure 5 Principle of vibro-acoustography. The ultrasound beam is used to produce a localized oscillatory radiation stress to vibrate the object. Vibration of the object produces an acoustic emission field in the medium. This field, which is a function of the viscoelastic properties of the object, is detected by a sensitive hydrophone.

Figure 6 The coordinate system describing the position of the ultrasound beam and the observation point relative to the object. The beam travels in the z-direction.

Figure 7 Normalized stress field of the vibro-acoustography system with a 3 MHz confocal transducer.

Figure 8 Vibro-acoustography system. The object is vibrated by the radiation force of the confocal, two-beam transducer. Resulting vibrations are detected by the microphone (or hydrophone) and mapped into the image.

Figure 9 Vibro-acoustic image of an ex-vivo human iliac artery near the bifurcation. On the left is a photo of the cut-open artery specimen. Calcified areas are marked with letter "C". Vibro-acoustic image of the specimen is shown on the right. Calcified areas stand out as bright spots. This image was obtained with a 3 MHz confocal transducer as described in the text. The difference frequency was set at 44 kHz. The gray-level scale is in arbitrary units.

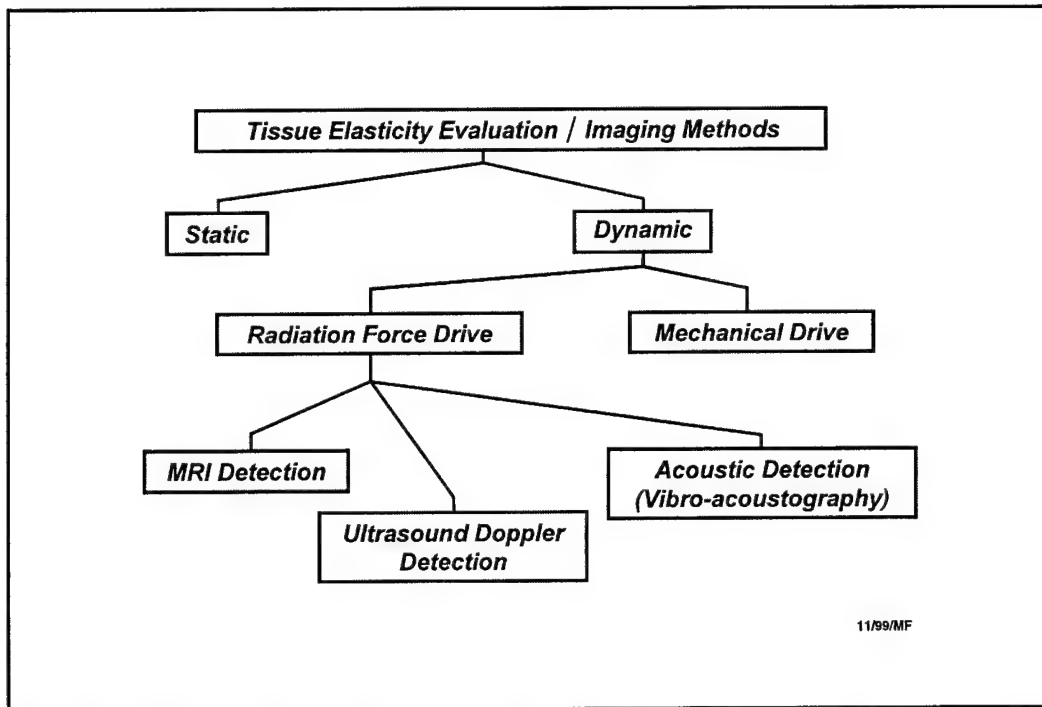


Figure 1

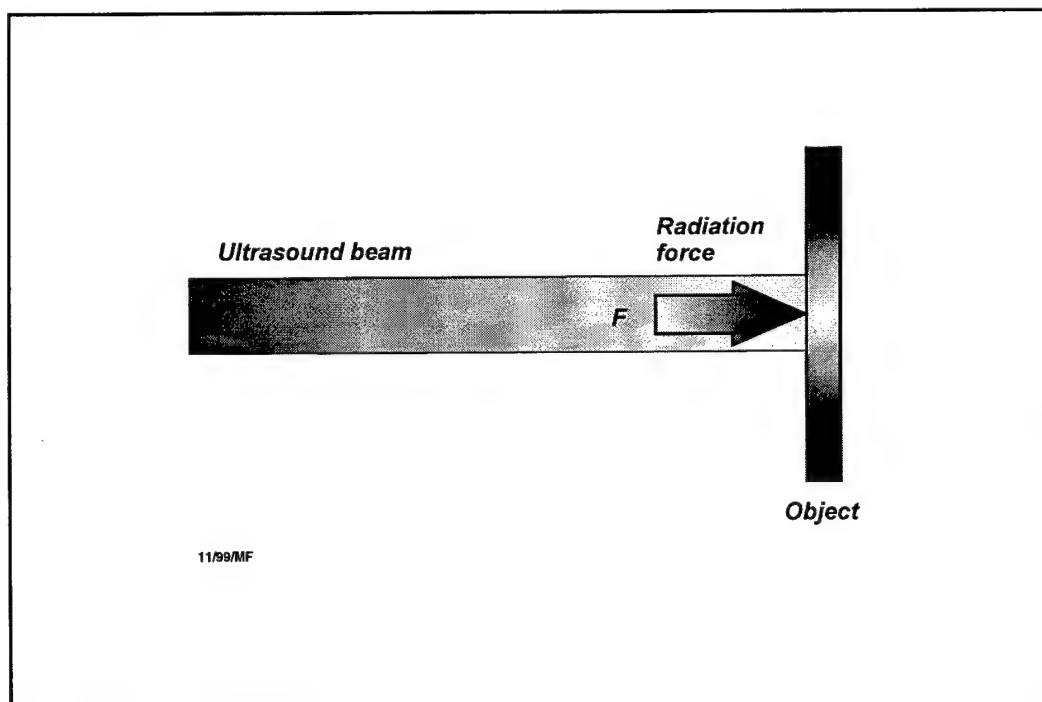


Figure 2

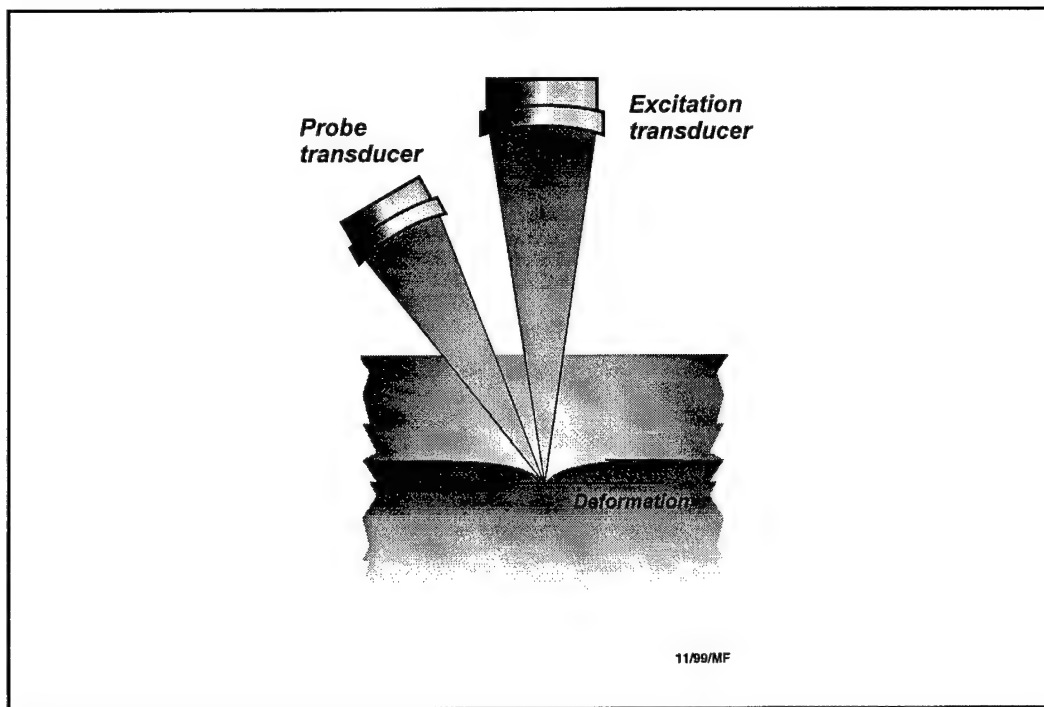


Figure 3

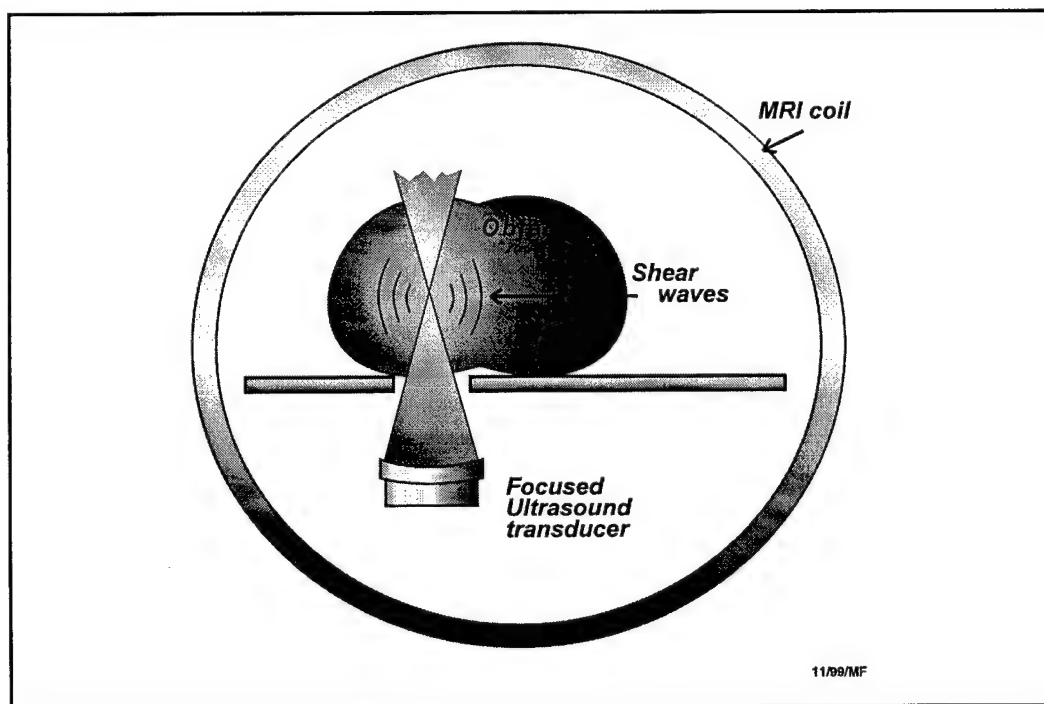


Figure 4

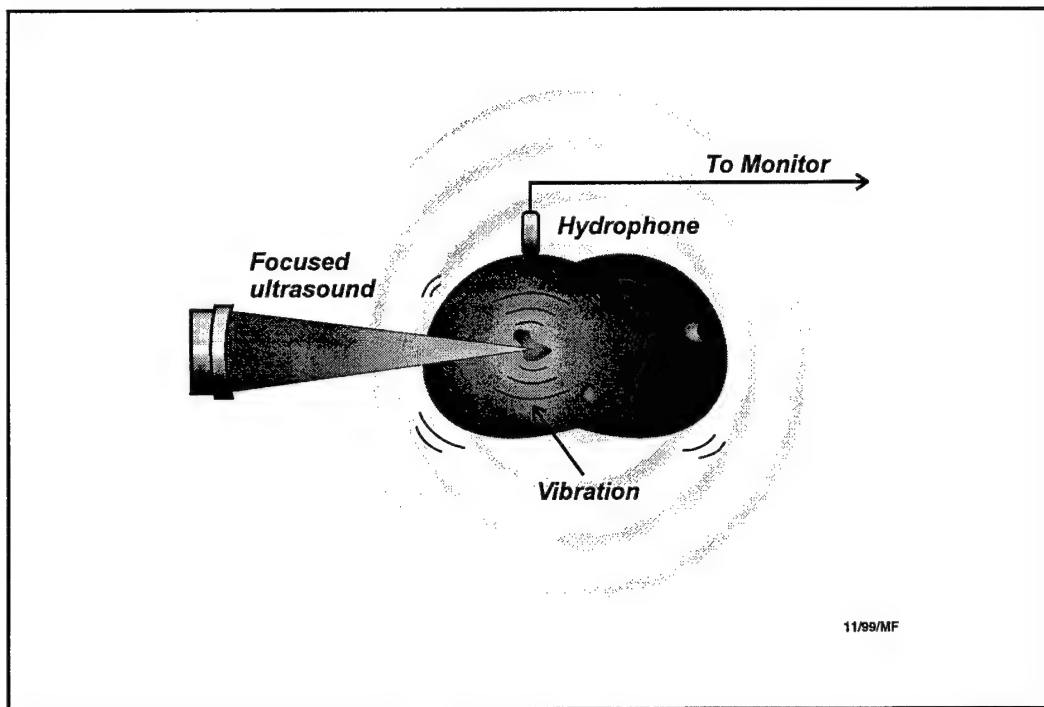


Figure 5

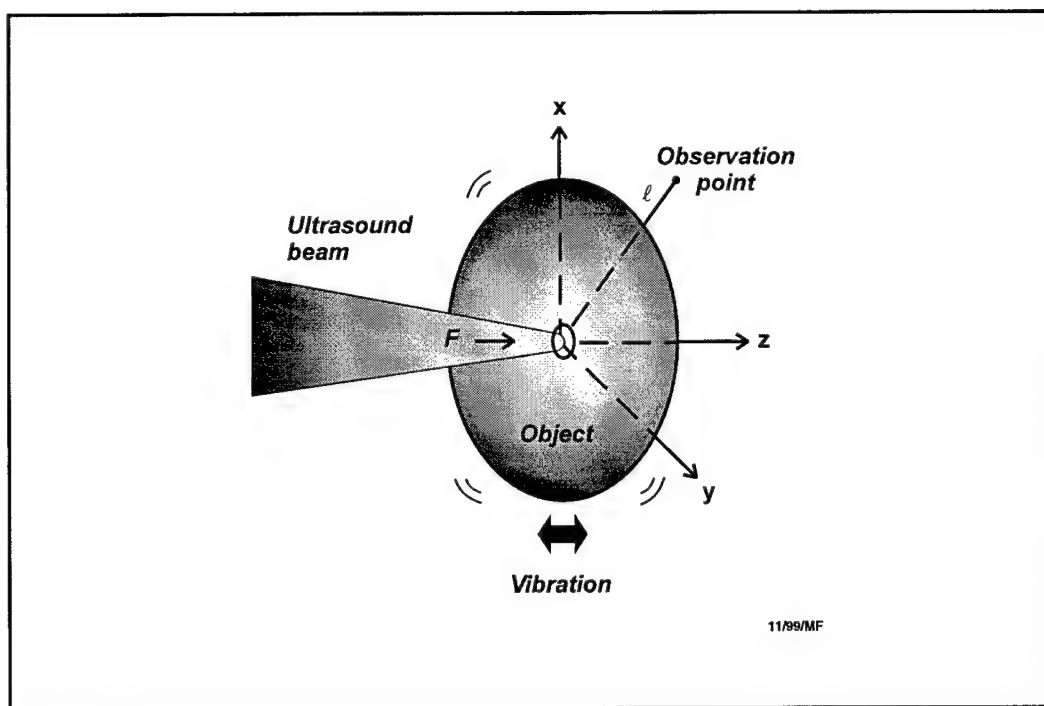


Figure 6

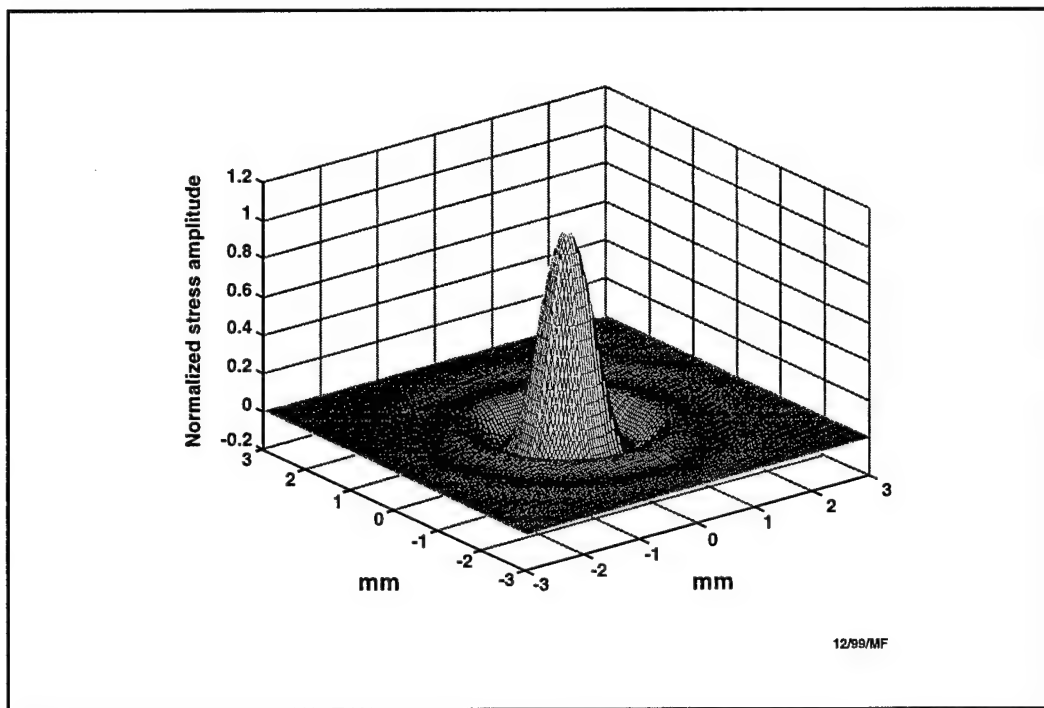


Figure 7

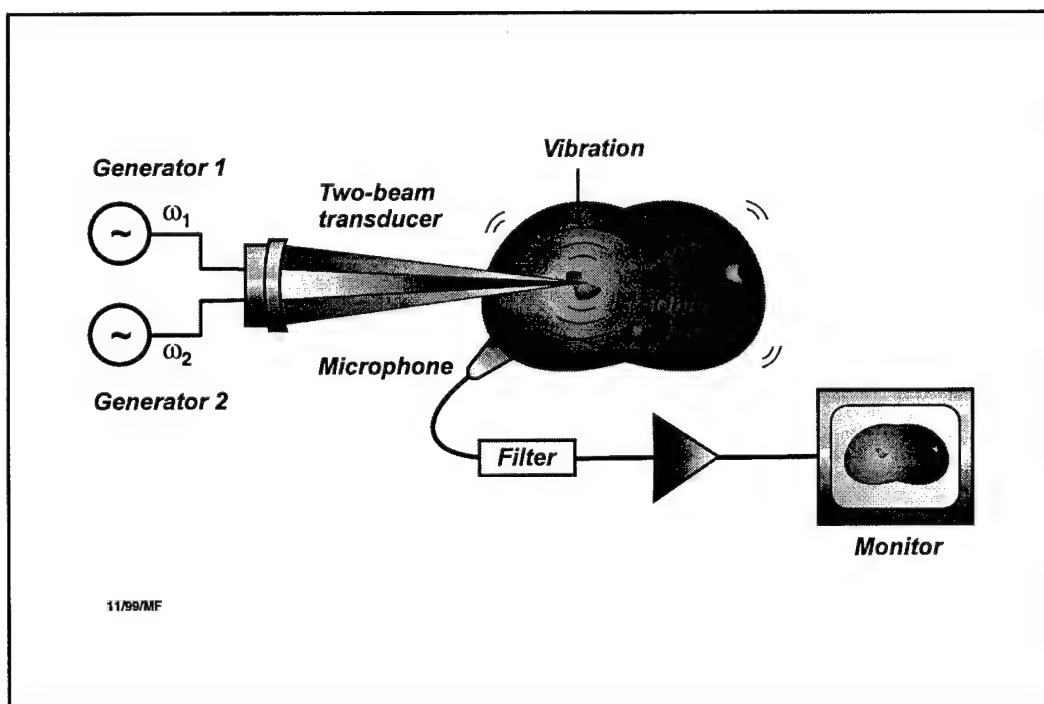


Figure 8

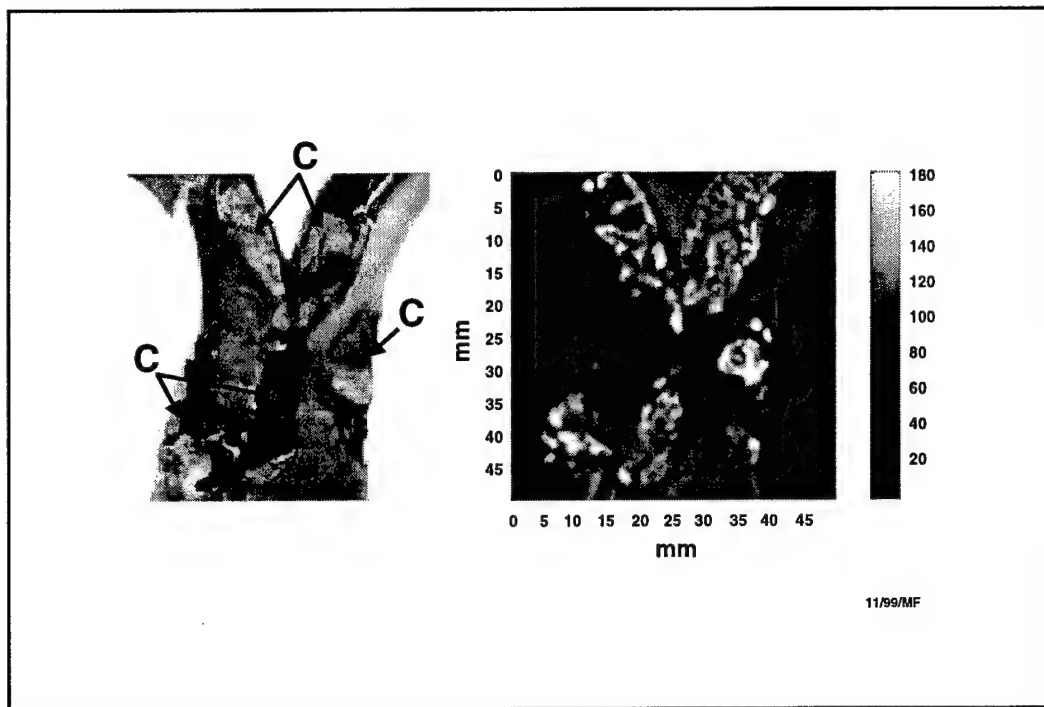


Figure 9

Application of Radiation Force in Noncontact Measurement of the Elastic Parameters

MOSTAFA FATEMI AND JAMES F. GREENLEAF

*Ultrasound Research
Department of Physiology and Biophysics
Mayo Clinic and Foundation
Rochester, MN 55905*

Ultrasound-stimulated vibro-acoustic spectrography is a recently-developed method that employs the radiation force of two intersecting continuous ultrasound beams to remotely vibrate an object at an arbitrary low frequency. Object vibration produces a sound field (acoustic emission) in the medium, which is a function of object mechanical properties. By measuring the acoustic emission field, one can obtain information about the mechanical parameters of the object. In this paper, we use this method for remote (noncontact) measurement of the dynamic Young's modulus of a rod based on its fundamental resonance frequency. Experimental results on an aluminum rod agree with the published data.

KEY WORDS: Acoustic emission; elasticity; noncontact measurement; radiation force; resonance; ultrasound-stimulated vibro-acoustic spectrography; Young's modulus.

INTRODUCTION

Estimation of material parameters using their mechanical response to externally-applied forces is of considerable interest in nondestructive inspection of materials, material science, and medical diagnosis. Normally, an applied force is used to produce displacement from which elastic constants, like spring constants, can be determined. In medical applications, ultrasound has been used to measure tissue displacement associated with externally applied compressive and cyclic forces.¹ In resonant ultrasound spectroscopy, an ultrasound source and a detector are used to measure the resonance frequencies of a sample with known size and mass. The resonances are related to mechanical parameters, including the elastic constants of the material.² In some applications, it is important to measure the elastic constants of a material at a particular frequency, since it is well known that the static and dynamic moduli of some materials, such as plastics, can differ substantially due to the existence of relaxation time effects that can make the modulus measured by the conventional quasi-static stress-strain curves significantly lower than the dynamic modulus. Acoustic resonators have been found to be valuable tools for investigating material properties. In general, resonance frequencies are functions of elastic constants and density, and resonator strength (or Q) is a function of the viscous loss and friction. Suitable measurement of the frequency response of resonators can therefore yield a wide range of information regarding the elastic properties and structure of materials. To study a material, normally a sample of known geometry, such as a rod or a tuning fork, is used. In the case of a rod, the Young's modulus can be determined from its resonance frequencies in various modes, such as flexural or longitudinal. The use of structures in their resonance modes insures high signal-to-noise ratio.³

Estimation of the elastic moduli by the resonance method requires some form of actuator and a motion detection device, such as piezoelectric or magnetic transducers.⁴ It has been realized that noncontact methods are superior to contact methods because contact with the object adds damping and stress, making object modeling more complex.³ Another consideration

is limitation in accessing the object when the object under test is very small compared to the measurement apparatus.

The Ultrasound-Stimulated Vibro-Acoustic Spectrography (USVAS) method³ utilizes a highly-localized radiation force,^{6,7} of two intersecting ultrasound beams to excite the object at arbitrary low frequencies and measures the frequency response of this object via a remote microphone. This method provides high spatial definition because it is capable of exerting an oscillatory force in a very small region of the object. This feature, plus the fact that object frequency response can be measured remotely, makes USVAS a potential candidate tool for material characterization.

In this paper, we introduce a noncontact technique, based on the USVAS method, for remotely measuring the Young's modulus of material. Here, we describe how ultrasound can be used to measure the Young's modulus of a metallic rod at frequencies much lower than the ultrasound frequency employed. This method allows us to avoid physical contacts in both the excitation and detection processes, while providing the convenience of accessing small objects and avoiding the surrounding structures by focusing the impinging ultrasound beam on the object. Our purpose is to present the methodology. Although the accuracy of the method can be similar to that of other resonance methods, we shall not focus on this issue here.

In the following sections, we will present the basic theory, method and some experimental results that show the utility of the method.

METHOD AND MATERIALS

Ultrasound-Stimulated Vibro-Acoustic Spectrography (USVAS)

When an acoustic wave is absorbed or reflected by an object, causing a change in the acoustic energy density, a steady force, which is called the radiation force, is exerted in the direction of the beam on that object. For a normal incident beam, the radiation force is given by:^{6,7}

$$F = d_r W / c \quad (1)$$

where W , c , and d_r are the total incident power on the object, speed of sound and a constant (the drag coefficient) that depends on the absorption and reflection properties of the object, respectively. The force decreases for incident angle less than 90° . For a total reflector, $d_r = 2$. For a total absorber, $d_r = 1$. When an amplitude modulated ultrasound beam impinges on the object, an oscillating radiation force is exerted on the object, causing vibration. This vibration is produced by direct conversion of ultrasound energy to low frequency elastic waves in the object. This conversion is a result of momentum change by the object. Noteworthy, neither the propagation medium nor the object material need to be acoustically nonlinear to allow such conversion.

USVAS employs the radiation force of two intersecting continuous ultrasound beams to remotely vibrate the object at an arbitrary low frequency.³ Object vibration produces a sound field that we named 'acoustic emission' in the medium, which is a function of object mechanical properties. The term 'acoustic emission' is used here to describe the acoustic field in response to a cyclic vibration of the object, and should not be confused with similar terminology used in the field of nondestructive testing of materials or in opto-acoustic imaging context, where 'acoustic emission' is used to describe the acoustic field resulting from structural deformation, cracking or thermal expansion of the object. By measuring the acoustic emission field, one can estimate some of the mechanical parameters of the object, including the elastic constants.

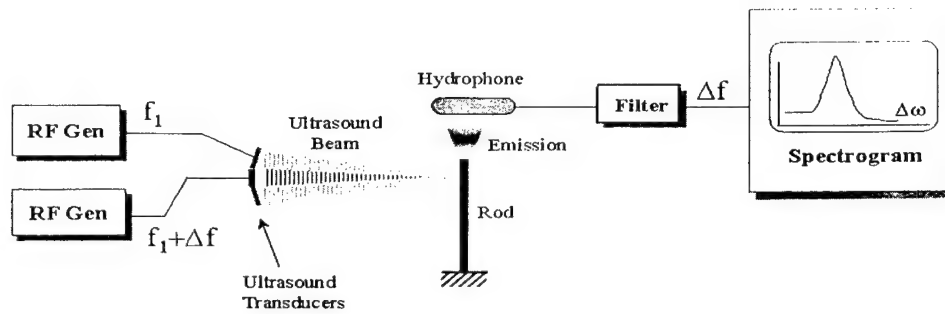


FIG. 1 USVAS system.

Figure 1 illustrates a USVAS system. The ultrasound energy is produced by means of a two-element confocal ultrasound annular array transducer, consisting of a center disc and an outer ring. The elements are driven by two cw sources, at frequencies equal to f_1 and $f_2 = f_1 + \Delta f$, where these frequencies are very close to the central frequency of the elements (f_0), and $\Delta f < f_0$. The beams interact only in a small region near the joint focal point. The object is placed at the joint focal point. The change in the energy density due to the reflection and absorption of ultrasound by the object produces a radiation force component in the beam direction on the object.⁷ This force oscillates at frequency Δf in response to the temporal changes in the energy density caused by pressure amplitude modulation. The oscillatory radiation force, in turn, vibrates the object at Δf . Object vibration elicits a sound field in the medium, which is received by a nearby microphone (or hydrophone) and recorded after digitization. Referring to reference 5, the amplitude of the acoustic emission signal $\Phi(\Delta f)$ can be written in terms of the frequency response of the object $Q(\Delta f)$ and the transfer function of the medium $H(\Delta f)$:

$$\Phi(\Delta f) = Cd_s H(\Delta f) Q(\Delta f) \quad (2)$$

where C is a constant proportional to the intensity of the impinging ultrasound beams. Hence, with some knowledge of $H(\Delta f)$, $\Phi(\Delta f)$ can be used to estimate $Q(\Delta f)$. This can be accomplished by sweeping Δf in the range of interest while keeping the amplitude of the impinging ultrasound fields constant. The resonance frequency(ies) of the object can be determined from the peak(s) of $Q(\Delta f)$. The positions of such peaks are independent of the constants C and d_s . In some applications, $H(\Delta f)$ may not be known or difficult to determine. Even, under these conditions we may still be able to use our method. That is because we only need to measure the resonance frequencies of $Q(\Delta f)$ — not the entire function of $Q(\Delta f)$. In many applications, the object is made to exhibit a sharp (high Q , or small relative bandwidth) resonances, which are indicated by sharp peaks in $Q(\Delta f)$, and hence, in $\Phi(\Delta f)$. In such cases, the positions of these peaks may not be sensitive to $H(\Delta f)$. Therefore, the resonance frequencies can be found directly from $\Phi(\Delta f)$, without a complete knowledge of $H(\Delta f)$. For example, assuming that we know $H(\Delta f)$ does not have a resonance within the frequency range of interest, then we can locate the resonance frequencies of the test object simply by determining the frequency values at sharp peaks of $\Phi(\Delta f)$.

Estimation of Young's modulus using the resonance frequency

To compress a rod (length l , square cross section, $b \times b$) by an amount dl requires a force $E_0 b^2 (dl/l)$, where the constant E_0 is called the Young's modulus⁸ and can be expressed in units of pressure. The Young's modulus of a material can be found by measuring the resonance

frequency of a rod made from that material. The resonance frequency depends on the boundary conditions of the rod, e.g., clamped on one end and free at the other, clamped at both ends, or free at both ends. A simple choice is to resonate a rod that is clamped at one end and free at the other. For this case, the Young's modulus of the rod, E_0 , can be calculated from the following relation:⁸

$$E_0 = 38.3 \frac{l^4 \rho}{b^2} f_R^2 \quad (3)$$

where f_R is the fundamental resonance frequency of the rod in vacuum and ρ is its mass density. In MKS units, E_0 is expressed in Newtons per square meter (or the pressure unit Pascal, Pa), l and b in meters, ρ in kilograms per cubic meter and f_R in Hz.

In practice, it is simpler to measure the resonance frequency of the rod in a fluid, like water. The resonance frequency in water is lower than in vacuum because of the loading effect of water mass. The resonance frequency in vacuum f_R can be calculated in terms of the resonance frequency in water (f_w) as:⁹

$$f_R = f_w \sqrt{1 + 119b^2 \rho_w / m} \quad (4)$$

where m is the mass per unit length of the rod, in kilograms per meter, and ρ_w is water density, in kilograms per cubic meter. The above derivation is not limited to square rods; similar relationships can be derived for nonsquare rods.

Excitation of a rod by the radiation force

Consider a rod, clamped at the bottom and free at the other end, placed in water. To vibrate the rod, we focus a modulated ultrasound beam on the free tip of the rod, with the beam axis in the direction of expected deflection of the rod. For a rod with a square cross section, we point the beam normal to one of the rod sides. The radiation force of the beam is applied to the rod via water molecules in the projected area. This force vibrates the rod; hence, the ultrasound energy is directly converted to vibrational energy in the rod. In contrast to some other resonance methods that use an attached actuator, this method excites the rod without any contact (except the surrounding liquid). Hence, there is no additional boundary condition imposed on the rod. The rod is free to vibrate (except at the clamped end) at its natural modes. Therefore, the position and the size of the excitation point along the length of the rod is immaterial, as long as it delivers the energy to the rod and the force is in the correct orientation. We also note that absorption of ultrasound by water can produce streaming.⁷ Streaming can potentially be another source of excitation to the rod. Because water absorption is low, we neglect this effect.

EXPERIMENT

The experimental setup is shown in figure 1. The free end of an aluminum alloy (Alloy 7129, Reynolds Metals Company, Richmond, VA) rod ($l = 6$ cm, $b = 9$ mm) was placed at the focal plane of the ultrasound beams in a water tank. The other end of the rod was screw clamped solidly to a heavy articulated frame that was rigid enough for the test. Water temperature was 18.5°C (not controlled).

The confocal transducer is constructed using a spherical piezoelectric cap. The two elements are constructed by dividing the back electrode of the piezoelectric wafer, with the radius of curvature to 70 mm, into a central disc and the outer ring, such that the elements have

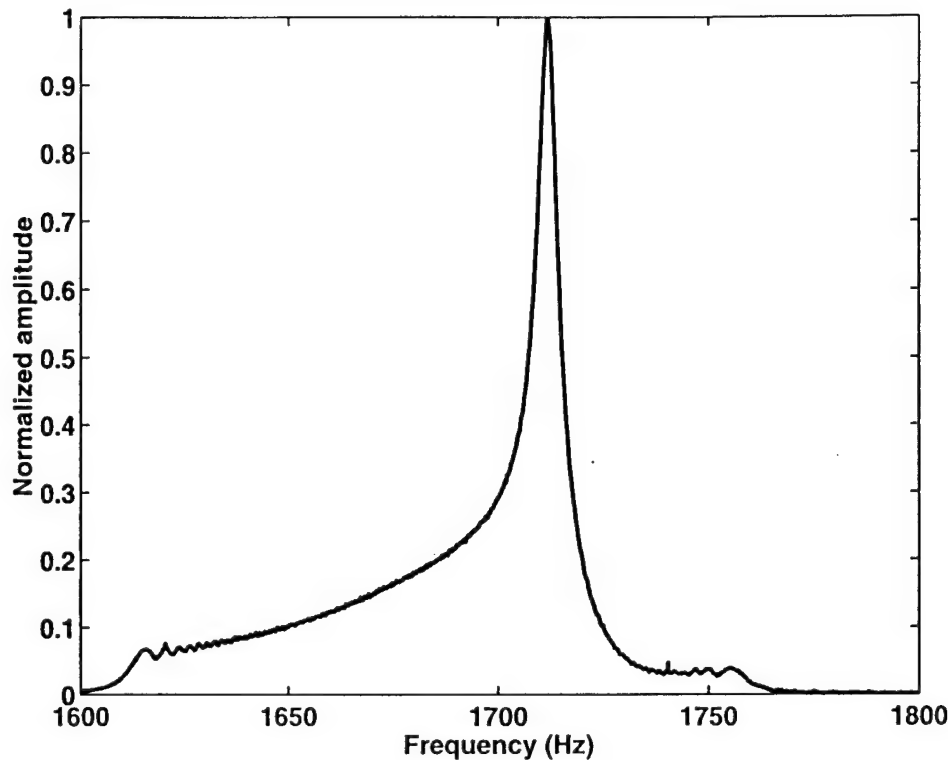


FIG. 2 Normalized frequency response of the rod in water.

identical beam axes and focal lengths. Radii of the elements are: $a_1 = 14.8$ mm (inner disc), $a_2 = 22.5$ mm (outer radius of the ring), and $a'_2 = 16.8$ mm (inner radius of the ring). The focal distance is 70 mm, and the center frequency, f_0 , is 3 MHz. The two beams emitted by this transducer interact at the focal region, producing an oscillatory radiation stress on the object in a circular area with a diameter of approximately $700 \mu\text{m}$.⁵ For a more detailed description of the stress field distribution on the target, refer to reference 10.

Transducer elements were driven by two stable rf synthesizers (HP 33120A and Analogic 2045) at frequencies of $f_1 = 3$ MHz and $f_2 = f_1 + \Delta f$, where Δf was swept slowly (in four seconds) from 1,600 to 1,800 Hz. The ultrasound intensity at the focal area was about 3.8×10^5 W/m². Sound produced by the object vibration was detected by a submerged audio hydrophone (ITC model 680, sensitivity: -154 dB re 1V/ μPa) placed within the water tank. The received signal was filtered and amplified by a programmable filter (Stanford Research Systems, SR650) to reject the noise, then digitized by a 12 bits/sample digitizer (HP model E1429A) at 20,000 samples per second. A total of 80,000 samples of acoustic emission data were recorded on a computer disc (Sun Sparc computer), and the spectrum was calculated using fast Fourier transform.

To ensure that the acoustics of the experiment set-up, including the water tank, was not affecting the estimation of the rod resonance frequency, we made an additional measurement with the rod replaced by a point object, consisting of a small glass bead (diameter < 0.5 mm), and obtained the resulting spectrum in the same frequency range (1,600-1,800 Hz). The glass bead was placed on a thin latex sheet. The latex sheet is almost transparent to the ultrasound, hence the radiation force on this sheet is negligible. The bead, however, presents a strong scatterer and acts as a point source when this sheet is vibrated by the radiation force.

RESULTS

Figure 2 shows the frequency response of the rod (acoustic emission amplitude versus frequency). The sharp peak indicating the fundamental resonance frequency of the rod in water, $f_w = 1,712$ Hz. Referring to Eq. (4), the corresponding resonance frequency in vacuum is $f_r = 2,051$ Hz. Finally, using Eq. (3), the Young's modulus of the aluminum alloy rod is found to be: $E_0 = 6.97 \times 10^{10}$ N/m² (or Pa). This value is in agreement with the value published¹¹ by the Aluminum Association for this aluminum alloy ($E_0 = 7 \times 10^{10}$ Pa), which is also close to the value for aluminum ($E_0 = 7 \times 10^{10}$ Pa) published in reference 11. The spectrum obtained from the glass bead showed no peaks in the frequency range of interest, and hence, validated our assumption that our measurement of ω was not influenced by the frequency response of the propagation medium.

DISCUSSION

The aim of this paper is to introduce a novel, noncontact method for evaluation of the dynamic Young's modulus of materials. This method employs the radiation force of ultrasound according to the USVAS technique to vibrate the object into its resonance. Hence, this method can be viewed as a resonance technique. Here, we discuss some features, advantages, limitations and applications of the method.

Measurement accuracy

Because the operation of the method is based on material resonance, its accuracy in measurement of the Young's modulus is basically similar to those of other resonance methods used for this purpose. In particular, since E_0 is proportional to the fourth power of l (Eq. (3)), accurate measurement of this parameter is of critical importance in the accuracy of the final result. The accuracy of this method can be improved by taking special care to measure the geometrical and frequency parameters with higher precision. However, we have not attempted to discuss these issues here.

In this paper, we used only one resonance frequency to determine the Young's modulus of the object. One can increase the accuracy of this method by measuring resonance frequencies in more than one mode. In that way, we have more data that relate to the same elastic parameter. This approach, in general, can lead to higher accuracy of the final result.³

Advantages

The main advantage of this method over other resonance methods is its capability of noncontact and remote excitation and detection. This can be desirable in a variety of applications, especially when the source of excitation and the detector must be set at some distance away from the resonator e.g., when measuring the elastic parameters of a material at high temperatures).

Another advantage of this method is its high sensitivity. Detection of object motion using the acoustic emission field can be very sensitive. It is shown that the hydrophone used in the experiment is sensitive enough to detect the acoustic emission due to oscillatory displacements of the order of a few nanometers.⁵ An implication of high sensitivity is that it allows the resonance to operate at its linear regime. It is well known that, at sufficiently high amplitudes, most resonators exhibit nonlinear behavior.^{12,13} Two common nonlinear phenomena are: a transition from sinusoidal to nonsinusoidal motion, which leads to harmonic genera-

tion, and a shift in the modal frequency. Modal frequencies can shift upwards or downwards at large amplitudes. If the effective spring constant of the resonator increases with amplitude, the frequency rises; if the effective spring constant decreases with amplitude, the frequency falls. This phenomena can, in general, lead to errors in estimation of the elastic constants by resonant methods. High sensitivity of motion detection in a USVAS system allows one to test the resonator at its linear regime by driving it at low oscillation amplitudes, and hence avoid the errors resulting from nonlinear behavior.

This method also offers high geometrical definition. By that, we mean it allows us to exert a dynamic force at a small projection region. The area of projection region depends on the characteristics of the ultrasound source, namely on the frequency and the aperture size. Having a small projection area is important when a miniaturized resonator is to be tested. The fact that the excitation is applied via a narrow ultrasound beam, permits system adaptability to a variety of resonator shapes.

Another advantage of USVAS is its relative insensitivity to the constituent material of the resonator. Since the method does not rely on electrical or magnetic properties of the resonator, it can be used to test a wide range of materials.

Practical issues

There are some issues to be considered when using USVAS to estimate the Young's modulus as proposed here. The frequency spectrum of the acoustic emission signal is a product of the object frequency response and the frequency response of the propagation medium (including the water tank).⁵ In order to assume that the latter would not have a major effect in determining the resonance frequency of the object, one must arrange the propagation medium to have a relatively flat frequency response in the vicinity of the object resonance frequency. Also a high Q (small relative bandwidth) resonating object would improve measurements precision. Temperature variations can change the Young's modulus of the object⁷ and the effect of water loading by changing the viscosity⁵. Therefore, the temperature needs to be controlled for more accurate estimation.

Limitations

The method presented here relies on the acoustic coupling of the medium to the resonator, both for excitation and detection. Hence, the acoustic properties of the medium surrounding the resonator are important in the success of the method. For example, the method can not operate in a vacuum. The method also fails if the acoustic path from the ultrasound source to the resonator is not suitable for directing the ultrasound beam. In practice, this might happen due to the existence of obstacles or high attenuation in the beam path.

Further applications

The method can also be used to study the variations of the elastic parameters with temperature. For this purpose, one can expand the method by adding a phase-locked-loop to the system to track the variations of the resonance frequency caused by temperature changes, in a temperature-controlled environment. The fact that the ultrasound source and the receiving hydrophone can be, in principle, thermally isolated while acoustically coupled to the object, provides the possibility of measuring the elastic moduli in a wide temperature range.

In some applications, air coupling may be preferred over liquid coupling, for example, to reduce the loading effects of the coupling medium or to measure the elastic parameters at high temperatures. In such cases, airborne ultrasound may be used. However, one must take into account the high attenuation and low sound speed of air when designing the system.

Taking advantage of the fact that soft tissues are good sound conductors, one may extend the principle presented here for biomedical applications, such as bone characterization. A modified version of the system may be used to measure the frequency response of the bone at low frequencies and evaluate its elastic parameters.

CONCLUSIONS

USVAS promises a new way for noncontact and remote measurement of the Young's modulus of materials. An airborne version of USVAS would provide further flexibility in applications where water coupling is not possible.

ACKNOWLEDGMENTS

Many thanks to Randall R.Kinnick for laboratory assistance, Thomas M.Kinter for software support, Elaine C.Quarve for secretarial assistance and Julie M.Patterson for graphic support.

REFERENCES

1. Gao, L., Parker, K.J., Lerner, R.M. and Levinson, S.F., Imaging of the elastic properties of tissue — a review, *Ultrasound Med. Biol.* 22, 959-977 (1996).
2. Maynard, J., Resonant ultrasound spectroscopy, *Physics Today*, 26-31 (1996)
3. Schindel, D.W., Hutchins, D.A. and Smith, S.T., A study of materials at high temperature using miniaturized resonant tuning forks and noncontact capacitance transducers, *J. Acoust. Soc. Am.* 102, 1296-1309 (1997).
4. Garrett, S.L., Resonant acoustic determination of elastic moduli, *J. Acoust. Soc. Am.* 88, 210-221 (1990).
5. Fatemi, M. and Greenleaf, J.F., Ultrasound stimulated vibro-acoustic spectroscopy. *Science* 280, 82-85 (1998).
6. Torr, G.R., The acoustic radiation force, *Am. J. Physics*, 52, 402-408 (1984).
7. Westervelt, P.J., The theory of steady force caused by sound waves, *J. Acoust. Soc. Am.*, 23, 312-315 (1951).
8. Morse, P.M.: *Vibration and Sound*, 3rd ed. (The Acoustical Society of America, USA, 1981).
9. Belvins, R.D., *Formulas for Natural Frequency and Mode Shape* (Van Nostrand Reinhold, New York, 1979).
10. Fatemi, M., and Greenleaf, J.F., Vibro-acoustography: an imaging modality based on ultrasound-stimulated acoustic emission, *Proc. Natl. Acad. Sci.* 96, 6603-6608 (1999).
11. Morse, P.M. and Ingard, K.U., *Theoretical Acoustics* (McGraw-Hill, New York, 1968).
12. Fletcher, N.H. and Rossing, T.D., *Physics of Musical Instruments* (Springer-Verlag, New York, 1991).
13. Rossing, T.D., Russell, D.A. and Brown, D.E., On the acoustic of tuning forks, *Am. J. Phys.* 60, 620-626 (1992).
14. *Aluminum Automotive Extrusion Manual* (Aluminum Association, Inc. Publication AT6, Washington, DC, Dec. 1998).

B-5 12:00 noon

POINT RESPONSE OF VIBRO-ACOUSTOGRAPHY SYSTEM

M. FATEMI* and J. F. GREENLEAF, Mayo Clinic and Foundation, Rochester, MN.

Vibro-acoustography is a method for imaging objects in terms of their response to a low frequency vibrational force [Science, 280(4):82-85, April 1998]. The vibrational force is produced by projecting an intensity modulated ultrasound beam on the object. The resulting radiation stress is highly localized and sufficiently strong to vibrate the object at the modulation frequency. Response of the system to a point object is of interest because it can be used to evaluate image resolution. The point response of a vibro-acoustography system is a function of the ultrasound beam shape. Here, we present system point response for three different beamforming methods: (1) single amplitude modulated beam; (2) x-focal method, in which two crossing single frequency ultrasound beams are used to generate a modulated field; and (3) confocal method which uses two coaxial single frequency beams. To compare the point responses, we considered the ultrasound sources used in these methods to be of equal areas. Theoretical results show that the confocal beam system has the smallest mainlobe width. The x-focal method offers the best sidelobe attenuation. The magnitude of the first sidelobes for single beam, confocal, and the x-focal systems are 17.6 dB, 19.5 dB, and 34.7 dB, below their respective mainlobes. Experimental results are in agreement with the theory.

This work was supported by grant DAMD17-98-1-8121 from the Army Medical Research and Material Command.

B-6 12:15 p.m.

COMPLEX-VALUED ABSOLUTE STIFFNESS ESTIMATION USING DYNAMIC DISPLACEMENT MEASUREMENTS AND LOCAL INVERSION OF CONSERVATION OF MOMENTUM

T. E. OLIPHANT*¹, J. L. MAHOWALD², R. L. EHMAN², and J. F. GREENLEAF¹
¹Ultrasound Research, Mayo Foundation, Rochester, MN, USA, and ²Magnetic Resonance Research, Mayo Foundation, Rochester, MN, USA.

It has been shown that elasticity can be estimated from direct displacement measurements measured using either ultrasonic or magnetic resonance (MRE) elastography methods. Most of the inversion techniques presented in the literature are based on inverting a displacement dataset that satisfies a static equation of shear motion resulting in only relative estimates of shear modulus. We present a robust method for estimating absolute shear-wave speed and attenuation from dynamic displacement data based on local inversion of the linearized differential equation satisfied by small-amplitude displacements in a source-free, possibly

VIBRO-ACOUSTOGRAPHY: SPECKLE FREE ULTRASONIC C-SCAN

James F. Greenleaf, Mostafa Fatemi and Randall R. Kinnick

Department of Physiology and Biophysics
Mayo Clinic and Foundation
Rochester, MN 55905 USA

INTRODUCTION

It is well known that changes in elasticity of soft tissues are often related to pathology. Traditionally, physicians use palpation as a simple method for estimating mechanical properties of tissue. The dynamic response of soft tissue to an oscillating or impulsive force is also valuable in medical diagnosis. For instance, rebound of tissue upon sudden release of pressure exerted by the physician's finger on the skin provides useful diagnostic information about the tissue. In vibro-acoustography ultrasound is used to produce an oscillating radiation force which then produces an acoustic response from tissues. Specifically acoustic energy is emitted from tissues in response to an oscillatory radiation force produced by interfering focused beams of ultrasound. Frequency spectra of ultrasound stimulated acoustic emission exhibit object resonances. Raster scanning the radiation force over the object and recording the amplitude and phase of the emitted sound results in data from which speckle free images related to elastic compositions of the acoustically emitting objects can be computed. We show here that intact and broken struts on prosthetic disk heart valves (convexo-concave Bjork-Shiley) can be distinguished by their resonant response to vibro-acoustography.

BACKGROUND

Quantitative measurement of the mechanical properties of tissues and their display in a raster format is the aim of a class of techniques generally called elasticity imaging or elastography (Gao et al., 1996). The general approach is to measure tissue motion caused by an external (or, in some methods, internal) force or displacement and use it to reconstruct the elastic parameters of the tissue. The excitation stress can be either static, or dynamic (vibration). Dynamic excitation is of particular interest because it provides more comprehensive information about tissue properties in a spectrum of frequencies. Because the motion is dynamic, derivatives of displacement in both space and time can be measured allowing the computation of elastic properties with low dependence on boundary condi-

tions. Magnetic resonance elastography is a recently developed method that employs a mechanical actuator to vibrate the body surface and then measures the strain waves with phase sensitive Magnetic Resonance Imaging resulting in a method termed Magnetic Resonance Elastography (Muthupillai et al., 1995). The majority of elasticity imaging methods are based on an external source of force, resulting in a spatially wide stress field distribution. This requires the stress field to pass through the superficial portion of the object before reaching the region of interest within the interior. This requirement can complicate estimation of stiffness because the stress field patterns vary with depth. An alternative strategy is to apply a stress directly to the localized region of interest. One way to accomplish this is to use the radiation pressure of ultrasound. An example is the use of ultrasound radiation pressure to vibrate the tissue and the use of MRI to measure the displacement (Sarvazyan et al., 1998 and Tau et al., 2000). The approach taken in this paper is to estimate the mode of vibration of an object from the acoustic emission resulting from the cyclic displacement.

Acoustic radiation force is the time average force exerted by an acoustic field on an object. This force is produced by a change in the energy density of an incident acoustic field (Beyer, 1978), for example, due to absorption or reflection. Several advantages may result from using ultrasound radiation force for evaluating tissue stiffness, including: a) acoustic (ultrasound) energy is a noninvasive means of applying force, b) current ultrasound technology and devices can be readily modified for this purpose, thus eliminating the need for developing a new technology, c) radiation force can be applied remotely inside tissue without disturbing its superficial layers, d) the radiation stress field can be localized, thus providing for precise positioning of the excitation point, and e) radiation force can be applied in a wide range of frequencies or temporal shapes. These features make radiation force methods highly attractive for creating remote stress fields within objects.

VIBRO-ACOUSTOGRAPHY THEORY

Study of radiation force and radiation pressure dates back nearly one century, to the time of Rayleigh (1902 and 1905). A historical review of radiation force and radiation pressure is presented in Beyer (1978), and a critical review of the subject can be found in Chu and Apfel (1982). Some recent developments of radiation force/pressure in attenuating medium, which may be applicable to biological tissues, are presented in Rudenko et al. (1996) and Jiang and Greenleaf (1996). Acoustic radiation force is a universal phenomenon in any wave motion that introduces some type of unidirectional force on absorbing or reflecting targets in the wave path. Radiation force in fluids is often studied in the context of radiation pressure. Definitions and theoretical developments of radiation force depend on the boundary conditions. Simple explanations of these definitions can be presented by considering a sound traveling inside, and along the axis of, a cylindrical container toward a wall (Beyer, 1978). Rayleigh radiation pressure is the excess pressure produced on the wall when the container's side wall is confining the fluid inside. Langevin radiation pressure is the excess pressure on the wall when the confining side wall is absent, so that the fluid is free to move. Here we will focus on Langevin radiation pressure because the conditions for which this pressure is defined apply to our experimental situation.

It can be shown that the Langevin radiation pressure of a plane wave impinging normally on a perfectly absorbing wall is equal to the total energy density $\langle E \rangle$, where $\langle \rangle$ represents the time average. If the wall is partially reflecting, this pressure would be equal to $(1+R)\langle E \rangle$, where R is the power reflection coefficient (Beyer, 1978). Thus, in general, we can write the radiation force of a normally impinging sound beam on a wall as $F = d_r \langle E \rangle$,

where F is the force in the beam direction, and d_r is the “radiation force function” or the drag coefficient. This dimensionless coefficient is defined per unit incident energy density and unit projected area. For a planar object, F is numerically equal to the force on the object. Physically, the drag coefficient represents the scattering and absorbing properties of the object (Westervelt, 1951). For a perfectly absorbing object, $d_r = 1$ and for a perfectly reflecting object $d_r = 2$. In the case of oblique incidence, the radiation force will have a normal as well as a transverse component. A more detailed description is presented in Westervelt (1951). To produce a time varying radiation force, the intensity of the incident beam can be modulated in various ways. For example, a short ultrasound pulse can produce a transient pulsed radiation force, and a sinusoidally modulated beam can result in a sinusoidally varying force.

METHODS

We interrogate the object by arranging the intersection of two focused continuous wave (CW) ultrasound beams of different frequencies to occur at a selected point on the object. Interference in the intersection region of the two beams produces sinusoidal modulation of the ultrasound energy density. Modulation of the energy density creates an oscillatory force, effectively vibrating the object at the selected region. The resulting vibration of the object produces an acoustic field (Fatemi and Greenleaf, 1998) that can be measured some distance away.

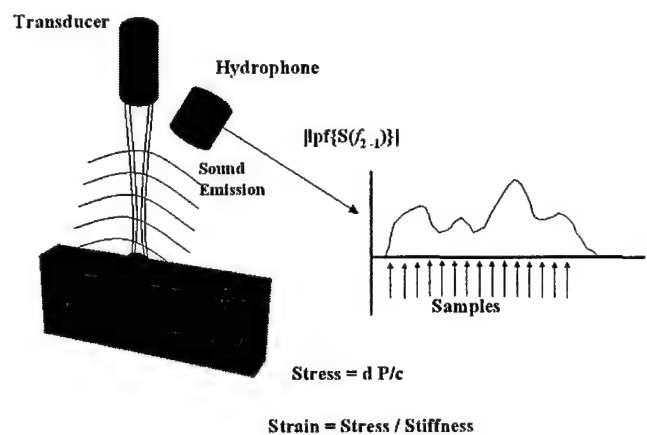


Figure 1. Ultrasound is made to interfere on the region of interest and the resulting acoustic emission is detected with a hydrophone or microphone to estimate the response of the object. The signal is digitized for analysis.

Ultrasound beams can be constructed in a variety of ways for this purpose (Fatemi and Greenleaf, 1999). We used two coaxial, confocal transducer elements of a spherically focused annular array (consisting of a central disc and an outer annulus) driven by two CW signals at slightly different frequencies f_1 and f_2 (Figure 1). The energy density at a point in this ultrasound field, say at the focus, is proportional to the square of the sum of the ultra-

sound fields from the two elements. Squaring the sum of two sines gives rise to sum and difference frequency terms. Thus, high frequency and low frequency variations in energy density result at the intersection of the two beams produced by the two elements. Ultrasound-stimulated acoustic emission results from the energy term that produces a low-frequency vibration. The low-frequency force on a target at the focal point can be computed with the following integration: $F_l = d_r \int_S \langle E \rangle da$, S is the area over which $\langle E \rangle$, the total

energy density in the focal plane, has significant value, and $\langle \rangle$ represents a short-term time average. For focused beams, the intersection region can be small enough that F_l , the low frequency force, can be considered to be an oscillating point force applied to the object at the focal intersection of the beams. To produce an ultrasound stimulated vibro-acoustic emission spectrogram, we vibrate a small region of the object with an oscillating radiation force of varying frequency. The complex amplitude of the resulting acoustic emission field, $\Phi(\Delta f)$, can be written: $\Phi(\Delta f) = d_r H(\Delta f) Q(\Delta f)$, where $Q(\Delta f)$ is a complex function representing the mechanical frequency response, or admittance, of the object at the selected point and $H(\Delta f)$ represents the combined frequency response, or transfer function, of the propagation medium and receiver and is assumed to be fixed and known (Fatemi and Greenleaf, 1999). Recording $\Phi(\Delta f)$ allows us to obtain $Q(\Delta f)$ for each point, within a constant multiplier. We raster scan the radiation force over the object to produce data that can be mapped into a pictorial format. The spatial resolution of the resulting image is determined by the region in which significant interference between the ultrasound beams occurs and is of the order of a few wavelengths at the ultrasound frequency. In a slight alteration of vibro-acoustography called vibrography we attach an accelerometer to the object to measure its vibration. The scan of the vibration inducing ultrasound beam remains the same. We show both types of images here.

RESULTS

To test the feasibility of using the technique to image mechanical properties of tissues, we measured the amplitude of acoustic emission from intact and broken struts on Bjork-Shiley convexo-concave (BSCC) prosthetic heart valves. The valves were scanned in a plane perpendicular to the ultrasound beam axis. Vibro-acoustography of the valve at 40 kHz resulted in an image of $Q(40k)$ and is illustrated in Figure 2. Also illustrated in Figure 2 are vibrography images representing $Q(7k)$ of a valve in which one leg of the small strut is broken. One can see that the strut vibrates differently when broken. The amplitude images are highly detailed and exhibit variations in acoustic emission from mechanical objects having different vibration characteristics. These differences are due to variations in the product of the reflection properties, d_r , and the effective mechanical vibration admittance properties of the object. Thus, both vibro-acoustography and vibrography are similar to conventional pulse echo ultrasound imaging, which is sensitive to the ultrasonic parameters of the object, but these two new imaging methods have the advantage of also being sensitive to the mechanical admittance at low frequencies.

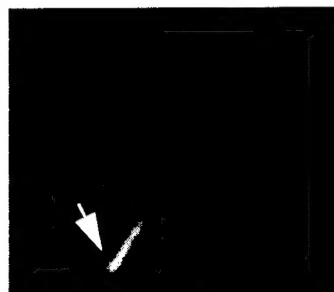
DISCUSSION

Several implications can be deduced from the results of this study. The results shown here imply that fractured struts could be found in similar types of valves implanted in

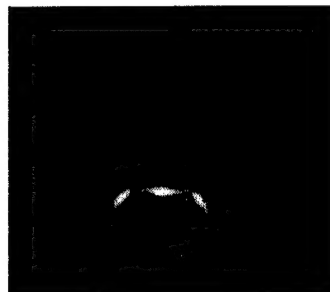
patients assuming an appropriate clinical instrument can be built. Vibration modes of complex objects could be characterized without having to touch the object. Motion induced by ultrasound and measured with ultrasound pulse echo has been used previously to study "hardness" (Dutt et al., 2000). However, the sensitivity of ultrasound pulse echo to motion at common ultrasound frequencies is limited to several micrometers. The advantage of ultrasound stimulated vibro-acoustic emission is its high displacement sensitivity. Cyclic displacement of 100 nm at 10 kHz produces an acoustic intensity of about $3.0 \times 10^3 \text{ W/cm}^2$. Hydrophones similar to the one used in these experiments are sensitive to as little as 10^{-15} W/cm^2 , and therefore, can detect very small cyclic displacements. The method will be more sensitive for higher frequency sound because acoustic power is proportional to the square of frequency for constant displacement amplitude.



48 kHz vibro-acoustography



Broken strut 2.04 kHz



Intact strut 7.4 kHz

Figure 2. Upper; vibro-acoustography image of artificial heart valve (BSCC) showing high detail and no speckle. Highlights on strut are due to reflection of ultrasound into the hydrophone which was at the right. Lower; images obtained with vibrography at the resonance of the broken (left) and intact (right) struts. The strut is broken at the arrow and the free end vibrates strongly when driven at frequency of 2.04 kHz, much lower than the 7.4 kHz resonance of the intact strut on the right.

Ultrasound stimulated vibro-acoustic spectrography may have application in at least two general areas. The first is nondestructive evaluation of materials, where material characteristics and structural flaws can be identified by measuring changes in the mechanical response to vibration at a point. The object under test could be remotely probed by beams propagating and interfering in either water or air. Beams propagating within the object could also be used to produce acoustic emission from flaws. The second general area of application is medical imaging and detection. Vibro-acoustography appears particularly suitable for noninvasive detection of hard tissue inclusions, such as imaging arteries with calcification, detecting breast micro-calcifications, visualizing hard tumors, and detecting foreign objects. Because changes of stiffness alter the vibration frequency response or damping of tissue, vibro-acoustography can potentially provide a noninvasive, remote, high-resolution, speckle

free "palpation" technique that can reach small abnormalities that are otherwise untouchable by conventional methods.

SUMMARY

In an *in vitro* experiment the acoustic emission characteristics of broken and intact struts on BSCC valves exhibited different frequency responses and different vibro-acoustography images. The images indicated that the vibration modes of the object could be deduced in addition to the structural integrity of the object. Structural integrity of such prostheses could be deduced using vibro-acoustography *in vivo*.

ACKNOWLEDGMENTS

The authors gratefully acknowledge the secretarial assistance of Elaine C. Quarve and the provision of heart valves by Edmond Rambod at the California Institute of Technology. This work was supported in part by a grant from the National Institutes of Health HL 61451 and a grant from the US Department of Defense DAMD 17-98-1-1821.

REFERENCES

- Beyer, R.T., 1978, Radiation pressure - the history of a mislabeled tensor, *J Acoust Soc Am* 63(4):1025.
- Chu B-T., and Apfel, R.E., 1982, Acoustic radiation pressure produced by a beam of sound. *J Acoust Soc Am* 72(6):1673.
- Dutt, V., Kinnick, R.R., Muthupillai, R., Oliphant, T.E., Ehman, R.L., and Greenleaf, J.F., 2000, Acoustic shear-wave imaging using echo ultrasound compared to magnetic resonance elastography, *Ultrasound Med Biol* 26(2) (to appear in Feb issue).
- Fatemi, M., and Greenleaf, J.F., 1998, Ultrasound-stimulated vibro-acoustic spectrography, *Science* 280:82.
- Fatemi M., and Greenleaf, J.F., 1999, Vibro-acoustography: an imaging modality based on ultrasound-stimulated acoustic emission, *Proc Natl Acad Sci USA* 96:6603.
- Gao, L., Parker, K.J., Lerner, R.M., and Levinson, S.F., 1996, Imaging of the elastic properties of tissue - a review, *Ultrasound Med Biol* 22(8):959.
- Jiang, Z-Y., and J.F. Greenleaf, J.F., 1996, Acoustic radiation pressure in a three-dimensional lossy medium. *J Acoust Soc Am* 100(2, Pt. 1):741.
- Lord Rayleigh, 1902, *Philos Mag* 3:338; also see Lord Rayleigh, 1905, *Philos Mag* 10:364.
- Muthupillai, R., Lomas, D.J., Rossman, P.J., Greenleaf, J.F., Manduca, A., and Ehman, R.L., 1995, Magnetic resonance elastography by direct visualization of propagating acoustic strain waves, *Science* 269:1854.
- Rudenko, O.V., Sarvazyan, A.P., and Emelianov, S.Y., 1996, Acoustic radiation force and streaming induced by focused nonlinear ultrasound in a dissipative medium, *J Acoust Soc Am* 99(5):1.
- Sarvazyan, A.P., Rudenko, O.V., Swanson, S.D., Fowlkes, J.B., and Emelianov, S.Y., 1998, Shear wave elasticity imaging: a new ultrasonic technology of medical diagnostics, *Ultrasound Med Biol* 24(9):1419.
- Wu, T., Felmlee, J.P., Greenleaf, J.F., Riederer, S.J., and Ehman, R.L., 2000, MR imaging of shear waves generated by focused ultrasound. *Magn Reson Med* 43:111.
- Westervelt, P.J., 1951, The theory of steady force caused by sound waves, *J Acoust Soc Am* 23(4):312.

COVER SHEET FOR PROPOSAL TO THE NATIONAL SCIENCE FOUNDATION

PROGRAM ANNOUNCEMENT/SOLICITATION NO./CLOSING DATE/If not in response to a program announcement/solicitation enter NSF 00-2					FOR NSF USE ONLY		
nsf99-168			01/18/00			NSF PROPOSAL NUMBER	
FOR CONSIDERATION BY NSF ORGANIZATION UNIT(S) (Indicate the most specific unit known, i.e. program, division, etc.)					0079804		
DATE RECEIVED	NUMBER OF COPIES	DIVISION ASSIGNED	FUND CODE	DUNS# (Data Universal Numbering System)	FILE LOCATION		
				006471700			
EMPLOYER IDENTIFICATION NUMBER (EIN) OR TAXPAYER IDENTIFICATION NUMBER (TIN)		SHOW PREVIOUS AWARD NO. IF THIS IS <input type="checkbox"/> A RENEWAL <input type="checkbox"/> AN ACCOMPLISHMENT-BASED RENEWAL		IS THIS PROPOSAL BEING SUBMITTED TO ANOTHER FEDERAL AGENCY? YES <input type="checkbox"/> NO <input checked="" type="checkbox"/> IF YES, LIST ACRONYMS(S)			
416011702							
NAME OF ORGANIZATION TO WHICH AWARD SHOULD BE MADE			ADDRESS OF Awardee ORGANIZATION, INCLUDING 9 DIGIT ZIP CODE				
Mayo Foundation			Mayo Foundation				
AWARDEE ORGANIZATION CODE (IF KNOWN)			200 First Street S. W.				
4004875000			Rochester, MN. 559050001				
NAME OF PERFORMING ORGANIZATION, IF DIFFERENT FROM ABOVE			ADDRESS OF PERFORMING ORGANIZATION, IF DIFFERENT, INCLUDING 9 DIGIT ZIP CODE				
PERFORMING ORGANIZATION CODE (IF KNOWN)							
IS Awardee ORGANIZATION (Check All That Apply) (See GPG II.D.1 For Definitions) <input type="checkbox"/> FOR-PROFIT ORGANIZATION <input type="checkbox"/> SMALL BUSINESS <input type="checkbox"/> MINORITY BUSINESS <input type="checkbox"/> WOMAN-OWNED BUSINESS							
TITLE OF PROPOSED PROJECT Acquisition of Low Level Sound and Vibration Measurements System							
REQUESTED AMOUNT \$ 350,661		PROPOSED DURATION (1-60 MONTHS) 12 months		REQUESTED STARTING DATE 07/01/00		SHOW RELATED PREPROPOSAL NO., IF APPLICABLE	
CHECK APPROPRIATE BOX(ES) IF THIS PROPOSAL INCLUDES ANY OF THE ITEMS LISTED BELOW							
<input type="checkbox"/> BEGINNING INVESTIGATOR (GPG 1.A.3)				<input type="checkbox"/> VERTEBRATE ANIMALS (GPG II.D.12) IACUC App. Date _____			
<input type="checkbox"/> DISCLOSURE OF LOBBYING ACTIVITIES (GPG II.D.1)				<input type="checkbox"/> HUMAN SUBJECTS (GPG II.D.12)			
<input type="checkbox"/> PROPRIETARY & PRIVILEGED INFORMATION (GPG II.D.10)				Exemption Subsection _____ or IRB App. Date _____			
<input type="checkbox"/> NATIONAL ENVIRONMENTAL POLICY ACT (GPG II.D.10)				<input type="checkbox"/> INTERNATIONAL COOPERATIVE ACTIVITIES: COUNTRY/COUNTRIES _____			
<input type="checkbox"/> HISTORIC PLACES (GPG II.D.10)				<input type="checkbox"/> FACILITATION FOR SCIENTISTS/ENGINEERS WITH DISABILITIES (GPG V.G.)			
<input type="checkbox"/> SMALL GRANT FOR EXPLOR. RESEARCH (SGER) (GPG II.D.12)				<input type="checkbox"/> RESEARCH OPPORTUNITY AWARD (GPG V.H)			
<input type="checkbox"/> GROUP PROPOSAL (GPG II.D.12)							
PI/PD DEPARTMENT Department of Physiology and Biophysics			PI/PD POSTAL ADDRESS 200 First St. Sw				
PI/PD FAX NUMBER 507-266-0361			Rochester, MN 55901				
			United States				
NAMES (TYPED)	High Degree	Yr of Degree	Telephone Number	Electronic Mail Address			
PI/PD NAME Mostafa Fatemi	Ph.D	1979	507-284-0608	fatemi@mayo.edu			
CO-PI/PD							
CO-PI/PD							
CO-PI/PD							
CO-PI/PD							

PROJECT SUMMARY

2. Project Summary

The general direction of our research activities is measurement of sound and vibration in response to micro-force. The majority of our projects are centered on the hypothesis that by measuring the sound and/or vibration resulting from such small forces we will be able to obtain important information about the object. In most of our projects this micro-force is produced by the radiation force of ultrasound, which is in mN range, and the resulting vibration is in nanometer or angstrom range.

We have shown that by measuring the acoustic field resulting from such vibration we can obtain estimates of the mechanical properties of the object, image the object at high resolutions, and detect small particles. We also have shown that the radiation force of ultrasound can stimulate the fetus. It appears that this field of science has great potential in material science, non-destructive evaluations, and medicine.

The aim of this proposal is to acquire instrumentation that would enable us to measure low level sound and vibration. With such capabilities, we would be able to validate our models, measure different modes of vibration and differentiate them, and improve our measurement techniques.

This proposal is for the acquisition of 4 main components: (1) an anechoic chamber, (2) a scanning laser vibrometer, (3) a dual channel compact fiber vibrometer, and (4) a de-aeration system. The anechoic chamber allows us to reduce the background noise and vibration in our experiments. Presently, the background noise is our main limiting factor in our newly developed imaging method called vibro-acoustography. The scanning laser vibrometer allows us to directly measure vibrations in angstrom range. Also we can use this device to obtain the spatial distribution of motion in response to a small point force. The dual-channel fiber vibrometer will be used to simultaneously measure vibration at two points of the object. These instruments would enable us to measure the transition time and the phase of vibration. Also this instrument allows us to measure vibrations directly under water, where most of our experiments are performed. Finally, the de-aeration system is necessary to provide clean and completely degassed water for our water tank experiments. Noting that gas bubbles interfere with our imaging technique and produce a significant amount of noise in the experimental water tank, de-aeration system would be a valuable tool for reducing errors in most of our experiments.

Graduate students, research trainees and fellows, and senior investigators will use the above instrumentation. Addition of these equipment to our laboratory will help us to attract more qualified students in the Biomedical Imaging track.